MINISTRY OF DEFENCE (PROCUREMENT EXECUTIVE)

AERONAUTICAL RESEARCH COUNCIL
REPORTS AND MEMORANDA

Experiments in Turbulent Boundary Layers with Foreign Gas Injection

By D. I. A. DUNBAR and L. C. SQUIRE

Cambridge University Engineering Department

LONDON: HER MAJESTY'S STATIONERY OFFICE

1972

PRICE £2·80 NET

Experiments in Turbulent Boundary Layers with Foreign Gas Injection

By D. I. A. DUNBAR and L. C. SQUIRE
Cambridge University Engineering Department

Reports and Memoranda No. 3696*
April, 1971

Summary.

An investigation has been made of the properties of turbulent boundary layers in negligible pressure gradient with homogeneous injection of carbon dioxide through a porous surface. Experiments were carried out at Mach numbers of 0·55, 1·8, 2·5 and 3·5 at various blowing rates, the highest rate at $M = 3{\cdot}5$ giving symptoms of incipient 'blow-off'. Velocity, temperature and concentration profiles were measured at various stations along the layer and these results have been used to determine skin-friction and shear-stress profiles in the boundary layer.

This report contains the full results in tabular form and also presents a preliminary analysis of the results.

LIST OF CONTENTS

* Replaces A.R.C. No. 32904.

---

1. Introduction.

There is now considerable interest in the injection of fluid through a porous surface into a turbulent boundary layer. In the first place this system is a powerful method of cooling a surface exposed to a hot stream of gas. Secondly it has been suggested that turbulent diffusion through the porous surface may provide a suitable mechanism for the introduction of fuel into a supersonic combustion process. In both uses there is the need to study the injection of gases different from the gas of the main stream, i.e., the use of so-called foreign gas injection.

Most of the previous work in this field has concentrated on the measurement of overall skin-friction and heat transfer rates, Leadon and Scott[1], Pappas and Okuno[2a, b]. The detailed effect of foreign gas injection on the incompressible boundary layer was investigated by Romanenko and Kharchenko[3]. However, instead of measuring the concentration profiles directly, they assumed a correlation between local concentration and velocity which has been shown by the present results to be inaccurate (Dunbar

and Squire[4]) although the error introduced into their overall results is relatively small. Scott, Anderson and Elgin[5] measured concentration profiles for helium injection into a supersonic flow and found that the concentration and velocity boundary layers were of equal thickness. However, they did not attempt a detailed investigation of the layer. While these early results show some of the main features of foreign gas injection, they are not sufficient to define the main parameters of the flow, or to serve as test cases for computer methods.

The present report gives an account of experiments made to provide a full set of data on turbulent boundary layer development with foreign gas injection. The experiment was carried out on the same equipment as used by Jeromin[6] and Squire [12] for their studies on air injection. Boundary layer developments were measured at Mach numbers of 0·55, 1·8, 2·5 and 3·5 for various rates of injection of carbon dioxide into a stream of air. For each set of conditions measurements were made of the velocity, temperature and concentration profiles along the layer.

In addition to the basic results the present report contains a brief account of the preliminary analysis of the results. Further analysis will be found in Ref. 4 and Squire[7].

2. Description of the Apparatus and the Experimental Procedure.

2.1. The wind tunnel.

The investigation was carried out in the Cambridge University Engineering Laboratory supersonic wind tunnel. This is an intermittent blow-down wind tunnel of working section (in standard mode) 115 mm × 180 mm.

The air is stored in a reservoir at a maximum pressure of 70 atmos. This is reduced to the required working section stagnation pressure by a manually operated throttle valve, this pressure being variable in the range 1–10 atmos. gauge. The stagnation temperature varies slightly during each run and from run to run, there being no means of control. The approximate mean value of the stagnation temperature was 292 degrees K, with a maximum variation of ± 4 degrees C, the typical variation during a run being about 2 degrees C.

Liners were available suitable for working section Mach numbers of about 1·8, 2·5 and 3·5, the $M = 3{\cdot}5$ liner being visible in Fig. 1. In order to extend the scope of the investigation to include near-isothermal flows, an arrangement was designed enabling the wind tunnel to be run at the subsonic Mach number of about 0·55. This can be seen in Fig. 2. It consists of a wooden liner, continuing the contraction from the settling chamber into a parallel portion at the working section, followed by a throat just before the diffuser. The throat is formed by a symmetrical duralumin aerofoil section spanning the tunnel at the rear of the parallel portion. Small variations in Mach number can be obtained by rotating the aerofoil about a horizontal axis through a point chosen such that for small rotations the throat areas above and below the aerofoil remain equal. This facility was included in case the injection caused a significant variation in working section Mach number but, in the event, this variation proved negligible and the throat geometry was kept constant throughout the subsonic experiments.

At the Mach numbers of 0·55, 1·8, 2·5 and 3·5 the wind tunnel was operated at stagnation pressures of 0·05, 0·083, 0·207 and 0·730 MN/m^2, gauge respectively. These operating conditions corresponded approximately to Reynolds numbers per metre of 1·68, 2·62, 3·18 and $5{\cdot}0 \times 10^7$ respectively.

2.2. The installed injection apparatus.

The apparatus installed in the wind tunnel was essentially that designed and described in great detail in Ref. 6, with a few minor modifications. Therefore, only the important features will be described here.

In order to fit any injection apparatus into the wind tunnel it was necessary to encroach on the standard working section. Therefore, for simplicity, the flat plate injection area was located almost on the centre line of the standard working section, thereby requiring only one liner instead of the usual symmetrical pair. This reduced the working section area to 115 mm × 90 mm but had the beneficial effect of doubling the maximum tunnel running time to 150 *s*.

A cross section of the injection apparatus is shown in Fig. 3 and it can be seen installed in the wind tunnel in Figs. 1 and 2. It consists of a plenum chamber with the porous injection surface at the top and

a second plate in the middle of the chamber to act as a filter and also to smooth the distribution of the injected gas. In order to minimise the time taken to purge the system of air when foreign gas was being injected, most of the possible dead-space below the lower plate was filled with Perspex, leaving two pentahedral spaces for gas to pass from the inlets to the lower surface of the plate. The gas was led from outside the tunnel to the two inlets through two tubes in the back closing plate.

The injection surface was made from $\frac{1}{4}$ in. (6·3 mm) thick, Grade A Porosint (a sintered bronze filter material made by Sintered Products Ltd.) to pass particles of maximum diameter 0·0001 in. (0·0025 mm) with a rolled surface. It was found by Jeromin[6] that this provided a surface which was effectively aerodynamically smooth. Another factor in the choice of this particular grade of material was that the pressure difference across the plate required for a given mass flow rate was larger than for the other possibilities, so that irregularities in the local mass flow rate, due to spatial pressure variations in the working section, would be minimised. However, a small correction was still required to take account of this. Jeromin[6] found that the spatial variation of mass flow rate due to variations in material porosity was about ± 5 per cent, which is good for most common porous materials.

The injection area measured 86 mm × 395 mm, thus spanning most of the tunnel width and allowing sufficient length for development of the boundary layer beyond the start of injection, since the first measurements were made 210 mm downstream of the start of injection. Small copper-constantan thermocouples were let into the plate for measuring the surface temperature, the connecting wires being led through a plug in the front of the plenum chamber and thence out of the tunnel.

2.3. The traverse gear.

Difficulties in introducing a traverse gear into the working section are inherent in the use of a porous surface. Two possibilities are passing the probe through the porous surface, with problems in sealing, and traversing from the opposite wall, which in this arrangement would produce tunnel blockage and probe rigidity problems. The method used in this apparatus was to position, immediately behind the porous surface, a very rigid traverse gear from which the probes could be extended forward to the measuring station. This traverse gear can be seen in Figs. 1, 2 and 3, and comprises a probe holder mounted on two rigidly connected pillars sliding in locating bushes. The vertical position of the probe was varied by means of a micrometer mounted on the outside of the tunnel, connected to the traverse gear through a universally jointed shaft. Any play in the system was taken up by a compression spring acting on the probe holder, since backlash allowed oscillations of the traverse gear when the tunnel was running.

The position of the traverse gear was determined using a linear potentiometer wound with 0·0005 in. (0·0125 mm) dia. wire mounted on the traverse gear frame, the moving contact being attached to the probe holder assembly, thereby ensuring that the output of the potentiometer was a measure of probe holder position only.

This system was very rigid and provided a sensitive means of traversing the probes and measuring their position.

2.4. The external injection apparatus.

The carbon dioxide for injection was obtained in non-syphon cylinders containing 22·5 kg each. One disadvantage of using carbon dioxide is that in these cylinders it is liquid and, in order to generate gas at the desired rate of up to 2 kg/min, a high rate of heat addition is required. This entails either using a very large number of cylinders manifolded, or using syphon cylinders with heating apparatus, in which case the temperature of the gas would be unsteady. For this investigation it was decided to use an intermediate reservoir for storing sufficient carbon dioxide in gaseous form. The vessel used was a 0·6 m^3 high pressure cylinder, similar to those used for storing the wind tunnel air, pressurised to about 30 atmos. During a tunnel run, carbon dioxide could be drawn from this at a high rate, and it was kept charged by bleeding continuously at a low rate from three carbon dioxide cylinders, manifolded together.

The metering apparatus connecting the reservoir to the wind tunnel injection system can be seen in Fig. 2. The gas passes from the reservoir through a control valve, reducing the pressure into the range

0–3 atmos. gauge measured by a gauge, before passing through a non-standard metering orifice, whose pressure tappings are connected to a single tube high-pressure alcohol manometer. The outlet from the orifice is a pipe which is bifurcated before connection to the wind tunnel apparatus, in order to feed the two plenum chamber inlets.

2.5. The pilot traverse apparatus.

The probe used for pitot pressure traversing is shown in Fig. 4. The probe tip was made from 1·05 mm O.D. hypodermic tube which was bored out at one end and flattened to an overall height of 0·18 mm, with a mouth height of 0·05 mm, the mouth centre line being 0·08 mm from the lower edge. The tip was joined to a length of straight 3·2 mm O.D. brass tube which formed the main supporting member of the probe. In order to give rigidity when the probe was in its farthest forward position, three triangular metal fins were joined to the brass tube, and it was by these fins that the probe was held on the probe holder. The internal volume of the probe is made small (to give fast response to changes in pressure) by continuing the hypodermic throughout the length of the probe.

To enable complete pitot traverses of the boundary layer to be carried out in the duration of a single tunnel run, it was necessary to use an electric pressure transducer. For the supersonic flows, a Solartron absolute pressure transducer of the diaphragm-strain gauge type of range 0–5 atmos. absolute was used, which was mounted on the traverse gear frame and connected by a short piece of plastic tube to the hypodermic tube at the rear of the probe. The transducer was mounted in an assembly which gave the minimum possible volume above the diaphragm and the response speed of the complete system was very fast.

For the subsonic experiments where it was necessary to measure tunnel static pressure, a differential pressure transducer was used, mounted externally on the tunnel. One side of the transducer was connected to a static pressure tapping in the tunnel wall, while the other was connected by a length of tube to the probe. The dead volume of this system was necessarily greater than that of the system described above but, nevertheless, the response speed was found to be adequate.

Both the transducers mentioned above gave an electrical output which, to sufficient accuracy, varied linearly with pressure and could be taken directly to the input of an X–Y pen recorder.

2.6. The temperature probe.

Following the practice of Danberg et al[8] and Jeromin[6], the temperature probe used for this investigation was of the 'equilibrium temperature' type. This description is used for a probe of such a shape that the supersonic flow about the probe is known. The body used in this investigation was an acute angle cone, as in the experiments of Danberg and Jeromin. It is then assumed that the temperature of the probe is the laminar recovery temperature of the theoretical flow at the cone surface corresponding to conditions immediately in front of the cone apex (allowance being made, if necessary, for heat conduction away from the conical tip). Thence the static temperature at the cone apex can be deduced, as will be shown in Appendix I.

For this temperature probe, which is shown in Fig. 4, a stainless steel cone of semi-angle 5 degrees, and maximum diameter about 1·5 mm was used. This was let into a short length of ceramic tube of the same diameter, which was joined to a brass wedge. This assembly was joined to a support of brass tube with fins of exactly the same type as that used for the pitot probe.

For measuring the temperature of the cone, a copper-constantan thermocouple was soldered into a hole in the metal, the leads being taken, through the wedge and the brass tube, out of the rear of the probe. It is sometimes necessary with this type of probe to make allowance for heat conduction along the support (in this case the ceramic tube), and for this a thermocouple would have been required in the wedge. However, Jeromin found that for this type of probe, working in conditions essentially similar to those in this investigation, the effect of heat conduction was negligible (due to the low thermal conductivity of the ceramic).

The output of the thermocouple, with its reference cold junction in an ice-water mixture was suitable

for direct connection to the input of an X–Y pen recorder.

2.7. The measurement of gas composition.

The most important preliminary investigation to be carried out before the main experimental programme, was the evaluation of methods of gas analysis to find the best and most convenient system for the determination of the concentration profiles. A factor which simplifies the problem is that the gases which comprise the mixture are known (i.e., air and carbon dioxide), so that true analysis of the sample is not required. It is only necessary to determine the relative proportion of the constituent gases.

The analysis of gas mixtures can be effected by considering either their chemical or physical properties, or both. In general, physical methods are more convenient for quick processing of a number of samples, especially when the constituents do not have to be identified. For this investigation, in order not to restrict further work using different gases, it was important that the chosen method should be applicable to as wide a range of gas mixtures as possible. Thus, methods which relied on a peculiarity of the injected gas were not considered acceptable. It was also essential that an accurate analysis should be possible from a small sample (of 100 ml or less).

An instrument which would satisfy these requirements extremely well is the mass spectrometer but, since access to one was not readily available, this possibility was rejected on the grounds of expense. Another common analyser is the gas chromatograph. This is also expensive when complete, but for a mixture of known gases the chromatograph column is unnecessary and only the detector is required. One type of detector is the katharometer, or thermal conductivity cell, whose basic component is an electrical conducting filament which is immersed in the gas to be analysed in a cavity. An electric current is passed through the filament, the temperature (and hence the resistance) of which is dependent on the thermal conductivity of the surrounding gas, a property which for most mixtures is a unique function of the concentration. The instrument is usually made in the form of a Wheatstone bridge network, with two of the arms being filaments immersed in the sample, and two filaments immersed in a reference gas. Thus the electrical output of the instrument is a direct measure of the gas composition. The only restrictions of the katharometer are that the thermal conductivity of the component gases must be sensibly different (which, in general, means that their molecular weights must be different), and that the thermal conductivity of the mixture should vary monotonically with concentration. On the grounds of its simplicity of operation and its versatility, the katharometer was chosen as the most suitable instrument for this investigation.

It would be convenient to be able to determine a complete concentration profile during a single tunnel run. This could be achieved by extracting gas from the boundary layer through a probe, the sample stream then being passed through the analysis instrument. By traversing the probe through the boundary layer, a continuous trace of concentration against position could be produced. However, this approach is complicated by the short duration of each run which would necessitate a total system response time of the order of two seconds. This can only be achieved using a through-flow type of katharometer in which the filaments are immersed directly in the gas stream, with the inherent disadvantage that the instrument is then flow-rate sensitive. Thus, in order to make accurate measurements, the flow rate must be stabilised, since the stagnation pressure at the probe mouth can vary from 0·015 to 0·27 MN/m^2 during a single run. A series of tests was carried out on a through-flow katharometer to determine whether this approach was feasible. It was found that the instrument's sensitivity to conditions would make it extremely difficult to obtain results of sufficient accuracy. It was therefore decided to abandon the continuous sampling method and, instead, to take discrete samples from the boundary layer, with a fixed probe position during each run. The sample could then be analysed after each run and, by using different probe positions, a concentration profile could be obtained.

2.7.1. *The concentration measuring apparatus.* The boundary layers to be measured varied in thickness from 5–12 mm, and so, for easiest measurement of the boundary layer combined with negligible interference to the flow, a five-probe rake was made and is shown in Fig. 4. The rake consists of five flattened probes with their mouths in a vertical line separated by 1·5 mm. Each probe is of similar construction to

the flattened pitot described in Section 2.5, being made from stainless steel hypodermic tube and having a mouth height of 0·05 mm with an overall height of 0·125 mm. The probe nearest to the surface was made with greater care so as to make the metal lips as thin as possible, thus minimising interference with the flow near the surface. The probes were held securely in a 5 degree semi-angle brass wedge which was joined to a flat plate which could be bolted in many positions to the traverse gear. In order to make the probe as stiff as possible, five tubes were soldered in a line above the plate (forming a fin) through which the hypodermic passed to the rear of the probe, making the overall length about 250 mm. For extra rigidity, the tubes were enclosed by two stainless steel plates.

It might be thought that a rake of this type would interfere with the flow in the boundary layer, so that the results from any one probe might be affected by the presence of the others. Therefore a schlieren study was made of the flow near the probe mouth, a typical result being shown in Fig. 5. In this case the boundary layer extends to the uppermost probe, and it can be seen that, even in the lower velocity region near the surface, the pressure field from one probe does not have a significant effect in the vicinity of another. It was therefore assumed that there was negligible interference between the probes of the rake.

For ease of manipulation, the equipment for collecting the samples is located just outside the wind tunnel. It consists of five cylindrical brass vessels of about 500 ml internal volume, whose inlets and outlets are controlled by means of ground glass taps. The inlets are connected by means of small-bore plastic tube to the rear of the sampling rake, passing through a blanking plate on the tunnel, while the outlets are connected to a rotary vacuum pump. The connections are such that the internal volume of the system between the probe mouth and the vessel inlet is very small compared with the volume of the vessel. This minimises contamination of the sample by residual gases in this tubing.

The sampling apparatus described above can be seen in position in Fig. 2. The instrument which was selected for measuring the sample composition was a Cambridge Instrument Company temperature controlled katharometer. This is a katharometer of the diffusion type which has two passages through one of which the sample is passed at low rate (of the order of 1 ml/sec). The other passage is used for passing the reference gas, which in this case was tunnel air, bled from the tunnel operating system. Off each passage there are two chambers into which the gas in the passage diffuses, and in each chamber there is one of the measuring filaments. The filaments are connected in a bridge form, the instrument being powered from a 350 mA constant current store. The output is measured on a digital voltmeter.

The bridge output can be adjusted to give zero for zero per cent carbon dioxide, and the 100 per cent carbon dioxide reading is approximately 130 mV.

It was found that the calibration of the instrument was almost linear and that the repeatability of zero and sensitivity was very good, so that it was unnecessary to calibrate the instrument each time using a reference mixture.

2.7.2. *Method for concentration measurement.* Before a concentration measuring run, the sampling vessels were evacuated by closing the inlet taps, opening the outlet taps and running thevacuum pump until a mercury manometer connected to the system gave a reading which differed by less than 0·05 mm from that of the barometer. The outlet taps were then closed and the tunnel started. When the tunnel conditions were steady, the inlet taps were opened, to be closed just before the end of the run.

The vessels were then disconnected from the tunnel, and the pressure of each sample was brought to atmospheric by connecting the 'outlet' to a reservoir of vacuum oil and opening the tap until the pressure equalised. Vacuum oil, with its low vapour pressure, was used in order to minimise the quantity of impurity introduced into the sample during this procedure. The 'inlet' was then connected to the katharometer and the sample passed through the instrument by slightly raising the reservoir of oil. The output of the instrument, as measured by the voltmeter, became steady after about two minutes, and this was taken as the value from which the sample composition could be found.

It might seem that the use of an evacuated vessel could induce such a flow through the probe mouth that the nearby flow might be distorted, thereby producing an unrepresentative sample. However, in a supersonic stream, the flow rate through the mouth can only be increased until the shock at the probe tip is ingested. Any further decrease in the suction pressure can only change the flow inside the probe and does not affect the external flow. In subsonic conditions, the probe mouth gas velocity did not exceed

the local undisturbed velocity and so the local effect would be expected to be negligible. The possibility of 'iso-kinetic' sampling, in which the probe mouth velocity is matched to the local velocity, was considered to introduce unnecessary complications since the gain in accuracy would have been negligible.

2.8. Experimental range and procedure.

The aim of the experimental programme was to provide a reasonable range of data under a variety of conditions. Therefore, experiments were carried out at three injection rates for each of the four Mach numbers which were available. In order to provide an indication of the degree of development of the boundary layer, and to be able to estimate the skin friction, it was necessary to measure profiles at a number of streamwise positions. The minimum number of stations to give the required information was two, but the greater the number the more reliable the information. As a compromise between accuracy and the time involved, the profiles were measured at three stations, each separated by 63 mm, the upstream station being about 210 mm downstream of the start of injection. In the figures and tables of this report, the profiles measured at the forward, centre and rear positions will be identified by the letters F, C, R.

The injection rates used at the three lower Mach numbers correspond to an injection parameter F before pressure gradient correction of $1{\cdot}2, 2{\cdot}4, 3{\cdot}6 \times 10^{-3}$. The maximum value was regulated by a reasonable consumption of carbon dioxide. At $M = 3{\cdot}5$, the maximum injection rate was regulated by what appeared to be blow-off, as will be described in Section 2.8.1 below. This occurred at the rear station at an injection parameter of $2{\cdot}4 \times 10^{-3}$, and so the injection rates used at this Mach number corresponded to values of F of $0{\cdot}8, 1{\cdot}6, 2{\cdot}4 \times 10^{-3}$.

Before profiles were measured at any Mach number, the injection apparatus was calibrated with the tunnel running to find the orifice pressure gauge reading which gave the required flow rates. Thereafter pressure gauge readings were used to specify the injection conditions.

2.8.1. *The pitot traverses.* For pitot traverses, the pressure transducer and traverse gear potentiometer were connected to the Y and X channels of an X–Y pen recorder. Before each run, the pitot was brought into contact with the surface and lowered a further distance of about 0·1 mm. The carbon dioxide supply was then turned on and allowed to flow for sufficient time to purge the system before the tunnel was started. During the run the pitot was traversed from the surface at a steady speed until the free stream was indicated by a constant pressure line on the plotter. After each run the pressure transducer was calibrated against a mercury manometer, and the probe holder potentiometer against the micrometer on the winding handle.

Two pitot profiles are shown in Fig. 6, where the effect on the pitot profile of increasing injection rate can be seen. At the start of the traces, there is a part where the pressure is constant until it suddenly starts to rise. This is the point at which the probe tip leaves the surface and it is from this point that all distances are measured. This point is easily distinguished in most profiles and so the surface position can be determined to less than 0·025 mm. However, at high blowing rates at $M = 3{\cdot}5$ the accuracy is slightly less (within 0·05 mm) on account of the small slope of the pitot profile near the wall.

At $M = 3{\cdot}5$ and a value of F over $2{\cdot}2 \times 10^{-3}$ an effect was observed which has been called 'blow-off', or separation of the boundary layer induced by transpiration. A pitot profile corresponding to this condition is shown in Fig. 7, where the trace near the surface becomes extremely unsteady with time (which appears on the profile as a spatial unsteadiness), remaining for most of the time at a value close to that registered when the pitot is on the surface. It is impossible to evaluate any mean quantities when these fluctuations occur.

2.8.2. *The temperature traverses.* For temperature traverses, the thermocouple in the temperature probe was connected to the Y-channel of the X–Y pen recorder, using an ice-water mixture at the cold junction. The traverse gear potentiometer was connected, as for the pitot traverse, to the X-channel. The running procedure was the same as that described in Section 2.8.1. However, in the temperature traverse, the probe was moved from the free stream to the surface. One reason for this was that it was not possible to use the same technique for determining the surface position as was used in the pitot traverse, since the

temperature probe was brittle and might easily have been broken during starting. Also, the surface temperature tended to an equilibrium level during each run and, by traversing towards the surface, temperature conditions near the surface had steadied by the time they were measured. This change in surface temperature had a negligible effect on the pitot profile.

A typical probe temperature trace is shown in Fig. 8. It was found that contact between the probe and the surface was indicated sensitively by a kick of the pen. Due to the size of the probe, no measurements could be made within 0·66 mm of the surface. However, it can be seen from this figure that the curve can reasonably be extrapolated to the temperature measured by the surface thermocouple. This was true for all the temperature traces. Since the variation in probe temperature is small compared with the variation in static temperature, the inaccuracies introduced by this approximate method are small.

The calibration of the thermocouple-plotter system was measured directly by immersing the probe in constant temperature surroundings. It was found that this calibration did not vary with time, so that a single calibration could be used for all the results.

2.8.3. *The concentration traverses.* The method used for extracting samples and finding their composition was described in Section 2.7.2. In order to obtain a complete concentration profile, several runs had to be made with the rake in different positions. It was found that, to produce a definitive profile, about eight positions of the rake were required, the actual positions being determined by a running plot of the measured concentrations.

The position of the surface had to be determined for every profile. This was done by connecting the bottom probe of the rake to a pressure transducer, whose output was measured by a digital voltmeter. With the tunnel running, the probe was then traversed from the surface and the point at which the lowest probe left the surface was determined. This was indicated by the reading of the voltmeter starting to rise from the steady value obtained when the probe was on the surface. It was found that in general this position could be determined to a repeatability of about 0·012 mm. The corresponding micrometer reading was noted and all further movements of the probe were measured using the micrometer. The positions of the other probes, relative to the lowest, were measured using a microscope.

A typical concentration traverse is shown in Fig. 9 in which it can be seen that the scatter is very small. Since, near the wall, the concentration changed rapidly with distance, the measuring positions in this region had to be close together in order to define the profile. However, when the lowest probe was further from the wall, in the region where the concentration gradient was lower, the rake could be moved a greater distance between runs, and still define the profile well.

It was found that if, on separate occasions, the injection rate, tunnel conditions and probe position were set to the same nominal values, the concentration reading was repeated to within 0·2 per cent carbon dioxide.

2.8.4. *The measurement of surface concentration.* An attempt was made to measure the concentration at the surface, using a porous plate with surface pressure tappings. Through these tappings gas was drawn at a very low rate to minimise distortion of the flow. Therefore the samples which were collected were very small (less than 10 ml) and, in order to analyse them, a Servomex micro-katharometer was used. This is a through-flow type katharometer of extremely small internal volume which is not as stable or accurate as the instrument used previously, but can measure much smaller samples.

The concentrations measured using this system were not consistent with the previously obtained profile as can be seen in Fig. 9, the value being lower than the final point measured using the rake. The 'surface concentration' remained constant with a varying sampling rate, and so the discrepancy cannot be accounted for by distortion of the flow due to sampling. However, the concentration varies very rapidly near the surface, falling by over a quarter of its surface value within 0·25 mm of the surface. The tappings are inherently regions with no injection, being solid walled brass tubes let into the porous surface, and are about 1·25 mm diameter. Thus it might be expected that over the diameter of the tapping, the concentration profile near the wall would change rapidly on account of the high concentration gradient. Therefore any surface concentration that is measured using a surface tapping, will not be representative of the uniform injection region and will be lower than in that region, as was found in this

investigation.

Scott et al[5] measured concentration profiles and surface concentrations with helium injection. They claimed that extrapolation of the profile to the surface agreed with the measured wall concentrations (determined by using a surface tapping sampling method), but it would appear that the scatter of their data near the surface makes it difficult to be certain of this agreement. They also state that their measured surface concentrations are less than those predicted by theory. This can be explained by the reasoning given above.

From this investigation it appears that in a transpired boundary layer, any interruption of the injection causes a rapid change in conditions near the surface. This conclusion is compatible with the results of McQuaid[10] for a discontinuity in air injection in incompressible flow. He found that on a non-injecting surface, following a region of uniform injection, the initial rate of change of skin friction was such as would increase c_f by 50 per cent in a distance downstream of about $\frac{1}{2}\delta$.

During the analysis of the results it was found that the concentration, ω, was almost a linear function of $\frac{u}{u_1}$. This result was used to extrapolate the experimental measurements to the wall and hence to find a value of the wall concentration. The values so found are given in Tables 13–16.

2.9. The accuracy of the basic experimental measurements.

The measurement of distance from the surface is common to all profiles, the only difference being that for pitot and temperature traverses it is measured using a potentiometer, whereas in the concentration traverse the measurement is taken directly from the traversing micrometer. The largest error near the wall comes from estimating the position of the surface. This can be determined to an accuracy of about 0·025 mm both with the potentiometer and the micrometer. The distance calibration of the potentiometer is determined to an accuracy of 0·2 per cent and the position can be read from the trace with an error of less than 0·012 mm. In the concentration traverse the micrometer can be set to an accuracy of 0·005 mm.

Since little is known about the effects of compressible shear flow on the reading of a flat pitot tube, no displacement or wall effect corrections have been applied to the results in this programme. MacMillan[9] showed that for incompressible flows the effective centre of a circular pitot is displaced by 15 per cent of the probe height, and McQuaid[10] showed that the correction was of a similar magnitude for a flattened pitot. If the effect were of a similar magnitude in these experiments then there would be a position error of about 0·018 mm.

The pitot pressure can be read to about 0·2 per cent of its total variation over the boundary layer (of the order of 350 N/m^2) and the linearity of the transducer response is within this accuracy. Errors in the pressure measurement are most likely to be caused by a slight drift in transducer zero during a run. This is usually small and never more than 0·6 per cent of the pressure range.

The probe temperature can be measured to about 0·3°C. Since all the temperatures measured by the probe are within 10°C of 280°K the relative error in the measured temperature is of the order 0·1 per cent.

Contamination of the samples by residual gases is kept to a minimum by making the system dead volume small and evacuating the collecting vessels to as low a pressure as possible. The effect of residual gases should change the sample concentration of carbon dioxide by less than 1 per cent of its value. The zero and calibration stability of the katharometer is extremely good and the accuracy of the instrument depends on the conditions in which it is used. As used in this programme, the composition of a sample can be measured to an accuracy better than 0·5 per cent carbon dioxide. That the accuracy is often even better than this is indicated by the lack of scatter in the concentration profiles.

The largest source of error in the programme is the evaluation of the local injection mass flow rate. Although the total mass flow can be measured to an accuracy better than 1 per cent, spatial variations in plate porosity and tunnel static pressure cause local mass flow rates per unit area to differ from the mean value by up to 7 per cent. A correction can be applied to make allowance for some of the pressure variation and this will be described in Section 3.2. However, this does not greatly reduce the possible errors in the local injection rate, and these inaccuracies may have a large effect in the evaluation of the skin friction, as will be shown later.

3. The Reduction of the Experimental Data and Description of Basic Results.

3.1. The reduction of the experimental data.

In Section 2 it was shown that the basic data obtained from the wind tunnel experiments is in the form of continuous pitot traverses, continuous temperature traverses and a concentration profile consisting of discrete measured points. The results are required in the form of a velocity profile, a static temperature profile and a concentration profile, these being the most convenient parameters for specifying the state of the fluid at any point.

The calculation method for a supersonic boundary layer is shown diagrammatically in Fig. 10. The relations which are used in this procedure are given in Appendix I. It is interesting to note the way in which the calculations are interconnected, so that the results are dependent on all the input quantities. Thus it was necessary to be able to specify the pitot pressure, probe temperature and carbon dioxide concentration at a given distance from the surface. This was easy for the continuous traverses of the pitot and temperature probes which could be read at any point. Using a variable epidiascope projector to match the scale with that of a scribed grid, any distance could be located without continuous use of the calibration. However, this method could not be used for the concentration traverse, where values were measured at discrete points, not necessarily those suitable for the calculation. However, it can be seen in Fig. 9 that on account of the small scatter, the complete profile is accurately specified by the measured points, so a profile can be drawn through these points and the value read at intermediate points to the same accuracy.

For the $M=0{\cdot}55$ profiles, the calculation procedure is changed slightly, since all the pitot pressures are measured relative to the static pressure. Thus, from the maximum pitot pressure and the stagnation pressure, the static pressure can be determined directly. From this point the calculation proceeds as before. Theoretically, the analysis used to find the static temperature from the probe temperature is only valid for supersonic flows. However, in the subsonic boundary layer, the analysis shows that the probe temperature is close to the local stagnation temperature, which is realistic. Since the difference between the local stagnation and static temperature is less than 5 per cent, the possible relative error in the determined static temperature is small, and, therefore, the error in the calculated velocity can be considered as negligible. However, on account of this approximation, the temperature profiles themselves must be considered as slightly suspect.

The distances from the surface at which the properties were calculated were chosen for each profile to give an accurate description of the property variations, the number of points used to define a profile being about forty. For the three profiles of each development, the distances from the surface were made the same. This was to facilitate their use for the calculation of shear stress profiles.

The procedure described above was programmed for calculation on the C.U. Engineering Laboratory IBM 1130 digital computer. The results are shown in tabular form in Tables 1 to 12. In each of these tables, the boundary layer profiles corresponding to one combination of Mach number and injection rate are shown. The distances from the wall at which the properties were calculated are the same for all the profiles in one table, and these distances are given in the left-hand column*. Then, for each measuring station, the profiles of Mach number (M), velocity (u/U_1), temperature (T/T_1), and carbon dioxide concentration (MF) are tabulated.

3.2. The correction of injection rate for pressure gradients.

Using the orifice in the injection apparatus, the total mass flow rate of carbon dioxide through the injection surface could be measured. In order to find the local mass flow rate, and hence the local injection parameter F, it was necessary to find the distribution of mass flow along the surface. This is affected by two factors, the porosity variation of the injection surface and the distribution of static pressure on the working section side of the porous plate. Spatial porosity variation is neglected since its length scale is

* Tables 1 to 12 are reproduced directly from the computer output and the distance from the wall is measured in inches. All other measurements are in S.I. Units.

of the order of the boundary layer thickness, and therefore the effect on the boundary layer is incalculable. Over the rear portion of the plate, where measurements were taken, there were small variations in static pressure due to slight pressure waves in the working section. These pressure differences were, however, small compared with the pressure drop across the plate which is of the order of one atmosphere. Therefore the fluctuations in local injection rate due to these disturbances were less than those due to changes in porosity and could be neglected. The largest effect was that due to the fact that at the start of injection the flow had not reached working section design conditions and so the static pressure on the front of the plate was falling with distance. Since the pressure across the injection surface was less at the front than at the rear, the mass flow per unit area at the measuring region was slightly higher than the value obtained from taking an average, using the total mass flow of carbon dioxide divided by the total injection area.

The effect is noticeable for all the supersonic tests, while pressure variations in the subsonic working section were negligible. In order to obtain a more accurate value of the injection parameter F, a correction must be applied to the averaged result. Since the correction was always relatively small, a sophisticated method was not required. By measuring the plenum chamber pressure at the various blowing rates, an approximate calibration of mass flow rate against pressure drop was found, using the average mass flow rate per unit area. From the measured pressure distribution and the calibration, an injection rate distribution was deduced and, by integration, the total mass flow rate calculated. Comparing this mass flow rate with the actual measured value, an approximate correction was applied to the calibration curve, and the procedure repeated until the two mass flow rates matched. Then from the corrected calibration curve, the injection rate at the measuring stations could be determined.

The corrections so obtained were negligible for $M=3{\cdot}5$ and largest for $M=1{\cdot}8$. Thus the corrected values of the injection parameter F were:

$$\text{For } M=0{\cdot}55 \quad F=1{\cdot}2,\ 2{\cdot}4,\ 3{\cdot}6\times10^{-3}$$

$$M=1{\cdot}8 \quad F=1{\cdot}3,\ 2{\cdot}6,\ 3{\cdot}8\times10^{-3}$$

$$M=2{\cdot}5 \quad F=1{\cdot}3,\ 2{\cdot}5,\ 3{\cdot}6\times10^{-3}$$

$$M=3{\cdot}5 \quad F=0{\cdot}8,\ 1{\cdot}6,\ 2{\cdot}4\times10^{-3}.$$

These injection rates are quoted to two significant figures since the accuracy implied by any further figures is not warranted on account of porosity variations. Throughout the remainder of the paper, and in the figures, boundary layer profiles will be specified by the injection parameter multiplied by 10^3. Thus, together with the measuring station notation given in Section 2.9, a typical profile name is $3{\cdot}5-F-1{\cdot}6$, indicating that the boundary layer referred to was measured at $M=3{\cdot}5$, an injection rate of $F=1{\cdot}6\times10^{-3}$ and at the forward measuring station.

3.3. Determination of skin-friction.

As mentioned in Section 2.8 only three profiles were measured along a layer for any given conditions of Mach number and injection rate. These three measurements are not really sufficient for accurate determination of skin-friction, but at least the order of magnitude of the skin-friction coefficient could be determined from the momentum integral equation,

$$\frac{c_f}{2}=\frac{d\theta}{dx}-F-\frac{\theta}{\rho_1 U_1^2}\frac{dp}{dx}(2+H-M^2).$$

Although the experiments in this investigation were carried out in nominally zero pressure gradient it was found that the pressure gradient term was significant* in certain cases at $M=1{\cdot}8$ and it was therefore included in the calculation of c_f. Typical variations of θ with x are shown in Fig. 11, and within the

* The maximum effect was a change of 0·0003 in c_f.

experimental scatter it will be seen that the variation is linear, thus $\frac{d\theta}{dx}$ and c_f, is approximately independent of position on the plate.

The resultant skin-friction coefficients are presented in Tables 13 to 16 and are plotted in Fig. 12 in the form c_f/c_{f_0} against $2F/c_{f_0}$, where c_{f_0} is the skin-friction in the absence of injection.

It is estimated that the possible error in the quoted values of c_f is $\pm 0{\cdot}0001$, i.e., ± 100 per cent at the highest blowing rates.

3.4. The choice of profiles for further analysis.

For a boundary layer on a solid wall in zero pressure gradient it is found that for a range of Reynolds numbers the velocity profiles are essentially similar when plotted as $\frac{u}{U_1}$ against $\frac{y}{\delta}$. This would be expected to occur in transpired boundary layers when the parameter $\frac{2F}{c_f}$ is kept constant and this has been observed by Tewfik[11]. In the present experimental programme, the skin-friction variation in the measuring region is very small, and the injection parameter F is effectively constant and so to reasonable accuracy the condition of constant $\frac{2F}{c_f}$ is satisfied. Thus it would be expected that in the absence of significant pressure gradients the three profiles of each development would be similar. This was found to be the case at $M = 0{\cdot}55$ (Fig. 13). The results at $M = 3{\cdot}5$ (Fig. 14) also showed a good collapse, apart from some anomalous behaviour at the rear station for $F = 1{\cdot}6 \times 10^{-3}$ which might be expected since this was the station at which apparent 'blow-off' was experienced at the highest injection rate. However, for $M = 1{\cdot}8$, $2{\cdot}5$ there were significant spatial pressure variations in the measuring section. These variations are reflected in the scatter of the non-dimensional profiles shown for these Mach numbers. This scatter is most noticeable in the profiles at $M = 2{\cdot}5$.

From the experiments of Jeromin[6] and Squire[12], performed with air injection using the same experimental arrangement, it is apparent that the pressure variations are in the form of a wave. It seemed most likely that this wave was caused by reflection of the compression wave formed at the start of the injection surface, where the gradient of the boundary layer displacement thickness changes abruptly. It appears that at $M = 1{\cdot}8$, $2{\cdot}5$ this reflection meets the back of the injection surface, whereas at $M = 3{\cdot}5$ the disturbance is downstream of the measuring region. Using air injection, where only the pitot profile need be measured to define the boundary layer profiles, Squire[12] was able to determine about ten velocity profiles for each development. He found that plotting non-dimensional velocity profiles, the quality of collapse was similar to that in this investigation (i.e., that at $M = 3{\cdot}5$ the collapse was good, whereas at $M = 1{\cdot}8$, $2{\cdot}5$, there was significant scatter of the profiles). However, he found that at $M = 1{\cdot}8$, $2{\cdot}5$ the front few profiles of each development tended to collapse onto a single curve with the discrepancies becoming more noticeable in the downstream profiles. This, together with the static pressure distribution indicated that the upstream profiles were not significantly affected by the pressure disturbances. It was assumed that the disturbances present with carbon dioxide injection would be qualitatively similar to those observed by Squire.

Therefore it was decided that, although all the profiles could be used in developments for calculating the skin friction (taking into account the pressure gradient term in the momentum integral equation), the centre and rear profiles at $M = 1{\cdot}8$, $2{\cdot}5$ could not be considered as representative of a transpired boundary layer in zero pressure gradient. Therefore, in most of the results and analysis presented in this paper, the only profiles which are used for detailed investigation are those measured at the forward station in each development. Since the pressure variation over the front half of the injection surface is negligible, it can be considered that these boundary layer profiles are fully developed injection profiles representative of zero pressure gradient conditions.

3.5. The basic results.

Typical boundary layers of velocity, temperature and concentration for various injection rates are plotted against y/δ in Figs. 15, 16 and 17. The general features of these results are discussed in the following paragraphs. Possible correlations of the profiles are discussed in Ref. 4.

It can be seen that injection at the wall changes the velocity profile throughout the boundary layer. The introduction of fluid with low streamwise momentum causes the velocity at all points in the boundary layer to be reduced. This effect is demonstrated in Fig. 18 where the velocity at $\frac{y}{\delta}=0{\cdot}2$ is plotted against F for all the Mach numbers. It was found by Squire[12] that for air injection these plots were linear for both incompressible and compressible transpired boundary layers. This linearity is not observed in Fig. 18 where all the curves have a slope which decreases with increasing F. However, it might be expected that the introduction of another variable property, the carbon dioxide concentration, would cause this non-linearity. Fig. 18 should not be considered as having any quantitative significance. However, it does give an indication of the magnitude of the change in the velocity profile caused by injection.

This reduction of velocity also reduces the non-dimensional wall velocity gradient, $\frac{d(u/U_1)}{d\left(\frac{y}{\delta}\right)}$. Also, the boundary layer thickness, δ, is increased by injection (under some conditions in this programme it is almost doubled) as shown in Fig. 19. These two effects combine to give a lower absolute wall velocity gradient, $\frac{du}{dy}$, and hence a lower skin friction, with increasing mass transfer rates, as is observed in the skin friction measurements.

It is interesting to note the effect of the zero injection skin friction, c_{f_0}, which increases with decreasing Mach number from 0·0012 at $M=3{\cdot}5$ to 0·0027 at $M=0{\cdot}55$. It is apparent from the velocity profiles that a given value of the injection parameter F has less effect at the lower Mach numbers, and this is demonstrated in Fig. 18. Here it can be seen that the change in velocity at $\frac{y}{\delta}=0{\cdot}2$ for a given value of F increases with Mach number. This observation is in agreement with the observed occurrence of 'blow-off' at $M=3{\cdot}5$ and an injection rate of $F=2{\cdot}4\times10^{-3}$. Although this injection rate was exceeded at all the other Mach numbers, the 'blow-off' condition was not achieved. The near 'blow-off' profile at $M=3{\cdot}5$ is notable for the low value $\frac{u}{U_1}$ which can be measured (about 0·1), indicating a comparatively low velocity gradient at the wall. A similar effect can be seen, only in the velocity profile for the highest injection rate at $M=2{\cdot}5$ (where the value of F is greater than at $M=3{\cdot}5$).

As stated previously, one of the parameters relevant to the transpired boundary layer is $\frac{2F}{c_f}$. Now although the reduction in $\frac{c_f}{c_{f_0}}$ with injection tends to be less at higher Mach numbers, as noted in Section 3.3, the value of c_{f_0} is lower. Therefore the skin friction values with injection tend to be lower at the higher Mach numbers and, hence, for a given value of F, the value of the parameter $\frac{2F}{c_f}$ is higher. Therefore it is to be expected that the magnitude of the effect of injection would show considerable dependence on the value of c_{f_0}. The fact that this is observed in the present experiments indicates that $\frac{2F}{c_f}$, or even $\frac{2F}{c_{f_0}}$, has a more general significance than the simple injection parameter F.

It can be seen in the temperature profiles (Fig. 16) that the wall temperature varies slightly, being generally lower at the higher injection rates. This was inevitable with the present experimental arrangement since there was no means for controlling the carbon-dioxide-plenum-chamber temperature. Nevertheless, the effects of injection are apparent in the profiles. It can be seen that, although the surface

temperature is lower at the higher injection rates, throughout the major part of the boundary layer the temperature at a given value of $\frac{y}{\delta}$ is increased. It is to be expected, on account of the reduced temperature gradients in the inner part of the boundary layer and the increase in boundary layer thickness with injection, that for a constant wall temperature the temperature gradient at the surface and therefore the heat transfer rate would be reduced. This has been observed by many experimenters, but cannot be verified here since the measurement of heat transfer from the temperature profile requires accurate measurement very close to the surface and there was no provision for measuring heat transfer directly. The zero injection adiabatic wall temperature (with a recovery factor $r=0{\cdot}89$) are shown on the temperature profiles. Other experimenters, including Bartle and Leadon[13] and Pappas and Okuno[2b], have noted that the adiabatic wall temperature is reduced by injection but its exact variation with injection rate for carbon dioxide is not determinate. However, for the present experiments the ratio $\frac{T_w}{T_r}$ is always greater than unity but never greater than 1·1, and thus it can be assumed that heat transfer has a negligible effect. In all experiments, except those at $M=0{\cdot}55$, the heat transfer is from the wall to the stream.

The concentration profiles (Fig. 17) show that the injected gas diffuses throughout the boundary layer and does not remain in the immediate vicinity of the wall. It can be seen that the concentration boundary layer thickness is, to experimental accuracy, the same as the velocity boundary layer thickness. This is apparent from the way in which the concentration tends to zero for values of $\frac{y}{\delta}$ just greater than unity. This result would be expected if the turbulent diffusion in the outer part of the boundary layer is very much greater than the molecular diffusion. Then the presence of carbon dioxide is associated with the movement of a discrete mass of fluid from the inner part of the boundary layer and is therefore inherently associated with a velocity defect. It is possible that with a rapidly diffusing gas such as helium, some molecular diffusion might be noticeable outside the region of turbulence and thus the two boundary layer thicknesses might not be equal.

It can be seen that the concentration profile has many of the same qualitative features as the velocity profile. These are a steady variation in the outer part of the boundary layer with a fairly well-defined edge (although not as well-defined as that of the velocity profile), and a high rate of change with distance near the surface.

3.6. A comparison of the present results with those of air injection.

Although this report is primarily an investigation of the effect of foreign gas injection, it is of interest at this stage to compare some of the results with those of Jeromin[6], Squire[12] and McQuaid[10] obtained under similar conditions using air injection.

Figs. 20 and 21 show comparisons between the velocity profiles obtained in these experiments and those measured by Squire[12] for air injection at Mach numbers of 1·8 and 2·5. The injection rates are nominally equal, but there may be slight differences due to inaccuracies in the flow rate measurement and because the correction to injection rate is higher for the denser carbon dioxide on account of its lower plenum-chamber pressure. The velocity profiles are plotted in the form of $\frac{u}{U_1}$ against $\frac{y}{\delta}$ and Fig. 19 compares the variation of δ with air and carbon dioxide injection. Only two of Squire's profiles are shown at $M=1{\cdot}8$, since his highest injection rate was not comparable with the present experiments.

The thickness of the boundary layer with air injection is greater than that with equivalent carbon dioxide injection. Although the injection mass flow rates are equal, carbon dioxide is denser than air, and so the volume flow through the surface into the boundary layer is less in the case of carbon dioxide injection. This being so, it might be expected that the boundary layer thicknesses would differ in the above manner. This observation is compatible with the fact that while the momentum thickness (which is a resultant of the effect of F and c_f) is greater with carbon dioxide injection than with air, the displacement thickness for a given injection rate is less with carbon dioxide injection than with air.

The differences between the air and carbon dioxide injection velocity profiles are fairly small. There is, however, a consistent tendency in the outer part of the boundary layer for the velocities with air injection to be higher than those for carbon dioxide. From the present data it is not possible to compare definitively the velocity profiles in the wall region since the scatter in this region is of the order of the difference between the profiles. The lower level of the velocity in the outer region with carbon dioxide injection can be explained by the greater density of carbon dioxide increasing the inertia of the fluid and thereby causing an increased velocity defect in the region where this is the relevant concept. In order to see the combined effect of the change in profile shape and in boundary layer thickness, the actual velocity profiles (plotted as $\frac{u}{U_1}$ against y) are shown for $M=2{\cdot}5$ in Fig. 22.

Fig. 12 compares the overall skin-friction results in the form of $\frac{c_f}{c_{f_0}}$ against $\frac{2F}{c_{f_0}}$. Many theories and experiments including those of Rubesin and Pappas[25], Pappas and Okuno[2] and Romanenko and Kharchenko[3], have shown that for a given injection parameter F, the higher the molecular weight of the gas the less is the reduction in skin friction. This can best be seen in Fig. 12 by comparing McQuaid's incompressible data with the $M=0{\cdot}55$ results of the present experiments, which would be expected to correspond closely to incompressible conditions. The carbon dioxide injection results show a considerably smaller reduction in skin friction than comparable air injection data. For a value of $\frac{2F}{c_{f_0}}$ of 2·0, the relative reduction in skin friction with air injection is about 1·5 times that with carbon dioxide injection. Similar effects are apparent at the higher Mach numbers, although since the skin friction reduction is less at higher Mach numbers, the difference between injection of the two gases is not so marked. The effect is most obvious in the compressible results when comparing the two sets of data, at $M=2{\cdot}5$.

3.7. Determination of the shear stress profiles.

The shear stress can be obtained by integrating the equations of motion and by using two or more profiles in the development to determine the x-derivatives in the equations. In the present results, the method is especially sensitive to errors in the velocity profiles in the wall region, where the scatter in the velocity at a given value of y is relatively large. Also, as discussed in Section 3.4 the downstream velocity profiles are perturbed from the flat plate profiles by the presence of pressure gradients. This would cause large inaccuracies in the shear stress profiles determined by the above method.

It was therefore decided that better profiles would be obtained by making use of Squire's result (Ref. 12) that the velocity profiles at the front of the measuring region are, within experimental error, similar and can be expressed in the form $\frac{u}{U_1}=f\left(\frac{y}{\theta}\right)$. Using this assumption, the local development can be defined by specifying the boundary layer profiles at one station (which give the relevant value of θ) and $\frac{d\theta}{dx}$. The shear stress is then found as described by Squire (Ref. 12). The profiles which were used for this calculation were those obtained at the front station under each set of conditions. The value of $\frac{d\theta}{dx}$ was that given by $\frac{d\theta}{dx}=F+\frac{c_f}{2}$ and pressure gradients were neglected.

The shear stress distributions for injected boundary layers obtained from this calculation method are shown in Figs. 23 to 26, together with the distributions for zero injection determined by Squire (1968).

It can be seen that injection radically alters the shear stress profile in a manner similar to an adverse pressure gradient. For zero injection the greatest shear stress occurs at the wall but with injection there is a maximum in the shear stress distribution. While the wall shear stress falls with increasing injection rate, the maximum shear stress in the boundary layer increases and its position moves away from the

surface so that for the highest injection rates at $M=2{\cdot}5$, $3{\cdot}5$ the maximum occurs at a value of $\frac{y}{\delta}$ greater than 0·4. The shear stress rises very rapidly near the wall and its value at the maximum is many times greater than that at the wall. In the most extreme case measured here, $F=2{\cdot}4\times10^{-3}$ at $M=3{\cdot}5$, the ratio of maximum to wall shear stress is about 12:1.

It is apparent that the effect of injection is greater at the higher Mach numbers and therefore at the higher values of $\frac{2F}{c_{f_0}}$ and $\frac{2F}{c_f}$. This can be seen from a qualitative comparison of the profiles at $M=0{\cdot}55$ and $M=3{\cdot}5$. This can be shown in a more quantitative form in Fig. 27 where $\frac{\tau_{\max}}{\tau_{0_{\max}}}$ is plotted against F and it can be seen that the value of the ordinate for a given injection rate increases with increasing Mach number. It is also interesting to note that if the results of Fig. 27 are plotted against $2F/c_{f_0}$ then they fall close to a single line (Fig. 28). Finally it should be noted that the overall effects of air and carbon dioxide injection on shear stress profiles are almost identical (see Fig. 25, for example). However, there are significant differences in the derived values of the eddy viscosity. These effects are discussed elsewhere in Ref. 7.

4. The Boundary Layer Profiles in the Inner and Outer Regions.

4.1. Law of the wall.

A number of authors have developed laws of the wall for boundary layers with air injection: here we consider the extension of these results to layers with foreign gas injection. As in previous work this extension will be based on a Couette flow analysis and on Prandtl's mixing length assumptions.

$$\frac{\partial}{\partial x}(\rho u)+\frac{\partial}{\partial y}(\rho v)=0 \tag{1}$$

$$\rho u\frac{\partial u}{\partial x}+\rho v\frac{\partial u}{\partial y}=\frac{\partial \tau}{\partial y}. \tag{2}$$

With the Couette flow assumption eqn. (1) reduces to:

$$\frac{\partial}{\partial y}(\rho v)=0, \quad \text{or } \rho v=\rho_w v_w, \tag{3}$$

while eqn. (2) becomes:

$$\rho_w v_w\frac{\partial u}{\partial y}=\frac{\partial \tau}{\partial y}, \quad \text{or } \tau-\tau_w=\rho_w v_w u. \tag{4}$$

Combination of eqn. (4) with the mixing length assumption:

$$\tau=\rho k^2 y^2\left|\frac{\partial u}{\partial y}\right|^2 \tag{5}$$

gives

$$ky\frac{du}{dy}=\frac{(\tau_w+\rho_w v_w u)^{\frac{1}{2}}}{\rho^{\frac{1}{2}}}. \tag{6}$$

This equation may be integrated to give after some re-arrangement:

$$G(u^*) \equiv \int_0^{u^*} \frac{\sqrt{\rho^*}\,du}{\left(F\bar{u} + \frac{c_f}{2}\right)^{\frac{1}{2}}} = \frac{1}{k} \log \frac{u_\tau y}{\nu_w} + B \tag{7}$$

where $u^* = u/U_1$, $\rho^* = \rho/\rho_1$. This equation reduces to the laws derived by other workers when their particular conditions are applied. For example with air injection:

$$\rho^* = T_1/T = (T_1/T_w) \Big/ \left(1 + \frac{T_r - T_w}{T_w} u^* + \frac{(T_1 - T_r)}{T_w} u^{*2}\right) \tag{8}$$

and so (7) reduces to the law of the wall proposed by Squire[14] and Danberg[8]. While for incompressible flow (6) reduces to the law proposed by Stevenson[15].

The function $G(u^*)$ was evaluated for all the boundary layers by numerical integration of the experimental results, and the results are plotted in Figs. 29–32. It can be seen that in all the injected profiles there is a linear region, extended out to about $y/\delta = 0{\cdot}2$. However, as with air injection, the level of the curves, i.e., the constant B tends to fall with increasing injection. Before discussing this variation in more detail it will be helpful to discuss the possible errors in Figs. 29–32. Apart from the errors in the basic profile data which will produce a random scatter in the results there are three quantities which can introduce a systematic error into the profiles. These are the values of skin-friction coefficient, the injection parameter F and the wall conditions. From a consideration of the possible errors in F and wall concentration it seems unlikely that these will produce errors greater than about 2 per cent in the slope of the linear portion or in the parameter B. However, the errors in c_f can produce large systematic errors. This is illustrated in Fig. 33 where results are plotted for one blowing rate and Mach number with $c_f = 0{\cdot}001$ and $c_f = 0{\cdot}001 \pm 0{\cdot}0002$. From this figure it is apparent that the change in slope of the linear portion is negligible, but the level is changed considerably. The same type of effect occurs with all profiles, but since the possible error in c_f is an absolute quantity (about $\pm 0{\cdot}0001$) the possible variation in the position of the curve is greatest at lower values of c_f, i.e., at the highest injection rates.

Danberg and Squire systematised their law of the wall profiles by considering the variation of the constant B in equation (7) with injection rate at a given Mach number. This approach has also been adopted here. It can be seen from Figs. 29 and 32 that all the injected profiles lie below the corresponding solid wall profile. Taking the line drawn through the solid wall results as the datum for each Mach number, the change in B caused by injection is equal to the distance parallel to the G-axis between the straight lines drawn through each profile. This distance is not sensitive to changes in the gradient chosen for the law of the wall, since it is basically the distance between the experimental points measured at a given value of $\log \frac{u_\tau y}{\nu_w}$. The results of this analysis are shown in Fig. 34 where, for each Mach number, the change in the constant B is plotted against F. The variations shown are not very systematic, but there are two features apparent in the figure. The change of the constant B with injection appears to be greater at higher Mach numbers and, at each Mach number, the rate of change of $-\Delta B$ with F decreases with increasing injection and may become negative.

The results shown in Fig. 34 have been replotted in Fig. 35 using separate origins for each Mach number for the sake of clarity. On each point is superimposed the possible range of values corresponding to possible variations of $\pm 0{\cdot}0001$ in skin friction. The possible inaccuracy increases with decreasing skin friction and, therefore, with increasing Mach number and injection rate and for the highest injection rate at $M = 3{\cdot}5$ the uncertainty in ΔB is very large. Thus the curves shown in Fig. 34 cannot be considered as very accurate, and they give only an indication of the type of behaviour to be expected. However, even with the allowance made for errors in skin friction, the two features noted in the previous paragraph are still apparent. But the phenomenon that at higher injection rates the value of B rises again (a feature that

can be seen in Fig. 34) is not certain since in Fig. 35 curves can be drawn through the spread points along which B decreases continuously with increasing F.

The variation of ΔB with F found in Refs. 8, 10 and 14 for air injection are compared with the results of this investigation in Fig. 36. Since McQuaid[10] found that the injection law of the wall was universal at low Mach numbers, his results form the line $\Delta B=0$. The curves for air injection are nearly linear, in contrast to those for carbon dioxide injection. However, the value of B is dependent on conditions in the sublayer, one parameter of which is the surface carbon dioxide concentration. This increases rapidly with F at low injection rates. Thus it might be expected that the rate of change of B with F for carbon dioxide injection would be greatest at the origin. From Fig. 36 it appears that the value of B for carbon dioxide injection is lower than for the corresponding air injection except, possibly, at high injection rates. Evidence of this may be doubtful at the higher Mach numbers, where the possible errors are relatively large, but from a comparison of the carbon dioxide results at $M=0{\cdot}55$ and McQuaid's incompressible data, this observation is valid at low Mach numbers.

4.2. The outer part of the boundary layer.

Analysis of the velocity profile in the outer part of the turbulent boundary layer in zero pressure gradient has, in general, been approached in two ways. The first is to apply a correction to the law of the wall which is negligible in the inner region. An example of this method is the intermittency hypothesis of Sarnecki[16]. The second approach (first proposed by Darcy[17]) is to consider the velocity defect as a function of $\frac{y}{\delta}$. This approach has been found useful in the consideration of incompressible flat plate boundary layers without injection. Stevenson[18] and McQuaid[19] found that the velocity defect concept could be used to give good correlation of their experimental data for incompressible boundary layers with air injection. Squire[12] extended McQuaid's approach to give good agreement with his supersonic boundary layer experiments with air injection. It was therefore interesting to discover whether McQuaid's velocity defect law could be extended to cover the present results for carbon dioxide injection.

The velocity defect law for incompressible turbulent boundary layers on a solid flat plate in its usual form:

$$\frac{U_1-u}{u_\tau}=f\left(\frac{y}{\delta}\right) \tag{9}$$

has been verified by many experimenters. Mellor and Gibson[20] found that for large adverse pressure gradients where u_τ becomes small, a more useful velocity scale is u_p, where

$$u_p^2=\frac{\delta^*}{\rho}\frac{dp}{dx}. \tag{10}$$

McQuaid[19] found that a single velocity scale could be used in both the above cases. This scale was:

$$U_*=U_1\left(\frac{d\theta}{dx}\right)^{\frac{1}{2}} \tag{11}$$

since for zero pressure gradient with no injection this becomes $U_*=u_\tau$, while for $u_\tau=0$ the velocity scale becomes a simple multiple u_p. McQuaid analysed his air injection profiles using the velocity defect law based on U_*, and found that his results were in close agreement with the solid wall zero pressure gradient curves.

Squire[12] extended McQuaid's approach to compressible boundary layers with air injection by showing that, in order to make the skin friction contribution in the velocity scale equal to u_τ, U_* must be defined as:

$$U'_* = U_1\left(\frac{T_w}{T_1}\frac{d\theta}{dx}\right)^{\frac{1}{2}}. \tag{12}$$

Basing the velocity defect law on U'_*, Squire found that his experimental results agreed well with the incompressible curve of McQuaid, although some divergence from universality was noted in the results of other workers for Mach numbers greater than about 5.

The most obvious method for incorporating the effect of foreign gas injection into the velocity defect law would be to stipulate that the skin friction part of the velocity scale should remain as u_τ. This necessitates defining the velocity scale as

$$U''_* = U_1\left(\frac{\rho_1}{\rho_w}\frac{d\theta}{dx}\right)^{\frac{1}{2}} \tag{13}$$

where $\frac{\rho_1}{\rho_w}$ is a function of surface carbon dioxide concentration as well as $\frac{T_w}{T_1}$.

However, from consideration of the experimental results it was found that correlation was worse when using U''_*, than for U'_*.

Boundary layer profiles for all the experimental conditions were analysed in velocity defect form using the scale defined by eqn. (12) so that the law takes the form:

$$\frac{1-u^*}{\left(\frac{T_w}{T_1}\frac{d\theta}{dx}\right)^{\frac{1}{2}}} = f\left(\frac{y}{\delta}\right). \tag{14}$$

The local value of $\frac{d\theta}{dx}$ was found from the zero pressure gradient momentum integral equation:

$$\frac{d\theta}{dx} = F + \frac{c_f}{2}$$

and $\frac{T_w}{T_1}$ was taken from the experimental measurements.

All the results analysed in this way are shown on a single graph in Fig. 37 with the measurement conditions unspecified to minimise confusion. It can be seen that the results lie in a narrow band with a scatter no worse than that normally associated with the incompressible velocity defect law. A representative curve has been drawn through the band and in Figs. 38 to 41 the results for each Mach number have been plotted, together with the representative curve. It appears that there is no systematic deviation from this curve although there is, perhaps, a small tendency for profiles with a higher injection rate to show a greater velocity defect than profiles at the same Mach number and lower injection rate.

For most profiles, agreement with the curve is good down to a value of $\frac{y}{\delta}$ of 0·2, below which the collapse of the profiles at a single Mach number deteriorates, except at $M = 3{\cdot}5$, where good collapse is found down to $\frac{y}{\delta} = 0{\cdot}1$. At $M = 0{\cdot}55$ noticeable deviation from the curve occurs below $\frac{y}{\delta} = 0{\cdot}3$, although even at $\frac{y}{\delta} = 0{\cdot}2$ the difference is not great, and since the velocity defects, $(1-u^*)$, are smaller than at the higher Mach numbers, the error in the value of u^* deduced from the curve would be small.

5. Conclusions.

Measurements have been made of the development of compressible turbulent boundary layers with carbon dioxide injection. The technique of concentration measurement, using a discrete sampling method with a diffusion-type katharometer as gas analyser, is simple and accurate, but is very laborious. The same method can be used to find concentrations in layers with the injection of any other foreign gas, provided the molecular weight of the injected gas is sensibly different from that of air. The surface concentration could not be measured directly since it appears that any interruption in the uniform injection caused a very rapid change in the flow properties near the surface.

The basic results are presented in tabular form, and these results are used to derive shear stress distributions through the layers. The results have also been used to derive a law of the wall and a velocity defect law. In general the overall effects of carbon dioxide injection are similar to those with air injection.

LIST OF SYMBOLS

c_v, c_p	Specific heats of gas
c_f	Skin-friction coefficient
F	Injection parameter $(\rho_w v_w/\rho_1 U_1)$
H	Boundary layer shape parameter (δ^*/θ)
k	Molecular coefficient of thermal conductivity
M	Mach number
M	Molecular weight of gas
p	Pressure; static unless otherwise qualified
Pr, Pr_t	Molecular and turbulent Prandtl numbers
R	Specific gas constant
u, U	Velocity in the x-direction
u_τ	Friction velocity $(\tau_w/\rho_w)^{\frac{1}{2}}$
u_p, U_*, U'_*, U''_*	Velocity defect scales
v	Velocity in the y-direction
x	Distance parallel to the surface in the stream direction
y	Distance normal to the surface
γ	Ratio of specific heats
δ	Boundary layer thickness $(u/U_1 = 0{\cdot}995)$
δ^*	Displacement thickness
θ	Momentum thickness
ρ	Density
τ	Shear stress
ω, MF	Mass fraction of injected gas

Subscripts

a	Main stream gas (air)
c	Injected gas (carbon dioxide)
r	Recovery or adiabatic condition
st	Stagnation conditions
w	Wall conditions
0	Zero-injection conditions
1	Conditions at edge of boundary layer.

REFERENCES

No.	Author(s)	Title, etc.
1	B. M. Leadon and C. J. Scott	Transpiration cooling experiments in a turbulent boundary layer at $M=3$. J. Aero. Sci. Vol. 23, p. 798. (1956).
2a	C. C. Pappas and A. F. Okuno	Measurements of skin friction of the compressible turbulent boundary layer on a cone with foreign gas injection. J. Aero/Space Sci. Vol. 27. p. 231. (1960).
2b	C. C. Pappas and A. F. Okuno	Measurements of heat transfer and recovery factor of a compressible turbulent boundary layer on a sharp cone with foreign gas injection. NASA TN D–2230 (1964).
3	P. N. Romanenko and V. N. Kharchenko	The effect of transverse mass flow on heat transfer and friction drag in a turbulent flow of compressible gas along an arbitrarily shaped surface. Int. J. Heat and Mass Transfer, Vol. 6, p. 727. (1963).
4	D. I. A. Dunbar and L. C. Squire	Correlations of concentration temperature and velocity profiles in compressible boundary layers with foreign gas injection. Int. J. Heat and Mass Transfer, Vol. 14, p. 27. (1971).
5	C. J. Scott, G. E. Anderson and D. R. Elgin	Laminar, transitional and turbulent mass transfer cooling experiments at Mach numbers from 3 to 5. University of Minnesota, Institute of Technology, Res. Rpt. No. 162. AFOSR TN 59–1305. (1959).
6	L. O. F. Jeromin	An experimental investigation of the compressible turbulent boundary layer with air injection. A.R.C. R. & M. 3526. (1966).
7	L. C. Squire	Eddy viscosity distribution in compressible turbulent boundary layers with injection. Aero. Quart. Vol. XXIII, p. 169. (1971).
8	J. E. Danberg, E. M. Winkler and P. K. Chang	Heat and mass transfer in a hypersonic turbulent boundary layer. Proceedings of Heat Transfer and Fluid Mechanics Institute. (1965).
9	F. A. MacMillan	Experiments on pitot tubes in shear flow. A.R.C. R. & M. 3028. (1956).
10	J. McQuaid	Incompressible turbulent boundary layers with distributed injection. Ph.D. Dissertation, University of Cambridge. (1966).
11	O. E. Tewfik	Some characteristics of the turbulent boundary layer with air injection. AIAA Journal, Vol. 1, p. 1306. (1963).

12 L. C. Squire .. .. .. Further experimental investigations of compressible turbulent boundary layers with air injection.
A.R.C. R. & M. 3627. (1968).

13a E. R. Bartle and B. M. Leadon Experimental evaluation of heat transfer with transpiration cooling in a turbulent boundary layer at $M = 3{\cdot}2$.
J. Aero/Space Sci. Vol. 27, p. 78. (1960).

13b E. R. Bartle and B. M. Leadon The compressible turbulent boundary layer on a flat plate with transpiration cooling.
Convair Scientific Research Laboratory, Res. Rep. 11. (1960).

14 L. C. Squire .. .. .. A law of the wall for compressible turbulent boundary layers with air injection.
J. Fluid Mech. Vol. 37, p. 449. (1969).

15 T. N. Stevenson .. .. A law of the wall for turbulent boundary layers with suction or injection.
A.R.C. 26 025. (1963).

16 A. J. Sarnecki .. .. .. The turbulent boundary layer on a permeable surface.
Ph.D. dissertation, University of Cambridge. (1959).

17 H. Darcy .. .. .. Recherches experementales relative aux mouvements de l'eau dans tuyaux.
Mem. pres. a l'Academie des Sciences de l'Institut de France, Vol. 15, p. 141. (1858).

18 T. N. Stevenson .. .. A modified velocity defect law for turbulent boundary layers with injection.
A.R.C. 25 797. (1963).

19 J. McQuaid .. .. .. A velocity defect relationship for the outer part of equilibrium and near-equilibrium turbulent boundary layers.
A.R.C. C.P. 885. (1965).

20 G. L. Mellor and D. M. Gibson Equilibrium turbulent boundary layers.
J. Fluid Mech. Vol. 24, p. 225. (1966).

21 J. L. Sims .. .. .. Tables for supersonic flow around right circular cones at zero angle of attack.
NASA SP–3004. (1964).

22 C. R. Wilke .. .. .. A viscosity equation for gas mixtures.
J. Chem. Phys. Vol. 18, p. 517. (1950).

23 E. A. Mason and S. C. Saxena An approximate formula for the thermal conductivity of gas mixtures.
Phys. of Fluids, Vol. 1, p. 361. (1958).

24 W. T. Strike and B. B. Norton — Flow properties of an unyawed 10-deg cone for $\gamma = 1{\cdot}28$ to $1{\cdot}40$ at Mach numbers of 1·5 to 8.
AEDC–TN–60–178. (1960).

25 M. W. Rubesin and C. C. Pappas — An analysis of the turbulent boundary layer characteristics on a flat plate with distributed light gas injection.
NACA TN 4149. (1958).

APPENDIX I

The Formulae for the Reduction of the Experimental Data.

The purpose of this appendix is to explain in detail the formulae which were used to process the basic experimental data in order to give the required flow properties as described in Section 3.1. Throughout this appendix the quantities measured by the pitot and temperature probes will be denoted by p^* and T^* respectively, and perfect gas assumptions will be made. The subscript, *st*, denotes stagnation conditions.

The relation between the local static and stagnation pressures is given by:

$$\frac{p_{st}}{p}=\left(1+\frac{\gamma-1}{2}\mathrm{M}^2\right)^{\frac{\gamma}{\gamma-1}}. \tag{I.1}$$

In subsonic flows, the pressure measured by a pitot tube is the local stagnation pressure, so that $p^*=p_{st}$. However, in supersonic flows it is assumed that the pitot pressure is equal to the stagnation pressure behind a normal shock in the local flow conditions. Using the normal shock relations, the relationship between the pitot pressure and the local static pressure in the undisturbed flow is given by:

$$\frac{p^*}{p}=\left[\frac{(\gamma+1)\left[(\gamma+1)\mathrm{M}^2/2\right]^{\gamma}}{2(\gamma\mathrm{M}^2+1)-(\gamma+1)}\right]^{\frac{1}{\gamma-1}} \tag{I.2}$$

Equation (I.1) and (I.2) can be combined to give the relation between the local pitot and stagnation pressures:

$$\frac{p^*}{p_{st}}=\left[\frac{(\gamma+1)\left[(\gamma+1)\mathrm{M}^2/2\right]^{\gamma}}{\left[2(\gamma\mathrm{M}^2+1)-(\gamma+1)\right]\left[1+(\gamma-1)\mathrm{M}^2/2\right]^{\gamma}}\right]^{\frac{1}{\gamma-1}}. \tag{I.3}$$

From equation (I.1) or (I.2) it can be seen that the condition that the local flow is supersonic is given by:

$$\frac{p^*}{p}>\left(\frac{\gamma+1}{2}\right)^{\frac{\gamma}{\gamma-1}}. \tag{I.4}$$

At the outside of the boundary layer (I.3) can be used to find the local free stream Mach number and (I.2) then gives the static pressure. If this is constant through the layer (I.2) can then be used to find the local Mach number.

It should be remembered that in boundary layers with foreign gas injection the value of γ which is used is a function of the local gas composition (*see* Appendix II).

It is now necessary to find the relation between the temperature measured by the probe and the local static temperature. It is assumed that the flow is conical in the region of the cone surface (conditions at the surface in the absence of viscous effects being denoted by the subscript *s*) and that the stagnation temperature is constant in this region and equal to that in front of the probe tip. It is also assumed that heat transfer effects are sufficiently small that the probe temperature is equal to the adiabatic surface temperature.

Now the relationship between the local undisturbed static and stagnation temperatures is given by:

$$T_{st}=T\left(1+\frac{\gamma-1}{2}\mathrm{M}^2\right) \tag{I.5}$$

and that between the stagnation temperature and the static temperature in the region near the cone surface is given by:

$$T_{st} = T_s\left(1 + \frac{\gamma - 1}{2} M_s^2\right). \tag{I.6}$$

The adiabatic surface temperature, T^*, is given by:

$$T^* = T_s + r \left(T_{st} - T_s\right) \tag{I.7}$$

where r is the recovery factor which, making the assumption that the cone boundary layer is laminar, is equal to $\sqrt{Pr}$. Combination of equation (I.6) and (I.7) gives:

$$T^* = T_s\left(1 + r\left(\frac{\gamma - 1}{2}\right)M_s^2\right) = T_{st} \left(\frac{1 + r\left(\frac{\gamma - 1}{2}\right)M_s^2}{1 + \left(\frac{\gamma - 1}{2}\right)M_s^2}\right) \tag{I.8}$$

and combining equations (I.8) and (I.5), the relationship between the probe temperature and the local undisturbed static temperature is given by:

$$T = T^* \left[\frac{1 + \left(\frac{\gamma - 1}{2}\right)M_s^2}{\left(1 + r\left(\frac{\gamma - 1}{2}\right)M_s^2\right)\left(1 + \left(\frac{\gamma - 1}{2}\right)M^2\right)}\right] \tag{I.9}$$

It only remains to define the relationship between M_s and M. It has been shown by Strike and Norton[24] that, for values of γ in the range 1·33 to 1·40 and Mach numbers up to 3·5, this relation is independent of γ to the accuracy required by the present programme. Therefore, the relation which is used here is that computed by Sims[21] for a 5 degree semi-angle cone in air. It was found that these results could be given to the required accuracy by the relation

$$M_s = 0{\cdot}984M - 0{\cdot}0065M^2. \tag{I.10}$$

The calculation procedure for a supersonic boundary layer is summarised as follows:

(i) Knowing the free-stream stagnation and pitot pressures, equation (I.3) is used to find the free stream Mach number.

(ii) Equation (I.1) is used to find the static pressure which is assumed to be constant throughout the boundary layer.

Then considering a point in the boundary layer:

(iii) The relation (I.4) is used to find whether the local flow is supersonic or subsonic.

(iv) Knowing the local pitot and static pressures and γ, either equation (I.1) (subsonic) or equation (I.2) (supersonic) is used to find the local Mach number.

(v) Introducing the local Prandtl number and probe temperature, equations (I.10) and (I.9) are used to find the local static temperature.

(vi) Introducing the local value of R, the local velocity can be found from the relation:

$$u = M\sqrt{\gamma RT}. \tag{I.11}$$

For a boundary layer which is entirely subsonic, the only difference in the calculation procedure is caused by the fact that the static pressure can be found directly. Therefore, in this case, the calculation starts at (iv).

APPENDIX II

The Properties of Gas Mixtures.

The purpose of this appendix is to define methods for calculating the properties of gas mixtures which are required for the analyses presented in this dissertation. Throughout the present work it is assumed that the gas mixtures behave as perfect gases under the conditions of the investigation and that the properties evaluated at about 275°K can be considered as representative.

The calibration of the katharometer is in % carbon dioxide by volume, n, and for further calculations it is useful to express the concentration as the mass fraction ω. These two quantities are connected by the relation:

$$\omega=\frac{nM_c}{nM_c+(100-n)M_a}. \tag{II.1}*$$

The specific heats at constant volume and pressure c_v and c_p, and the gas constant per unit mass, R, are given by:

$$c_v=(1-\omega)c_{v_a}+\omega c_{v_c} \tag{II.2}*$$

$$c_p=(1-\omega)c_{p_a}+\omega c_{p_c} \tag{II.3}*$$

$$R=(1-\omega)R_a+\omega R_c \tag{II.4}*$$

and the ratio of the specific heats, γ, is found from the division of eqn. (II.3) by eqn. (II.2)

$$\gamma=\frac{(1-\omega)c_{p_a}+\omega c_{p_c}}{(1-\omega)c_{v_a}+\omega c_{v_c}}. \tag{II.5}*$$

The density of the mixture can be found from the perfect gas state equation:

$$\rho=\frac{p}{RT} \tag{II.6}$$

where the value of R is found from equation (II.4).

The mixture viscosity can be determined using the method of Wilke[22]. This is an approximate method which has been shown to give good agreement with experimental data. For these calculations the gases were considered as three-component mixtures of nitrogen, oxygen and carbon dioxide. For three-component mixtures the formula of Wilke becomes:

---

* M is the molecular weight; suffix a corresponds to air and suffix c to carbon dioxide.

$$\mu = \sum_{i=1}^{3} \frac{\omega_i \mu_i}{\sum_{j=1}^{3} \omega_j \Phi_{ij}}$$

where

$$\Phi_{ij} = \frac{1}{\sqrt{8}}\left(1+\frac{M_i}{M_j}\right)^{-\frac{1}{2}} \left[1+\left(\frac{\mu_i}{\mu_j}\right)^{\frac{1}{2}}\left(\frac{M_j}{M_i}\right)^{\frac{1}{4}}\right]^2 \tag{II.8}$$

and the subscripts 1, 2 and 3 refer to the three components of the mixture.

The variation of viscosity with carbon dioxide concentration which was calculated from equation (B.7) is shown in Fig. 42. It was found that to sufficient accuracy, this variation could be expressed as:

$$\mu = (17{\cdot}10 - 4{\cdot}65\omega + 1{\cdot}20\omega^2) \times 10^{-6} \text{ kg/ms}. \tag{II.9}$$

It is also necessary to consider the variation of the mixture viscosity with temperature. This is usually well defined by Sutherland's formula:

$$\mu = \mu_{273}\left(\frac{T}{273}\right)^{\frac{3}{2}}\left(\frac{D+273}{D+T}\right) \tag{II.10}$$

where μ_{273} is the viscosity at 273°K and D is a constant for a particular gas mixture. Although the values of D have been found for pure air and carbon dioxide separately, no information is available on its value for mixtures of these gases. However, because the temperatures at which knowledge of the viscosity itself is required are close to 290°K, equation (II.10) acts as a correction and so it is thought to be sufficiently accurate to assume a linear variation of D with concentration. Therefore, D was assumed to be given by:

$$D = 114 + 220\omega \text{°K}. \tag{II.11}$$

The thermal conductivity of the mixtures can be found using the method of Mason and Saxena[23] which is analagous to the method of Wilke[22] for viscosity. The thermal conductivity is given as:

$$k = \sum_{i=1}^{3} \frac{\omega_i k_i}{\sum_{j=1}^{3} \omega_j \Phi_{ij}} \tag{II.12}$$

where Φ_{ij} is given by equation (II.8).

The laminar Prandtl number can now be found from its definition:

$$Pr = \frac{\mu c_p}{k} \tag{II.13}$$

since all its constituent properties have been defined. The variation with concentration of the Prandtl number of carbon dioxide-air mixtures at 273°K is shown in Fig. 43. It was found that this variation could be closely approximated by the linear relation:

$$Pr = 0{\cdot}720 + 0{\cdot}064\omega. \tag{II.14}$$

TABLE I

	0.55-F-1.2				0.55-C-1.2				0.55-R-1.2			
Y (ins)	M	U/U1	T/T1	MF	M	U/U1	T/T1	MF	M	U/U1	T/T1	MF
0.0032	0.191	0.343	1.052	0.229	0.191	0.339	1.046	0.226	0.196	0.350	1.058	0.229
0.0052	0.212	0.383	1.051	0.211	0.221	0.394	1.045	0.211	0.216	0.387	1.057	0.212
0.0072	0.230	0.417	1.051	0.197	0.248	0.443	1.043	0.199	0.228	0.411	1.057	0.200
0.0092	0.247	0.448	1.050	0.187	0.269	0.485	1.042	0.190	0.241	0.435	1.056	0.191
0.0112	0.257	0.466	1.050	0.178	0.279	0.485	1.042	0.181	0.254	0.458	1.055	0.183
0.0132	0.265	0.482	1.050	0.171	0.276	0.495	1.042	0.174	0.266	0.480	1.055	0.177
0.0182	0.283	0.518	1.050	0.154	0.292	0.526	1.041	0.162	0.286	0.518	1.053	0.166
0.0232	0.297	0.544	1.049	0.140	0.300	0.541	1.041	0.152	0.298	0.539	1.052	0.157
0.0282	0.308	0.564	1.048	0.131	0.309	0.558	1.041	0.144	0.307	0.557	1.052	0.149
0.0332	0.317	0.583	1.047	0.123	0.317	0.573	1.040	0.137	0.314	0.570	1.051	0.142
0.0382	0.326	0.598	1.046	0.116	0.323	0.584	1.039	0.131	0.320	0.582	1.050	0.136
0.0432	0.332	0.610	1.045	0.109	0.328	0.594	1.039	0.125	0.328	0.596	1.049	0.131
0.0482	0.338	0.622	1.044	0.104	0.335	0.606	1.038	0.120	0.333	0.606	1.048	0.127
0.0532	0.343	0.632	1.043	0.099	0.340	0.616	1.037	0.115	0.338	0.615	1.047	0.123
0.0632	0.355	0.654	1.041	0.091	0.349	0.635	1.036	0.107	0.347	0.633	1.046	0.115
0.0732	0.366	0.675	1.040	0.082	0.359	0.652	1.035	0.099	0.357	0.651	1.045	0.108
0.0832	0.375	0.693	1.038	0.073	0.368	0.669	1.034	0.092	0.364	0.665	1.044	0.102
0.0932	0.383	0.709	1.037	0.066	0.376	0.685	1.032	0.086	0.372	0.680	1.043	0.096
0.1032	0.392	0.725	1.036	0.060	0.384	0.700	1.031	0.079	0.379	0.693	1.042	0.090
0.1132	0.400	0.741	1.035	0.054	0.392	0.714	1.030	0.073	0.387	0.708	1.040	0.084
0.1232	0.409	0.757	1.033	0.048	0.400	0.730	1.029	0.067	0.394	0.721	1.039	0.079
0.1332	0.417	0.773	1.032	0.043	0.407	0.743	1.028	0.062	0.401	0.735	1.038	0.074
0.1432	0.425	0.787	1.031	0.038	0.413	0.755	1.027	0.056	0.408	0.747	1.036	0.069
0.1532	0.433	0.802	1.029	0.034	0.420	0.769	1.026	0.052	0.415	0.760	1.035	0.065
0.1732	0.448	0.831	1.027	0.026	0.435	0.795	1.024	0.044	0.428	0.784	1.033	0.056
0.1932	0.463	0.858	1.023	0.020	0.448	0.820	1.021	0.037	0.440	0.807	1.031	0.049
0.2132	0.476	0.882	1.021	0.015	0.461	0.844	1.019	0.030	0.451	0.827	1.029	0.042
0.2332	0.489	0.905	1.018	0.010	0.475	0.869	1.017	0.024	0.462	0.848	1.026	0.036
0.2532	0.500	0.927	1.016	0.007	0.487	0.892	1.016	0.019	0.473	0.868	1.024	0.030
0.2732	0.511	0.945	1.014	0.004	0.498	0.912	1.014	0.014	0.484	0.888	1.022	0.025
0.2932	0.520	0.962	1.012	0.003	0.509	0.931	1.012	0.010	0.494	0.906	1.020	0.020
0.3132	0.528	0.976	1.010	0.001	0.517	0.947	1.011	0.007	0.503	0.923	1.018	0.016
0.3332	0.534	0.987	1.008	0.001	0.526	0.962	1.009	0.005	0.512	0.940	1.016	0.013
0.3532	0.538	0.993	1.006	0.000	0.533	0.974	1.007	0.003	0.521	0.955	1.015	0.009
0.3732	0.540	0.996	1.004	0.000	0.538	0.983	1.006	0.001	0.528	0.969	1.012	0.007
0.3932	0.542	0.999	1.002	0.000	0.541	0.989	1.005	0.001	0.535	0.979	1.010	0.004
0.4132	0.543	0.999	1.001	0.000	0.544	0.994	1.004	0.000	0.539	0.987	1.008	0.003
0.4332	0.543	1.000	1.000	0.000	0.546	0.997	1.003	0.000	0.543	0.993	1.005	0.001
0.4532					0.547	0.999	1.002	0.000	0.545	0.996	1.003	0.001
0.4732					0.548	0.999	1.001	0.000	0.546	0.998	1.002	0.000
0.4932					0.548	1.000	1.000	0.000	0.547	0.999	1.001	0.000
0.5132									0.548	1.000	1.000	0.000

TABLE 2

	0.55-F-2.4				0.55-C-2.4				0.55-R-2.4			
Y(ins)	M	U/U1	T/T1	MF	M	U/U1	T/T1	MF	M	U/U1	T/T1	MF
0.0032	0.166	0.284	1.041	0.412	0.167	0.284	1.035	0.399	0.173	0.292	1.034	0.413
0.0052	0.182	0.314	1.042	0.379	0.193	0.332	1.036	0.372	0.192	0.328	1.034	0.375
0.0072	0.197	0.342	1.043	0.357	0.212	0.366	1.037	0.353	0.208	0.357	1.035	0.353
0.0092	0.211	0.368	1.045	0.335	0.226	0.392	1.037	0.338	0.222	0.383	1.036	0.341
0.0112	0.225	0.394	1.045	0.320	0.239	0.414	1.037	0.323	0.235	0.406	1.036	0.325
0.0132	0.238	0.419	1.045	0.308	0.249	0.433	1.037	0.314	0.243	0.421	1.037	0.315
0.0152	0.256	0.452	1.046	0.284	0.267	0.467	1.038	0.291	0.262	0.457	1.037	0.296
0.0232	0.270	0.479	1.046	0.264	0.278	0.489	1.038	0.275	0.276	0.483	1.038	0.281
0.0282	0.282	0.502	1.046	0.249	0.288	0.507	1.038	0.259	0.287	0.503	1.038	0.268
0.0332	0.292	0.522	1.045	0.235	0.295	0.522	1.038	0.248	0.297	0.521	1.038	0.258
0.0382	0.299	0.536	1.045	0.225	0.301	0.534	1.038	0.238	0.304	0.534	1.037	0.249
0.0432	0.308	0.553	1.044	0.216	0.309	0.549	1.038	0.230	0.310	0.546	1.037	0.242
0.0482	0.315	0.566	1.044	0.207	0.315	0.560	1.037	0.222	0.316	0.557	1.036	0.235
0.0532	0.322	0.579	1.043	0.198	0.320	0.569	1.036	0.215	0.322	0.569	1.035	0.229
0.0632	0.332	0.593	1.042	0.183	0.330	0.589	1.036	0.203	0.330	0.583	1.034	0.216
0.0732	0.344	0.622	1.041	0.170	0.339	0.606	1.035	0.191	0.338	0.599	1.034	0.205
0.0832	0.353	0.640	1.040	0.156	0.347	0.621	1.035	0.180	0.346	0.614	1.033	0.195
0.0932	0.362	0.653	1.039	0.142	0.356	0.639	1.034	0.168	0.353	0.629	1.033	0.184
0.1032	0.372	0.677	1.038	0.130	0.365	0.655	1.032	0.159	0.361	0.644	1.032	0.175
0.1132	0.380	0.694	1.037	0.120	0.373	0.670	1.031	0.149	0.367	0.656	1.032	0.167
0.1232	0.389	0.710	1.036	0.110	0.381	0.686	1.030	0.140	0.375	0.670	1.031	0.159
0.1332	0.397	0.726	1.035	0.101	0.387	0.699	1.030	0.130	0.382	0.684	1.030	0.151
0.1432	0.405	0.743	1.034	0.092	0.395	0.714	1.029	0.122	0.388	0.696	1.029	0.142
0.1532	0.413	0.758	1.033	0.084	0.402	0.727	1.028	0.113	0.394	0.707	1.028	0.136
0.1732	0.430	0.790	1.030	0.068	0.416	0.755	1.026	0.099	0.406	0.731	1.027	0.122
0.1932	0.446	0.820	1.027	0.054	0.429	0.781	1.025	0.085	0.418	0.754	1.025	0.108
0.2132	0.460	0.848	1.024	0.042	0.443	0.807	1.023	0.072	0.430	0.776	1.023	0.096
0.2332	0.475	0.877	1.022	0.032	0.456	0.831	1.021	0.061	0.441	0.798	1.022	0.085
0.2532	0.488	0.901	1.020	0.023	0.469	0.856	1.019	0.051	0.452	0.819	1.021	0.075
0.2732	0.501	0.925	1.017	0.016	0.481	0.880	1.017	0.041	0.463	0.841	1.019	0.064
0.2932	0.512	0.945	1.014	0.012	0.494	0.902	1.015	0.033	0.475	0.862	1.018	0.055
0.3132	0.522	0.963	1.012	0.008	0.505	0.923	1.012	0.025	0.485	0.881	1.016	0.047
0.3332	0.530	0.978	1.010	0.004	0.515	0.941	1.010	0.018	0.496	0.902	1.015	0.039
0.3532	0.536	0.988	1.008	0.002	0.523	0.957	1.007	0.013	0.505	0.920	1.013	0.031
0.3732	0.540	0.995	1.006	0.001	0.531	0.971	1.005	0.009	0.514	0.938	1.012	0.024
0.3932	0.542	0.998	1.004	0.000	0.537	0.982	1.004	0.006	0.523	0.953	1.010	0.018
0.4132	0.544	0.999	1.001	0.000	0.541	0.990	1.003	0.003	0.529	0.965	1.008	0.014
0.4332	0.544	1.000	1.000	0.000	0.544	0.995	1.002	0.002	0.535	0.975	1.007	0.010
0.4532					0.546	0.998	1.001	0.001	0.539	0.983	1.005	0.006
0.4732					0.547	0.999	1.000	0.000	0.543	0.991	1.004	0.004
0.4932					0.547	1.000	1.000	0.000	0.545	0.994	1.002	0.002
0.5132									0.547	0.997	1.001	0.000
0.5332									0.548	0.998	1.000	0.000
0.5532									0.549	1.000	1.000	0.000

TABLE 3

Y (ins)	0.55-F-3.6 M	U/U1	T/T1	MF	0.55-C-3.6 M	U/U1	T/T1	MF	0.55-R-3.6 M	U/U1	T/T1	MF
0.0032	0.144	0.237	1.025	0.541	0.147	0.241	1.026	0.528	0.153	0.250	1.026	0.540
0.0052	0.163	0.270	1.027	0.508	0.179	0.296	1.027	0.493	0.175	0.287	1.019	0.509
0.0072	0.179	0.300	1.029	0.479	0.197	0.329	1.029	0.470	0.192	0.319	1.021	0.473
0.0092	0.196	0.330	1.030	0.455	0.212	0.354	1.030	0.452	0.208	0.347	1.022	0.452
0.0112	0.209	0.353	1.031	0.435	0.223	0.376	1.031	0.435	0.223	0.374	1.023	0.434
0.0132	0.222	0.377	1.032	0.419	0.230	0.389	1.033	0.422	0.234	0.393	1.024	0.421
0.0182	0.239	0.410	1.035	0.389	0.247	0.421	1.034	0.397	0.252	0.427	1.027	0.397
0.0232	0.253	0.437	1.037	0.365	0.258	0.442	1.036	0.376	0.263	0.447	1.029	0.379
0.0282	0.264	0.457	1.039	0.346	0.269	0.462	1.037	0.359	0.273	0.467	1.030	0.364
0.0332	0.271	0.471	1.041	0.329	0.278	0.479	1.038	0.346	0.280	0.480	1.030	0.351
0.0382	0.278	0.487	1.042	0.315	0.286	0.494	1.038	0.334	0.287	0.492	1.030	0.341
0.0432	0.286	0.501	1.041	0.304	0.294	0.510	1.038	0.325	0.292	0.502	1.030	0.332
0.0482	0.292	0.513	1.041	0.293	0.299	0.520	1.038	0.315	0.297	0.512	1.030	0.323
0.0532	0.298	0.525	1.041	0.283	0.304	0.530	1.038	0.307	0.302	0.522	1.030	0.315
0.0632	0.309	0.547	1.041	0.263	0.314	0.548	1.038	0.293	0.312	0.541	1.029	0.300
0.0732	0.321	0.569	1.040	0.246	0.324	0.567	1.037	0.278	0.321	0.557	1.029	0.287
0.0832	0.331	0.589	1.040	0.229	0.332	0.583	1.037	0.264	0.328	0.572	1.029	0.275
0.0932	0.339	0.605	1.040	0.213	0.340	0.599	1.036	0.249	0.336	0.587	1.028	0.262
0.1032	0.347	0.622	1.039	0.199	0.348	0.614	1.036	0.235	0.343	0.601	1.028	0.252
0.1132	0.356	0.640	1.039	0.186	0.356	0.629	1.035	0.224	0.349	0.611	1.027	0.240
0.1232	0.366	0.659	1.037	0.172	0.363	0.644	1.034	0.212	0.354	0.623	1.027	0.230
0.1332	0.375	0.676	1.036	0.160	0.370	0.658	1.033	0.202	0.362	0.637	1.026	0.221
0.1432	0.383	0.693	1.035	0.149	0.378	0.672	1.032	0.191	0.368	0.650	1.026	0.211
0.1532	0.392	0.709	1.034	0.138	0.385	0.687	1.032	0.180	0.375	0.662	1.026	0.203
0.1732	0.410	0.746	1.032	0.116	0.399	0.714	1.031	0.160	0.388	0.688	1.025	0.186
0.1932	0.426	0.777	1.030	0.098	0.412	0.741	1.030	0.141	0.400	0.711	1.025	0.170
0.2132	0.441	0.806	1.028	0.081	0.426	0.768	1.029	0.124	0.412	0.735	1.023	0.155
0.2332	0.457	0.837	1.025	0.065	0.439	0.793	1.027	0.108	0.423	0.757	1.022	0.140
0.2532	0.471	0.864	1.023	0.051	0.452	0.819	1.025	0.093	0.435	0.779	1.021	0.126
0.2732	0.485	0.891	1.021	0.039	0.465	0.843	1.023	0.081	0.446	0.801	1.020	0.112
0.2932	0.498	0.916	1.018	0.029	0.478	0.867	1.020	0.068	0.456	0.820	1.019	0.101
0.3132	0.510	0.939	1.015	0.020	0.489	0.889	1.018	0.056	0.467	0.842	1.017	0.089
0.3332	0.521	0.958	1.013	0.014	0.501	0.912	1.015	0.045	0.478	0.864	1.015	0.076
0.3532	0.530	0.974	1.010	0.008	0.512	0.932	1.013	0.035	0.489	0.884	1.014	0.065
0.3732	0.536	0.985	1.008	0.004	0.522	0.951	1.010	0.027	0.498	0.903	1.012	0.055
0.3932	0.540	0.992	1.006	0.002	0.530	0.966	1.008	0.020	0.507	0.920	1.011	0.045
0.4132	0.543	0.997	1.004	0.001	0.536	0.977	1.007	0.014	0.516	0.937	1.009	0.037
0.4332	0.545	0.999	1.002	0.000	0.540	0.985	1.005	0.009	0.524	0.952	1.008	0.030
0.4532	0.545	0.999	1.001	0.000	0.544	0.993	1.003	0.005	0.531	0.965	1.007	0.023
0.4732	0.546	1.000	1.000	0.000	0.547	0.997	1.001	0.003	0.536	0.975	1.006	0.017
0.4932					0.548	0.998	1.000	0.001	0.541	0.984	1.005	0.012
0.5132					0.549	1.000	1.000	0.000	0.544	0.990	1.004	0.008
0.5332									0.547	0.996	1.003	0.004
0.5532									0.548	0.998	1.002	0.002
0.5732									0.549	0.999	1.001	0.000
0.5932									0.549	1.000	1.000	0.000

TABLE 4

	1.8-F-1.3				1.8-C-1.3				1.8-R-1.3			
Y(ins)	M	U/U1	T/T1	MF	M	U/U1	T/T1	MF	M	U/U1	T/T1	MF
0.0032	0.607	0.383	1.520	0.289	0.583	0.374	1.547	0.278	0.534	0.350	1.530	0.273
0.0052	0.667	0.419	1.502	0.273	0.652	0.416	1.525	0.263	0.632	0.412	1.501	0.257
0.0072	0.723	0.453	1.483	0.259	0.697	0.444	1.509	0.252	0.682	0.443	1.484	0.244
0.0092	0.759	0.475	1.471	0.247	0.739	0.470	1.493	0.240	0.722	0.468	1.470	0.234
0.0112	0.801	0.500	1.456	0.234	0.782	0.495	1.477	0.231	0.750	0.485	1.458	0.226
0.0132	0.827	0.516	1.446	0.224	0.805	0.509	1.467	0.224	0.781	0.504	1.446	0.219
0.0182	0.876	0.545	1.427	0.204	0.852	0.554	1.435	0.207	0.834	0.535	1.424	0.204
0.0232	0.924	0.573	1.407	0.187	0.922	0.577	1.417	0.194	0.879	0.561	1.404	0.192
0.0282	0.965	0.596	1.390	0.174	0.959	0.598	1.400	0.183	0.909	0.581	1.397	0.182
0.0332	1.003	0.618	1.374	0.163	0.991	0.616	1.386	0.174	0.942	0.598	1.375	0.174
0.0382	1.038	0.638	1.360	0.153	1.012	0.627	1.376	0.166	0.963	0.610	1.366	0.167
0.0432	1.077	0.659	1.343	0.145	1.040	0.643	1.363	0.157	0.987	0.624	1.356	0.160
0.0482	1.112	0.677	1.329	0.137	1.063	0.656	1.353	0.151	1.007	0.635	1.348	0.155
0.0532	1.142	0.694	1.316	0.129	1.087	0.669	1.343	0.144	1.029	0.648	1.339	0.149
0.0632	1.202	0.725	1.291	0.115	1.133	0.694	1.323	0.133	1.068	0.669	1.323	0.140
0.0732	1.263	0.757	1.266	0.100	1.178	0.718	1.304	0.120	1.107	0.691	1.306	0.130
0.0832	1.328	0.790	1.238	0.086	1.222	0.741	1.285	0.109	1.142	0.710	1.291	0.122
0.0932	1.392	0.821	1.211	0.073	1.261	0.761	1.268	0.099	1.177	0.729	1.276	0.112
0.1032	1.453	0.850	1.195	0.060	1.307	0.785	1.248	0.089	1.214	0.749	1.261	0.103
0.1132	1.511	0.876	1.160	0.049	1.351	0.807	1.229	0.079	1.249	0.768	1.247	0.095
0.1232	1.570	0.902	1.135	0.040	1.403	0.832	1.206	0.071	1.287	0.787	1.231	0.088
0.1332	1.623	0.925	1.111	0.030	1.446	0.852	1.188	0.061	1.321	0.805	1.216	0.079
0.1432	1.675	0.946	1.098	0.022	1.484	0.870	1.172	0.053	1.359	0.823	1.200	0.073
0.1532	1.725	0.965	1.065	0.015	1.526	0.889	1.153	0.045	1.393	0.840	1.185	0.066
0.1632	1.764	0.979	1.046	0.010	1.568	0.907	1.134	0.037	1.426	0.856	1.171	0.059
0.1732	1.795	0.989	1.029	0.006	1.614	0.927	1.113	0.030	1.459	0.871	1.157	0.053
0.1832	1.813	0.994	1.018	0.003	1.654	0.943	1.095	0.025	1.487	0.885	1.145	0.047
0.1932	1.824	0.998	1.011	0.002	1.692	0.957	1.078	0.020	1.518	0.899	1.131	0.041
0.2032	1.832	0.999	1.007	0.001	1.724	0.969	1.061	0.015	1.555	0.915	1.116	0.035
0.2132					1.754	0.980	1.046	0.010	1.586	0.929	1.102	0.030
0.2232					1.776	0.987	1.034	0.006	1.615	0.941	1.089	0.025
0.2332					1.796	0.993	1.021	0.003	1.643	0.952	1.075	0.021
0.2432					1.808	0.996	1.014	0.001	1.670	0.963	1.062	0.017
0.2532					1.815	0.998	1.009	0.000	1.694	0.972	1.050	0.013
0.2632					1.821	0.999	1.005	0.000	1.714	0.979	1.040	0.010
0.2732					1.825	1.000	1.002	0.000	1.731	0.985	1.031	0.008
0.2832									1.747	0.990	1.021	0.006
0.2932									1.756	0.993	1.015	0.004
0.3032									1.765	0.995	1.011	0.003
0.3132									1.773	0.997	1.005	0.001
0.3232									1.778	0.999	1.002	0.000
0.3332									1.781	1.000	1.000	0.000

TABLE 5

	1.8-F-2.6				1.8-C-2.6				1.8-R-2.6			
Y(ins)	M	U/U1	T/T1	MF	M	U/U1	T/T1	MF	M	U/U1	T/T1	MF
0.0032	0.498	0.300	1.514	0.504	0.468	0.289	1.539	0.473	0.441	0.276	1.513	0.473
0.0052	0.554	0.336	1.501	0.472	0.543	0.335	1.520	0.445	0.509	0.319	1.497	0.436
0.0072	0.604	0.366	1.489	0.445	0.592	0.366	1.507	0.424	0.566	0.356	1.483	0.412
0.0092	0.642	0.390	1.479	0.425	0.631	0.390	1.496	0.408	0.611	0.384	1.471	0.400
0.0112	0.672	0.409	1.471	0.408	0.672	0.415	1.484	0.395	0.641	0.402	1.463	0.386
0.0132	0.70[illegible]	0.426	1.464	0.395	0.700	0.432	1.475	0.383	0.668	0.419	1.454	0.375
0.0182	0.761	0.463	1.445	0.367	0.764	0.471	1.454	0.358	0.729	0.457	1.435	0.353
0.0232	0.807	0.491	1.430	0.342	0.804	0.496	1.440	0.339	0.765	0.480	1.423	0.333
0.0282	0.840	0.512	1.419	0.325	0.838	0.516	1.428	0.323	0.799	0.500	1.412	0.320
0.0332	0.880	0.535	1.405	0.308	0.869	0.535	1.417	0.310	0.827	0.518	1.402	0.308
0.0382	0.912	0.555	1.393	0.293	0.895	0.550	1.407	0.299	0.853	0.533	1.393	0.298
0.0432	0.947	0.574	1.381	0.282	0.919	0.565	1.397	0.288	0.878	0.548	1.384	0.289
0.0482	0.973	0.590	1.371	0.271	0.939	0.577	1.389	0.279	0.899	0.561	1.376	0.282
0.0532	0.998	0.604	1.362	0.262	0.962	0.590	1.380	0.271	0.916	0.571	1.370	0.275
0.0632	1.050	0.633	1.341	0.242	1.005	0.614	1.364	0.254	0.950	0.591	1.356	0.261
0.0732	1.103	0.663	1.320	0.221	1.044	0.637	1.348	0.239	0.983	0.610	1.343	0.247
0.0832	1.155	0.692	1.299	0.200	1.081	0.658	1.333	0.224	1.016	0.630	1.331	0.234
0.0932	1.210	0.722	1.277	0.179	1.119	0.680	1.318	0.208	1.045	0.647	1.319	0.222
0.1032	1.267	0.753	1.254	0.160	1.157	0.701	1.302	0.192	1.076	0.664	1.308	0.209
0.1132	1.323	0.782	1.232	0.142	1.194	0.721	1.287	0.179	1.104	0.681	1.297	0.198
0.1232	1.382	0.811	1.209	0.126	1.233	0.742	1.271	0.166	1.137	0.699	1.284	0.187
0.1332	1.436	0.838	1.186	0.109	1.277	0.765	1.252	0.152	1.170	0.718	1.270	0.175
0.1432	1.486	0.863	1.165	0.092	1.318	0.787	1.235	0.138	1.200	0.734	1.258	0.164
0.1532	1.538	0.888	1.143	0.075	1.361	0.809	1.218	0.126	1.229	0.750	1.247	0.155
0.1632	1.607	0.919	1.113	0.056	1.420	0.838	1.193	0.109	1.279	0.777	1.227	0.140
0.1832	1.681	0.950	1.080	0.040	1.477	0.866	1.170	0.092	1.323	0.800	1.210	0.126
0.1932	1.739	0.973	1.053	0.027	1.530	0.891	1.146	0.076	1.368	0.824	1.192	0.113
0.2132	1.781	0.989	1.030	0.014	1.583	0.918	1.120	0.061	1.414	0.847	1.173	0.099
0.2232	1.804	0.996	1.016	0.006	1.639	0.940	1.098	0.047	1.458	0.869	1.155	0.088
0.2432	1.81[illegible]	0.999	1.00[illegible]	0.002	1.691	0.961	1.073	0.030	1.504	0.891	1.136	0.076
0.2632					1.739	0.977	1.053	0.023	1.548	0.912	1.117	0.064
0.2732					1.770	0.989	1.041	0.016	1.588	0.930	1.100	0.053
0.2832					1.786	0.994	1.022	0.008	1.627	0.947	1.082	0.043
0.3032					1.797	0.997	1.013	0.005	1.668	0.964	1.064	0.033
0.3132					1.803	0.999	1.006	0.001	1.700	0.977	1.047	0.025
0.3332									1.725	0.987	1.034	0.018
0.3432									1.742	0.993	1.024	0.012
0.3632									1.754	0.997	1.017	0.0[illegible]7
0.3732									1.762	0.999	1.010	0.004

TABLE 6

Y(inch)	1.8-F-3.8 M	1.8-F-3.8 U/U1	1.8-F-3.8 T/T1	1.8-F-3.8 MF	1.8-C-3.8 M	1.8-C-3.8 U/U1	1.8-C-3.8 T/T1	1.8-C-3.8 MF	1.8-R-3.8 M	1.8-R-3.8 U/U1	1.8-R-3.8 T/T1	1.8-R-3.8 MF
0.0032	0.390	0.223	1.508	0.655	0.413	0.244	1.509	0.621	0.415	0.251	1.501	0.612
0.0052	0.453	0.266	1.493	0.610	0.480	0.285	1.497	0.586	0.479	0.286	1.490	0.559
0.0072	0.506	0.299	1.490	0.590	0.529	0.311	1.490	0.559	0.510	0.312	1.481	0.534
0.0092	0.553	0.319	1.483	0.568	0.569	0.335	1.482	0.536	0.546	0.335	1.473	0.515
0.0112	0.597	0.342	1.476	0.549	0.588	0.352	1.476	0.521	0.573	0.352	1.466	0.499
0.0132	0.636	0.355	1.472	0.531	0.603	0.368	1.472	0.503	0.599	0.368	1.460	0.487
0.0152	0.647	0.386	1.460	0.495	0.674	0.405	1.456	0.479	0.652	0.401	1.446	0.464
0.0232	0.687	0.411	1.451	0.471	0.719	0.429	1.446	0.459	0.689	0.424	1.435	0.443
0.0252	0.724	0.434	1.441	0.450	0.758	0.452	1.434	0.441	0.719	0.443	1.427	0.427
0.0332	0.758	0.452	1.432	0.433	0.775	0.467	1.427	0.428	0.741	0.457	1.419	0.414
0.0352	0.786	0.472	1.422	0.419	0.802	0.483	1.418	0.416	0.768	0.474	1.411	0.401
0.0432	0.816	0.490	1.413	0.405	0.823	0.495	1.411	0.405	0.793	0.490	1.402	0.391
0.0452	0.844	0.507	1.404	0.392	0.843	0.507	1.404	0.394	0.809	0.499	1.397	0.383
0.0532	0.870	0.523	1.394	0.381	0.859	0.517	1.399	0.384	0.829	0.511	1.390	0.375
0.0552	0.893	0.538	1.386	0.367	0.873	0.531	1.395	0.365	0.862	0.531	1.378	0.361
0.0732	0.952	0.577	1.369	0.333	0.934	0.561	1.378	0.346	0.890	0.548	1.368	0.346
0.0832	1.009	0.604	1.345	0.309	0.983	0.575	1.361	0.329	0.916	0.564	1.359	0.332
0.0932	1.061	0.634	1.325	0.294	0.996	0.590	1.340	0.310	0.941	0.579	1.349	0.317
0.1032	1.110	0.662	1.307	0.283	1.034	0.621	1.331	0.294	0.963	0.595	1.339	0.304
0.1132	1.160	0.691	1.289	0.268	1.066	0.640	1.324	0.277	0.997	0.612	1.329	0.292
0.1232	1.213	0.719	1.268	0.251	1.102	0.660	1.309	0.262	1.024	0.629	1.319	0.279
0.1332	1.266	0.748	1.248	0.238	1.141	0.682	1.295	0.247	1.049	0.643	1.309	0.267
0.1432	1.311	0.773	1.230	0.189	1.174	0.700	1.283	0.234	1.077	0.659	1.298	0.254
0.1532	1.360	0.798	1.211	0.163	1.209	0.720	1.269	0.219	1.105	0.675	1.288	0.242
0.1732	1.463	0.850	1.169	0.131	1.281	0.759	1.241	0.192	1.159	0.706	1.268	0.221
0.1932	1.551	0.903	1.133	0.099	1.344	0.799	1.213	0.166	1.212	0.736	1.247	0.199
0.2132	1.645	0.935	1.098	0.069	1.421	0.832	1.186	0.141	1.272	0.768	1.224	0.178
0.2332	1.724	0.967	1.065	0.044	1.498	0.870	1.155	0.116	1.330	0.799	1.201	0.157
0.2532	1.773	0.988	1.029	0.023	1.566	0.903	1.126	0.093	1.385	0.829	1.180	0.138
0.2732	1.801	0.998	1.012	0.009	1.633	0.933	1.097	0.071	1.441	0.857	1.157	0.120
0.2932	1.809	0.999	1.003	0.003	1.693	0.960	1.069	0.049	1.492	0.883	1.136	0.099
0.3132					1.744	0.981	1.045	0.032	1.536	0.910	1.113	0.079
0.3332					1.777	0.992	1.026	0.021	1.570	0.934	1.090	0.063
0.3532					1.792	0.998	1.015	0.011	1.644	0.954	1.068	0.049
0.3732					1.802	1.000	1.007	0.005	1.687	0.972	1.049	0.035
0.3932									1.717	0.984	1.033	0.024
0.4132									1.737	0.992	1.021	0.015
0.4332									1.749	0.995	1.013	0.009
0.4532									1.756	0.998	1.006	0.004
0.4732									1.761	0.999	1.002	0.001

TABLE 7

Y(ins)	2.5-F-1.3 M	2.5-F-1.3 U/U1	2.5-F-1.3 T/T1	2.5-F-1.3 MF	2.5-C-1.3 M	2.5-C-1.3 U/U1	2.5-C-1.3 T/T1	2.5-C-1.3 MF	2.5-R-1.3 M	2.5-R-1.3 U/U1	2.5-R-1.3 T/T1	2.5-R-1.3 MF
0.0032	0.622	0.327	2.036	0.396	0.690	0.364	2.061	0.347	0.765	0.399	2.001	0.348
0.0052	0.700	0.368	1.999	0.358	0.777	0.407	2.015	0.328	0.832	0.432	1.966	0.326
0.0072	0.760	0.398	1.968	0.337	0.819	0.427	1.989	0.309	0.880	0.455	1.937	0.309
0.0092	0.814	0.425	1.939	0.320	0.870	0.452	1.959	0.294	0.923	0.476	1.910	0.298
0.0112	0.860	0.443	1.916	0.304	0.916	0.474	1.930	0.278	0.954	0.490	1.890	0.288
0.0132	0.895	0.459	1.896	0.292	0.948	0.489	1.907	0.272	0.982	0.503	1.871	0.281
0.0182	0.947	0.490	1.857	0.266	1.025	0.524	1.857	0.256	1.027	0.524	1.840	0.259
0.0232	1.003	0.516	1.821	0.247	1.077	0.546	1.819	0.240	1.077	0.546	1.808	0.243
0.0282	1.054	0.539	1.788	0.231	1.125	0.567	1.788	0.228	1.123	0.567	1.778	0.230
0.0332	1.101	0.560	1.759	0.217	1.163	0.584	1.763	0.216	1.160	0.583	1.754	0.220
0.0382	1.145	0.579	1.733	0.207	1.200	0.600	1.742	0.205	1.195	0.598	1.733	0.211
0.0432	1.184	0.601	1.705	0.196	1.228	0.612	1.724	0.196	1.222	0.609	1.717	0.204
0.0482	1.234	0.617	1.685	0.186	1.262	0.626	1.703	0.188	1.248	0.621	1.700	0.196
0.0532	1.256	0.632	1.664	0.176	1.288	0.637	1.687	0.182	1.274	0.632	1.684	0.188
0.0632	1.350	0.667	1.616	0.157	1.346	0.661	1.653	0.168	1.324	0.652	1.654	0.176
0.0732	1.429	0.699	1.571	0.140	1.400	0.683	1.621	0.155	1.371	0.671	1.625	0.164
0.0832	1.509	0.730	1.527	0.122	1.458	0.705	1.588	0.142	1.428	0.693	1.591	0.155
0.0932	1.593	0.761	1.480	0.109	1.518	0.729	1.543	0.130	1.477	0.712	1.562	0.144
0.1032	1.669	0.788	1.438	0.091	1.571	0.748	1.502	0.117	1.519	0.728	1.539	0.134
0.1132	1.749	0.816	1.394	0.077	1.629	0.762	1.481	0.112	1.565	0.745	1.513	0.123
0.1232	1.826	0.842	1.353	0.064	1.701	0.794	1.449	0.093	1.609	0.762	1.488	0.115
0.1332	1.903	0.867	1.309	0.052	1.761	0.815	1.415	0.084	1.657	0.779	1.461	0.105
0.1432	1.980	0.891	1.266	0.040	1.820	0.834	1.382	0.073	1.703	0.795	1.435	0.096
0.1532	2.069	0.913	1.224	0.032	1.881	0.853	1.349	0.063	1.753	0.811	1.407	0.089
0.1632	2.152	0.934	1.181	0.025	1.945	0.872	1.314	0.055	1.805	0.828	1.378	0.080
0.1732	2.225	0.951	1.143	0.019	2.014	0.892	1.277	0.047	1.952	0.843	1.353	0.072
0.1832	2.299	0.967	1.105	0.013	2.069	0.907	1.248	0.040	1.905	0.860	1.324	0.064
0.1932	2.367	0.981	1.069	0.008	2.130	0.923	1.215	0.033	1.954	0.874	1.299	0.058
0.2032	2.421	0.991	1.041	0.004	2.190	0.939	1.184	0.027	2.004	0.889	1.272	0.052
0.2132	2.452	0.996	1.024	0.003	2.244	0.950	1.155	0.021	2.050	0.902	1.248	0.045
0.2232	2.467	0.997	1.014	0.001	2.309	0.964	1.122	0.015	2.098	0.915	1.223	0.039
0.2332	2.479	0.999	1.007	0.001	2.366	0.975	1.091	0.011	2.146	0.927	1.199	0.034
0.2432	2.484	0.999	1.004	0.001	2.419	0.983	1.067	0.008	2.202	0.941	1.170	0.029
0.2532					2.440	0.990	1.046	0.005	2.251	0.952	1.145	0.024
0.2632					2.482	0.996	1.029	0.004	2.302	0.964	1.119	0.019
0.2732					2.501	0.998	1.017	0.002	2.342	0.972	1.099	0.015
0.2832					2.514	0.999	1.010	0.001	2.391	0.980	1.078	0.012
0.2932									2.419	0.987	1.058	0.009
0.3032									2.448	0.992	1.042	0.006
0.3132									2.466	0.994	1.030	0.003
0.3232									2.483	0.997	1.021	0.001
0.3332									2.494	0.998	1.014	0.000
0.3432									2.500	0.999	1.010	0.000
0.3532									2.505	0.999	1.007	0.000

TABLE 8

	2.5-F-2.5				2.5-C-2.5				2.5-R-2.5			
Y(ins)	M	U/U1	T/T1	MF	M	U/U1	T/T1	MF	M	U/U1	T/T1	MF
0.0032	0.426	0.214	2.089	0.621	0.488	0.247	2.073	0.561	0.496	0.252	2.067	0.570
0.0052	0.509	0.257	2.062	0.579	0.562	0.284	2.045	0.531	0.578	0.294	2.037	0.533
0.0072	0.556	0.282	2.043	0.551	0.635	0.321	2.016	0.510	0.637	0.324	2.010	0.504
0.0092	0.608	0.308	2.020	0.526	0.672	0.339	1.998	0.490	0.697	0.354	1.982	0.483
0.0112	0.636	0.323	2.007	0.509	0.714	0.360	1.978	0.473	0.729	0.370	1.965	0.466
0.0132	0.672	0.341	1.989	0.494	0.745	0.376	1.962	0.457	0.758	0.385	1.951	0.453
0.0182	0.743	0.376	1.952	0.463	0.815	0.410	1.926	0.429	0.799	0.405	1.926	0.428
0.0232	0.792	0.400	1.924	0.439	0.865	0.434	1.897	0.409	0.849	0.429	1.897	0.409
0.0282	0.843	0.425	1.895	0.417	0.911	0.456	1.871	0.391	0.895	0.451	1.870	0.391
0.0332	0.889	0.447	1.870	0.397	0.943	0.471	1.854	0.378	0.937	0.471	1.847	0.379
0.0382	0.921	0.463	1.851	0.381	0.982	0.490	1.833	0.365	0.956	0.481	1.836	0.367
0.0432	0.951	0.478	1.834	0.366	1.010	0.503	1.817	0.352	0.986	0.494	1.820	0.355
0.0482	0.989	0.495	1.814	0.353	1.028	0.511	1.807	0.342	1.003	0.503	1.810	0.345
0.0532	1.024	0.512	1.795	0.340	1.053	0.523	1.792	0.332	1.029	0.515	1.796	0.334
0.0632	1.081	0.539	1.763	0.315	1.102	0.545	1.765	0.314	1.070	0.534	1.772	0.317
0.0732	1.149	0.569	1.726	0.292	1.155	0.569	1.735	0.296	1.108	0.552	1.749	0.302
0.0832	1.217	0.600	1.688	0.268	1.205	0.591	1.708	0.278	1.152	0.571	1.724	0.287
0.0932	1.294	0.633	1.646	0.246	1.252	0.612	1.681	0.262	1.194	0.590	1.700	0.273
0.1032	1.353	0.658	1.613	0.222	1.303	0.634	1.652	0.246	1.234	0.607	1.678	0.259
0.1132	1.416	0.684	1.578	0.203	1.340	0.650	1.631	0.231	1.272	0.624	1.656	0.246
0.1232	1.491	0.714	1.537	0.183	1.394	0.671	1.601	0.216	1.315	0.642	1.632	0.234
0.1332	1.562	0.742	1.498	0.163	1.445	0.692	1.573	0.203	1.357	0.659	1.609	0.222
0.1432	1.629	0.767	1.462	0.144	1.488	0.710	1.549	0.186	1.402	0.678	1.583	0.209
0.1532	1.703	0.794	1.422	0.126	1.541	0.730	1.520	0.171	1.435	0.692	1.565	0.198
0.1682	1.820	0.834	1.358	0.102	1.621	0.760	1.475	0.151	1.493	0.715	1.533	0.180
0.1832	1.930	0.869	1.300	0.081	1.702	0.789	1.431	0.133	1.564	0.742	1.494	0.164
0.1982	2.048	0.903	1.238	0.060	1.779	0.816	1.390	0.113	1.622	0.764	1.462	0.148
0.2132	2.156	0.933	1.181	0.041	1.865	0.845	1.344	0.096	1.687	0.787	1.427	0.133
0.2282	2.273	0.960	1.120	0.027	1.948	0.871	1.301	0.081	1.750	0.809	1.394	0.119
0.2432	2.368	0.980	1.070	0.016	2.031	0.895	1.258	0.067	1.822	0.834	1.355	0.105
0.2582	2.431	0.991	1.036	0.009	2.114	0.918	1.215	0.054	1.888	0.855	1.320	0.092
0.2732	2.468	0.997	1.015	0.004	2.193	0.939	1.173	0.041	1.956	0.876	1.285	0.079
0.2882	2.477	0.998	1.008	0.001	2.270	0.958	1.134	0.028	2.013	0.893	1.255	0.068
0.3032	2.486	0.999	1.003	0.000	2.348	0.975	1.093	0.019	2.091	0.915	1.214	0.056
0.3182					2.401	0.985	1.065	0.012	2.162	0.934	1.177	0.045
0.3332					2.446	0.993	1.041	0.007	2.228	0.950	1.143	0.035
0.3482					2.465	0.995	1.029	0.004	2.288	0.963	1.111	0.027
0.3632					2.484	0.998	1.017	0.002	2.344	0.975	1.082	0.020
0.3782					2.493	0.999	1.010	0.000	2.388	0.984	1.058	0.014
0.3932					2.499	0.999	1.006	0.000	2.420	0.990	1.041	0.009
0.4082					2.503	1.000	1.002	0.000	2.445	0.994	1.027	0.005
0.4232									2.460	0.996	1.018	0.002
0.4382									2.472	0.998	1.010	0.001
0.4532									2.478	0.998	1.006	0.000
0.4682									2.485	0.999	1.003	0.000

TABLE 9

	2.5-F-3.6				2.5-C-3.6				2.5-K-3.6			
Y(ins)	M	U/U1	T/T1	MF	M	U/U1	T/T1	MF	M	U/U1	T/T1	MF
0.0032	0.238	0.144	2.082	0.774	0.458	0.217	2.083	0.742	0.415	0.203	2.061	0.725
0.0052	0.378	0.196	2.063	0.719	0.521	0.253	2.060	0.699	0.469	0.227	2.046	0.674
0.0072	0.423	0.210	2.049	0.699	0.558	0.272	2.046	0.689	0.499	0.242	2.031	0.654
0.0092	0.457	0.226	2.039	0.682	0.591	0.289	2.039	0.684	0.535	0.266	2.018	0.613
0.0112	0.484	0.239	2.029	0.646	0.612	0.300	2.022	0.617	0.560	0.283	1.997	0.598
0.0132	0.510	0.253	2.021	0.631	0.632	0.310	2.013	0.602	0.619	0.309	1.985	0.587
0.0152	0.538	0.296	1.987	0.606	0.705	0.346	1.981	0.579	0.681	0.338	1.956	0.561
0.0232	0.627	0.311	1.973	0.578	0.738	0.362	1.965	0.560	0.713	0.355	1.940	0.537
0.0252	0.659	0.341	1.947	0.557	0.797	0.390	1.937	0.538	0.743	0.370	1.926	0.520
0.0332	0.720	0.357	1.933	0.538	0.837	0.410	1.917	0.511	0.786	0.390	1.907	0.507
0.0352	0.750	0.372	1.918	0.521	0.856	0.419	1.907	0.496	0.811	0.403	1.894	0.493
0.0432	0.773	0.386	1.905	0.506	0.886	0.434	1.892	0.483	0.836	0.415	1.882	0.480
0.0452	0.817	0.405	1.887	0.491	0.900	0.445	1.880	0.473	0.860	0.427	1.870	0.471
0.0532	0.849	0.419	1.875	0.477	0.931	0.460	1.860	0.463	0.871	0.433	1.864	0.461
0.0552	0.880	0.440	1.847	0.461	0.972	0.475	1.847	0.443	0.914	0.453	1.842	0.441
0.0732	0.941	0.466	1.826	0.426	1.010	0.497	1.831	0.422	0.954	0.473	1.822	0.425
0.0832	0.996	0.493	1.797	0.400	1.056	0.514	1.801	0.403	0.991	0.490	1.802	0.408
0.0932	1.047	0.517	1.770	0.376	1.088	0.529	1.783	0.386	1.026	0.507	1.783	0.392
0.1032	1.100	0.546	1.737	0.352	1.120	0.547	1.760	0.368	1.051	0.519	1.769	0.378
0.1132	1.167	0.572	1.706	0.331	1.161	0.564	1.730	0.351	1.082	0.533	1.751	0.362
0.1232	1.221	0.596	1.677	0.312	1.203	0.588	1.715	0.333	1.112	0.547	1.734	0.348
0.1332	1.278	0.621	1.647	0.296	1.243	0.609	1.696	0.316	1.140	0.564	1.714	0.334
0.1432	1.338	0.647	1.618	0.283	1.283	0.614	1.674	0.309	1.173	0.579	1.695	0.321
0.1532	1.394	0.671	1.594	0.243	1.328	0.638	1.649	0.286	1.212	0.594	1.677	0.309
0.1732	1.526	0.724	1.519	0.204	1.418	0.672	1.598	0.257	1.286	0.624	1.639	0.284
0.1932	1.656	0.773	1.448	0.169	1.502	0.706	1.552	0.229	1.362	0.656	1.596	0.258
0.2132	1.788	0.820	1.372	0.133	1.596	0.742	1.490	0.200	1.434	0.685	1.556	0.237
0.2332	1.922	0.865	1.310	0.101	1.670	0.777	1.448	0.175	1.507	0.714	1.517	0.216
0.2532	2.065	0.903	1.252	0.072	1.737	0.811	1.397	0.149	1.586	0.744	1.474	0.195
0.2732	2.202	0.945	1.197	0.044	1.801	0.846	1.341	0.124	1.661	0.772	1.433	0.174
0.2932	2.331	0.975	1.150	0.024	1.900	0.877	1.289	0.098	1.736	0.800	1.393	0.152
0.3132	2.416	0.992	1.121	0.012	2.037	0.906	1.230	0.076	1.809	0.825	1.355	0.131
0.3332	2.458	0.999	1.013	0.003	2.109	0.936	1.189	0.058	1.902	0.856	1.337	0.110
0.3532	2.474	1.000	1.000	0.000	2.177	0.956	1.142	0.039	1.979	0.881	1.268	0.092
0.3732					2.366	0.976	1.096	0.027	2.057	0.904	1.223	0.073
0.3932					2.420	0.989	1.069	0.017	2.132	0.926	1.191	0.058
0.4132					2.474	0.997	1.037	0.009	2.211	0.947	1.151	0.044
0.4332					2.496	1.000	1.023	0.004	2.287	0.965	1.113	0.033
0.4532									2.345	0.978	1.083	0.022
0.4732									2.398	0.990	1.055	0.014
0.4932									2.423	0.993	1.040	0.009
0.5132									2.454	0.999	1.023	0.005
0.5332									2.469	1.000	1.013	0.002

TABLE 10

	3.5-F-0.8				3.5-C-0.8				3.5-R-0.8			
Y(ins)	M	U/U1	T/T1	MF	M	U/U1	T/T1	MF	M	U/U1	T/T1	MF
0.0032	0.640	0.301	3.151	0.338	0.737	0.344	3.095	0.321	0.646	0.303	3.084	0.302
0.0052	0.739	0.353	3.044	0.310	0.819	0.380	3.023	0.294	0.741	0.346	3.010	0.281
0.0072	0.808	0.409	2.953	0.292	0.890	0.410	2.956	0.278	0.833	0.377	2.807	0.266
0.0092	0.864	0.435	2.890	0.275	0.936	0.429	2.903	0.266	0.873	0.393	2.764	0.253
0.0112	0.907	0.449	2.853	0.263	0.986	0.449	2.859	0.256	0.910	0.408	2.731	0.243
0.0132	1.029	0.461	2.819	0.254	1.031	0.467	2.814	0.246	0.945	0.432	2.831	0.236
0.0152	1.116	0.494	2.727	0.235	1.114	0.498	2.725	0.226	1.023	0.463	2.753	0.221
0.0232	1.194	0.522	2.645	0.219	1.188	0.525	2.645	0.213	1.092	0.490	2.682	0.203
0.0282	1.254	0.543	2.580	0.203	1.234	0.541	2.590	0.202	1.155	0.513	2.618	0.190
0.0332	1.321	0.566	2.511	0.191	1.289	0.561	2.537	0.192	1.214	0.534	2.560	0.180
0.0382	1.375	0.585	2.463	0.178	1.331	0.575	2.496	0.183	1.269	0.553	2.510	0.182
0.0432	1.438	0.606	2.408	0.167	1.362	0.586	2.467	0.175	1.321	0.572	2.465	0.175
0.0482	1.484	0.622	2.364	0.156	1.401	0.600	2.431	0.168	1.362	0.585	2.426	0.169
0.0532	1.541	0.640	2.315	0.147	1.439	0.612	2.396	0.163	1.391	0.595	2.398	0.162
0.0632	1.629	0.668	2.236	0.130	1.512	0.636	2.330	0.149	1.465	0.620	2.333	0.151
0.0732	1.730	0.698	2.153	0.116	1.590	0.661	2.262	0.136	1.519	0.638	2.287	0.141
0.0832	1.817	0.722	2.090	0.103	1.656	0.682	2.206	0.122	1.570	0.654	2.244	0.131
0.0932	1.921	0.750	1.995	0.091	1.727	0.703	2.146	0.111	1.627	0.672	2.195	0.121
0.1032	2.027	0.777	1.914	0.076	1.802	0.725	2.084	0.100	1.691	0.692	2.143	0.112
0.1132	2.127	0.802	1.838	0.063	1.883	0.748	2.014	0.091	1.759	0.711	2.087	0.103
0.1232	2.229	0.825	1.764	0.053	1.964	0.768	1.954	0.081	1.825	0.730	2.035	0.093
0.1332	2.338	0.849	1.687	0.044	2.062	0.792	1.879	0.071	1.895	0.749	1.980	0.085
0.1432	2.443	0.868	1.617	0.036	2.131	0.809	1.827	0.062	1.956	0.765	1.933	0.077
0.1532	2.548	0.888	1.548	0.028	2.216	0.828	1.765	0.053	2.027	0.783	1.878	0.070
0.1682	2.737	0.918	1.431	0.018	2.343	0.855	1.676	0.041	2.127	0.805	1.805	0.059
0.1832	2.932	0.946	1.318	0.011	2.480	0.881	1.583	0.033	2.234	0.832	1.730	0.049
0.1982	3.151	0.972	1.204	0.007	2.624	0.906	1.490	0.024	2.337	0.853	1.663	0.040
0.2132	3.347	0.991	1.108	0.003	2.775	0.930	1.397	0.016	2.450	0.876	1.582	0.030
0.2282	3.469	0.999	1.047	0.002	2.941	0.951	1.299	0.010	2.569	0.897	1.505	0.023
0.2433	3.524	1.000	1.017	0.000	3.132	0.973	1.196	0.006	2.706	0.919	1.420	0.016
0.2582					3.291	0.987	1.113	0.003	2.841	0.939	1.348	0.010
0.2732					3.424	0.997	1.048	0.002	2.988	0.957	1.258	0.005
0.2882					3.482	1.000	1.020	0.001	3.132	0.973	1.191	0.003
0.3032									3.281	0.987	1.107	0.002
0.3182									3.382	0.995	1.059	0.001
0.3332									3.439	0.999	1.031	0.001
0.3482									3.469	1.000	1.016	0.000

TABLE II

	3.5-F-1.6				3.5-C-1.6				3.5-R-1.6			
Y (ins)	M	U/U1	T/T1	MF	M	U/U1	T/T1	MF	M	U/U1	T/T1	MF
0.0032	0.355	0.158	3.280	0.612	0.336	0.152	3.257	0.548	0.494	0.226	3.170	0.518
0.0052	0.444	0.198	3.235	0.573	0.478	0.217	3.190	0.510	0.588	0.268	3.115	0.482
0.0072	0.515	0.231	3.191	0.528	0.543	0.246	3.146	0.483	0.665	0.303	3.064	0.460
0.0092	0.576	0.259	3.151	0.497	0.581	0.263	3.115	0.460	0.731	0.332	3.013	0.441
0.0112	0.629	0.282	3.111	0.479	0.633	0.286	3.074	0.447	0.766	0.347	2.981	0.427
0.0132	0.662	0.297	3.083	0.464	0.664	0.299	3.048	0.436	0.810	0.366	2.945	0.414
0.0182	0.785	0.349	2.983	0.432	0.761	0.340	2.969	0.416	0.879	0.395	2.880	0.390
0.0232	0.853	0.377	2.919	0.407	0.841	0.373	2.901	0.396	0.948	0.423	2.816	0.373
0.0282	0.903	0.398	2.868	0.387	0.882	0.390	2.862	0.380	0.979	0.435	2.780	0.361
0.0332	0.958	0.420	2.819	0.368	0.937	0.413	2.812	0.365	1.023	0.452	2.738	0.352
0.0382	1.023	0.446	2.761	0.353	0.971	0.427	2.781	0.352	1.064	0.468	2.700	0.341
0.0432	1.067	0.463	2.721	0.338	1.019	0.445	2.742	0.340	1.090	0.478	2.675	0.332
0.0482	1.109	0.480	2.685	0.325	1.048	0.457	2.714	0.331	1.127	0.492	2.641	0.322
0.0532	1.148	0.495	2.648	0.311	1.077	0.468	2.689	0.321	1.150	0.501	2.618	0.313
0.0632	1.222	0.522	2.581	0.288	1.143	0.494	2.632	0.304	1.207	0.523	2.564	0.297
0.0732	1.301	0.552	2.512	0.266	1.204	0.517	2.578	0.286	1.250	0.538	2.522	0.282
0.0832	1.375	0.578	2.446	0.243	1.261	0.538	2.528	0.270	1.301	0.557	2.472	0.270
0.0932	1.464	0.608	2.368	0.222	1.326	0.561	2.470	0.253	1.340	0.571	2.436	0.257
0.1032	1.547	0.636	2.296	0.203	1.397	0.586	2.408	0.237	1.387	0.587	2.394	0.243
0.1132	1.625	0.661	2.229	0.184	1.473	0.612	2.343	0.220	1.432	0.603	2.351	0.230
0.1232	1.699	0.684	2.167	0.166	1.527	0.630	2.297	0.205	1.485	0.619	2.304	0.219
0.1332	1.801	0.714	2.085	0.148	1.597	0.652	2.240	0.191	1.535	0.637	2.259	0.205
0.1432	1.897	0.740	2.009	0.131	1.671	0.675	2.178	0.176	1.584	0.652	2.218	0.195
0.1532	1.995	0.766	1.932	0.116	1.742	0.696	2.119	0.163	1.631	0.667	2.179	0.184
0.1732	2.177	0.811	1.797	0.088	1.882	0.737	2.008	0.137	1.735	0.700	2.095	0.161
0.1932	2.368	0.854	1.664	0.063	2.026	0.775	1.897	0.113	1.840	0.730	2.011	0.141
0.2132	2.598	0.897	1.514	0.043	2.178	0.812	1.787	0.091	1.939	0.758	1.934	0.122
0.2332	2.832	0.934	1.372	0.026	2.343	0.849	1.674	0.071	2.057	0.788	1.845	0.103
0.2532	3.088	0.967	1.231	0.012	2.507	0.881	1.563	0.053	2.175	0.817	1.761	0.088
0.2732	3.337	0.991	1.103	0.004	2.671	0.910	1.458	0.037	2.297	0.845	1.677	0.072
0.2932	3.487	1.000	1.030	0.001	2.909	0.945	1.318	0.022	2.428	0.871	1.588	0.059
0.3132					3.158	0.974	1.184	0.011	2.567	0.897	1.497	0.046
0.3332					3.350	0.992	1.089	0.004	2.735	0.924	1.394	0.037
0.3532					3.443	0.998	1.041	0.001	2.902	0.947	1.296	0.028
0.3732					3.489	1.000	1.017	0.000	3.083	0.969	1.195	0.019
0.3932									3.256	0.986	1.110	0.011
0.4132									3.364	0.996	1.056	0.004
0.4332									3.415	0.998	1.029	0.001
0.4532									3.444	1.000	1.014	0.000

TABLE 12

	3.5-F-2.4				3.5-C-2.4			
Y (ins)	M	U/U1	T/T1	MF	M	U/U1	T/T1	MF
0.0032	0.272	0.116	3.243	0.790	0.243	0.105	3.231	0.720
0.0052	0.313	0.134	3.223	0.747	0.326	0.143	3.201	0.667
0.0072	0.348	0.151	3.201	0.707	0.360	0.159	3.179	0.637
0.0092	0.410	0.178	3.172	0.676	0.391	0.168	3.013	0.617
0.0112	0.436	0.190	3.153	0.649	0.445	0.196	3.132	0.600
0.0132	0.485	0.212	3.128	0.631	0.492	0.217	3.107	0.588
0.0182	0.527	0.231	3.096	0.597	0.573	0.252	3.056	0.565
0.0232	0.602	0.263	3.046	0.571	0.656	0.287	2.999	0.543
0.0282	0.666	0.291	3.003	0.550	0.726	0.317	2.949	0.528
0.0332	0.735	0.320	2.955	0.531	0.776	0.338	2.910	0.512
0.0382	0.796	0.345	2.911	0.514	0.810	0.352	2.884	0.499
0.0432	0.829	0.360	2.884	0.496	0.832	0.361	2.866	0.486
0.0482	0.870	0.377	2.851	0.480	0.862	0.374	2.841	0.474
0.0532	0.917	0.396	2.813	0.464	0.901	0.390	2.809	0.463
0.0632	0.968	0.417	2.770	0.437	0.936	0.405	2.780	0.440
0.0732	1.022	0.440	2.722	0.412	0.985	0.425	2.739	0.419
0.0832	1.085	0.465	2.669	0.386	1.031	0.444	2.700	0.401
0.0932	1.151	0.494	2.604	0.361	1.072	0.460	2.664	0.383
0.1032	1.220	0.517	2.552	0.338	1.125	0.481	2.619	0.366
0.1132	1.286	0.541	2.495	0.319	1.174	0.500	2.576	0.348
0.1232	1.357	0.567	2.433	0.297	1.220	0.517	2.536	0.332
0.1332	1.425	0.591	2.374	0.276	1.275	0.537	2.489	0.316
0.1432	1.489	0.613	2.320	0.257	1.327	0.556	2.444	0.302
0.1532	1.559	0.636	2.261	0.239	1.377	0.574	2.401	0.286
0.1732	1.712	0.684	2.134	0.203	1.480	0.609	2.315	0.257
0.1932	1.859	0.727	2.016	0.168	1.592	0.646	2.222	0.229
0.2132	2.033	0.774	1.883	0.136	1.718	0.686	2.118	0.200
0.2332	2.205	0.817	1.762	0.108	1.850	0.724	2.015	0.174
0.2532	2.392	0.858	1.634	0.081	1.986	0.761	1.911	0.151
0.2732	2.590	0.893	1.499	0.055	2.113	0.793	1.819	0.129
0.2932	2.819	0.934	1.366	0.034	2.261	0.828	1.715	0.108
0.3132	3.087	0.969	1.219	0.019	2.410	0.860	1.613	0.085
0.3332	3.314	0.992	1.104	0.007	2.576	0.892	1.506	0.066
0.3532	3.451	1.000	1.036	0.003	2.751	0.921	1.398	0.046
0.3732					2.967	0.953	1.275	0.027
0.3932					3.165	0.976	1.169	0.011
0.4132					3.332	0.992	1.086	0.006
0.4332					3.416	0.997	1.043	0.002
0.4532					3.465	1.000	1.019	0.001

TABLE 13

	M_1	Tw/T_1	F	c_f	$2F/c_f$	$2F/c_{f_o}$	δ (mm)	δ^* (mm)	θ (mm)	R_θ X 10^{-4}	H	w
0.55-F-1.2	0.54	1.053					9.12	1.86	1.18	1.98	1.58	0.42
0.55-C-1.2	0.55	1.050	0.0012	0.0021	1.15	0.9	10.62	2.08	1.37	2.30	1.51	
0.55-R-1.2	0.55	1.062					11.25	2.26	1.47	2.46	1.54	
0.55-F-2.4	0.54	1.039					9.42	2.11	1.36	2.28	1.56	0.66
0.55-C-2.4	0.55	1.038	0.0024	0.0015	3.2	1.8	11.00	2.32	1.58	2.66	1.47	
0.55-R-2.4	0.55	1.032					12.57	2.59	1.80	3.02	1.44	
0.55-F-3.6	0.55	1.027					10.21	2.40	1.56	2.63	1.54	0.82
0.55-C-3.6	0.55	1.027	0.0036	0.0009	8.0	2.7	11.73	2.59	1.80	3.03	1.44	
0.55-R-3.6	0.55	1.012					13.26	2.89	2.08	3.51	1.39	

TABLE 14

	M_1	Tw/T_1	F	c_f	$2F/c_f$	$2F/c_{f_o}$	δ	δ^*	θ	R_θ X 10^{-4}	H	w
1.8-F-1.3	1.84	1.615					4.67	1.54	0.533	1.40	2.89	0.59
1.8-C-1.3	1.83	1.637	0.00135	0.0015	1.8	1.35	6.02	1.91	0.665	1.75	2.87	
1.8-R-1.3	1.78	1.610					7.57	2.20	0.805	2.12	2.74	
1.8-F-2.6	1.82	1.573					5.66	1.95	0.711	1.87	2.74	0.80
1.8-C-2.6	1.81	1.591	0.0026	0.0009	5.8	2.6	7.30	2.45	0.896	2.36	2.73	
1.8-R-2.6	1.77	1.560					8.91	2.92	1.115	2.93	2.64	
1.8-F-3.8	1.81	1.552					6.68	2.43	0.907	2.39	2.68	0.93
1.8-C-3.8	1.81	1.546	0.0038	0.0005	15.2	3.8	8.61	3.02	1.158	3.05	2.61	
1.8-R-3.8	1.76	1.549					10.69	3.61	1.417	3.73	2.55	

TABLE 15

	M_1	Tw/T_1	F	c_f	$2F/c_f$	$2F/c_{f_o}$	δ (mm)	δ^* (mm)	θ (mm)	R_θ X 10^{-4}	H	w	Sc_t
2.5-F-1.3	2.49	2.17					5.31	2.23	0.531	1.69	4.20	0.72	0.65
2.5-C-1.3	2.53	2.23	0.0013	0.0010	2.6	1.6	6.60	2.67	0.637	2.03	4.20		
2.5-R-1.3	2.52	2.20					7.95	3.08	0.757	2.42	4.06		
2.5-F-2.5	2.49	2.16					6.68	3.05	0.729	2.33	4.18	0.88	0.70
2.5-C-2.5	2.51	2.15	0.0025	0.0007	8.5	3.1	8.76	3.73	0.917	2.93	4.07		
2.5-R-2.5	2.49	2.16					10.49	4.34	1.092	3.49	3.98		
2.5-F-3.6	2.48	2.10					8.05	3.96	0.932	2.98	4.25	0.96	0.80
2.5-C-3.6	2.52	2.16	0.0036	0.0004	18.2	4.5	10.34	4.75	1.165	3.72	4.08		
2.5-R-3.6	2.48	2.12					12.60	5.61	1.412	4.52	3.97		

TABLE 16

	M_1	Tw/T_1	F	c_f	$2F/c_f$	$2F/c_{f_o}$	δ	δ^*	θ	R_θ X 10^{-4}	H	w	Sc_t
3.5-F-0.8	3.55	3.39					5.54	3.10	0.429	2.12	7.20	0.60	0.60
3.5-C-0.8	3.52	3.38	0.0008	0.0008	2.1	1.3	6.83	3.66	0.513	2.54	7.14		
3.5-R-0.8	3.50	3.31					8.03	4.14	0.597	2.96	6.93		
3.5-F-1.6	3.53	3.35					7.03	4.24	0.579	2.89	7.34	0.80	0.65
3.5-C-1.6	3.52	3.34	0.0016	0.0005	6.6	2.7	8.64	5.08	0.709	3.54	7.16		
3.5-R-1.6	3.47	3.31					10.34	5.74	0.833	4.15	6.88		
3.5-F-2.4	3.50	3.27	0.0024	0.0002	24.5	4.0	8.61	5.33	0.726	3.62	7.35	0.97	0.70
3.5-C-2.4	3.50	3.27					10.67	6.37	0.897	4.47	7.10		

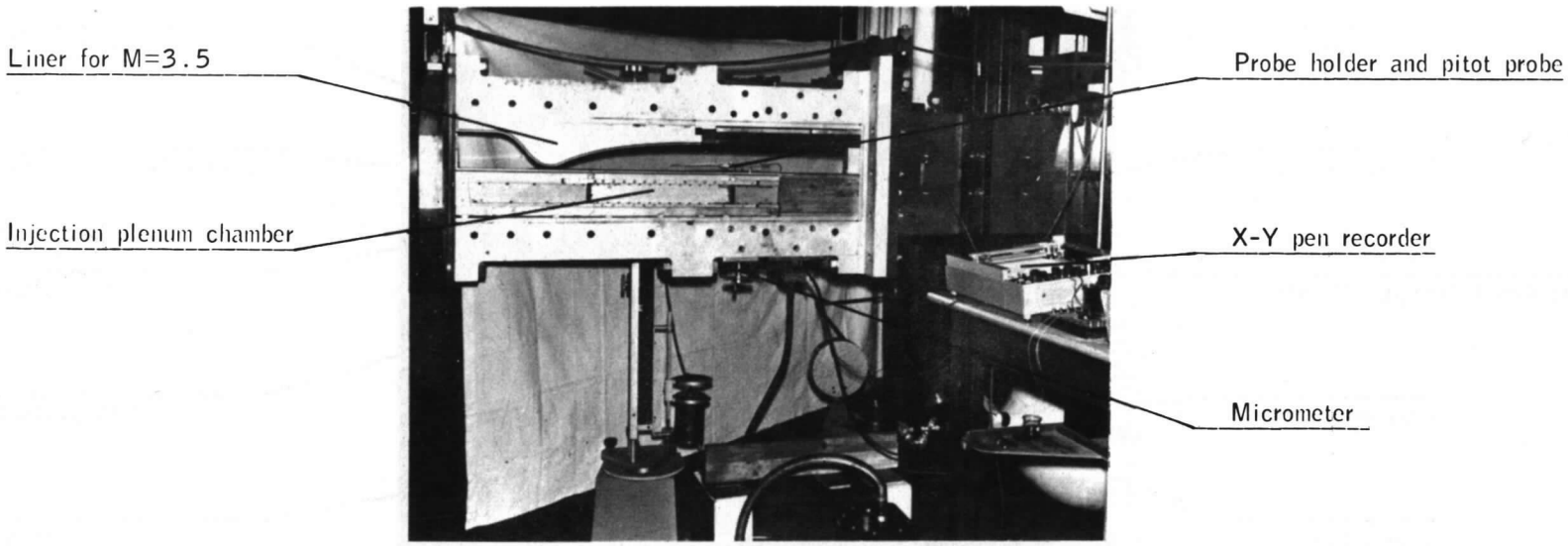

FIG. 1 Photograph of the wind tunnel with the liner for M=3.5

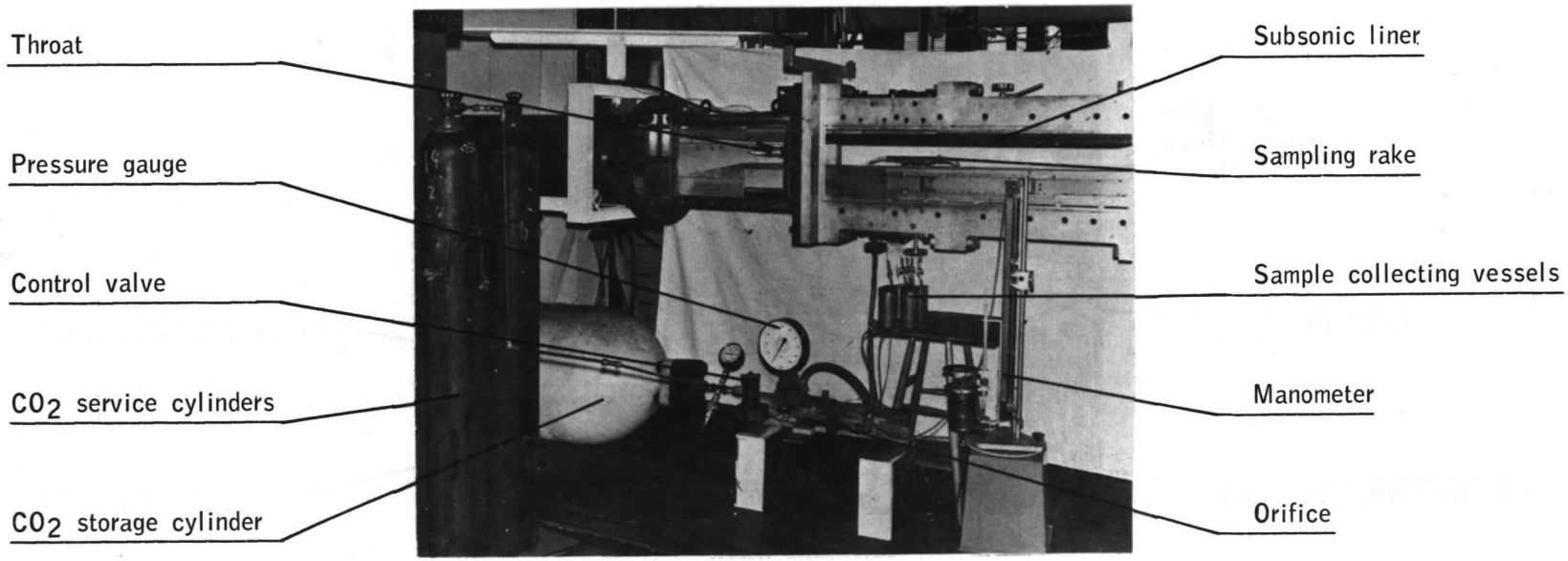

FIG. 2. Photograph of the external injection apparatus and the wind tunnel with the subsonic liner.

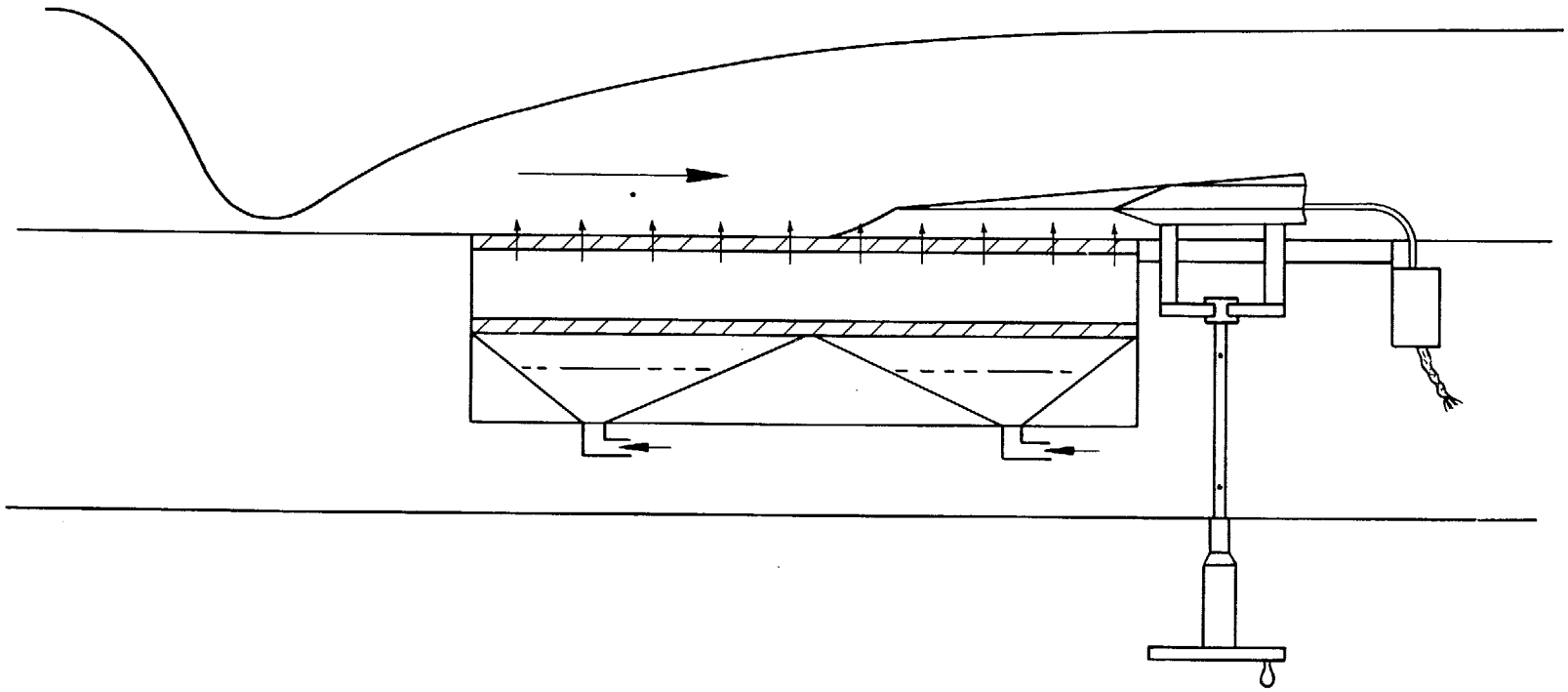

FIG. 3. Diagrammatic representation of the injection equipment.

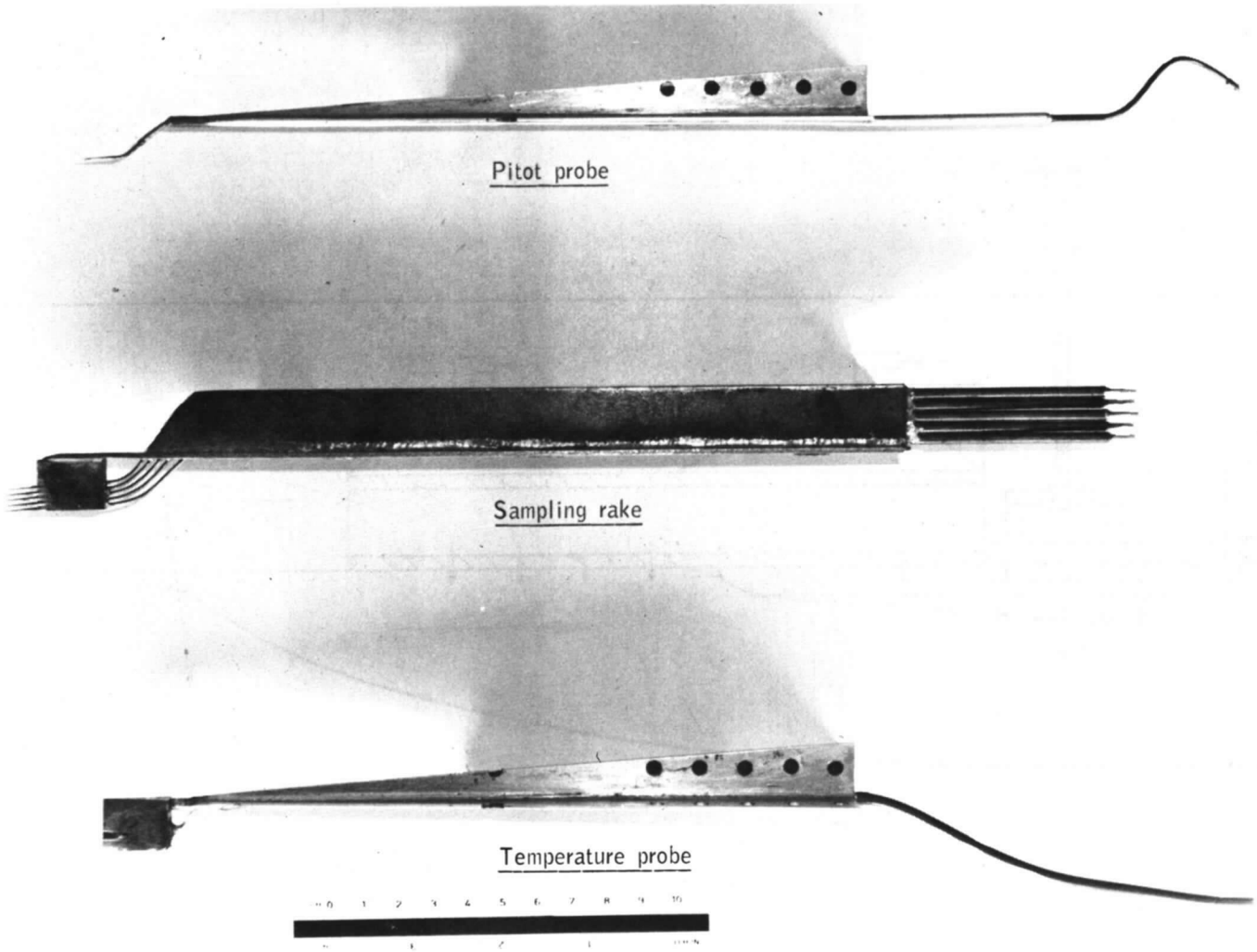

FIG. 4. The measuring probes.

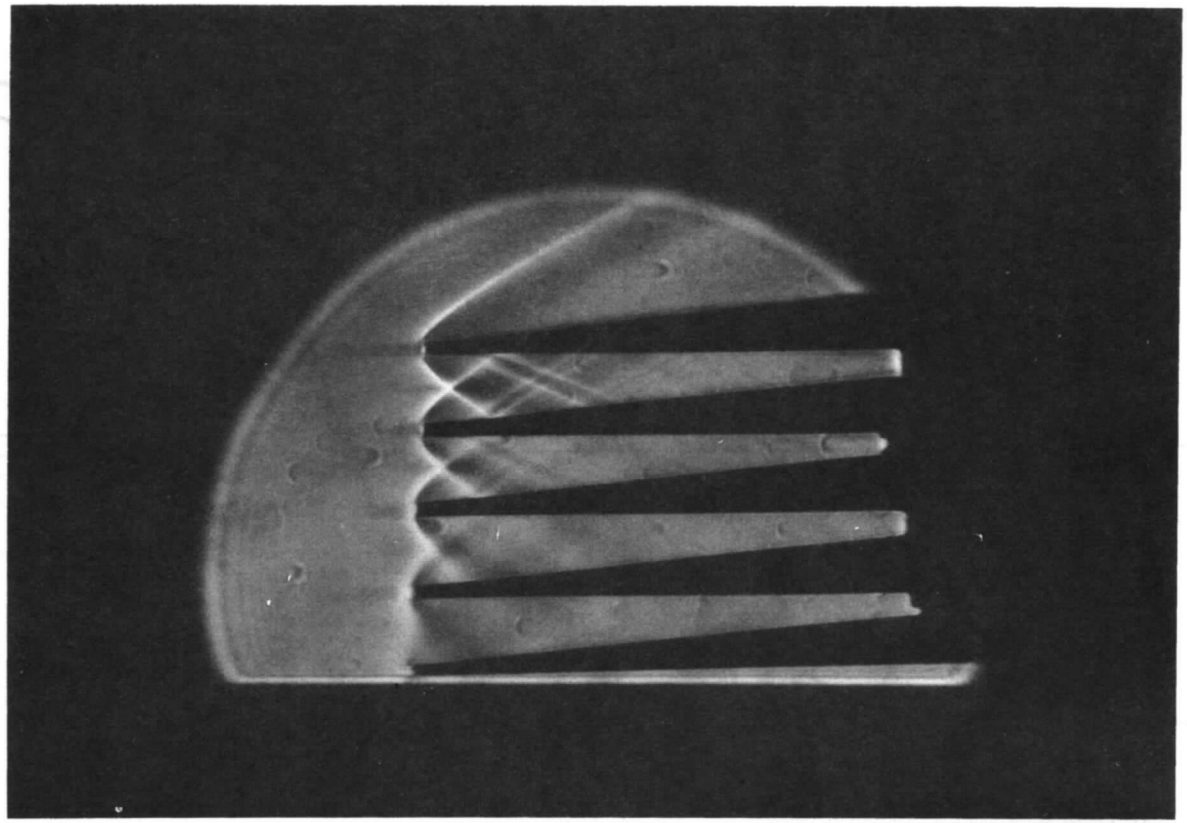

FIG. 5. Schlieren photograph of the sampling rake; approximately 7 × full size. M = 2·5.

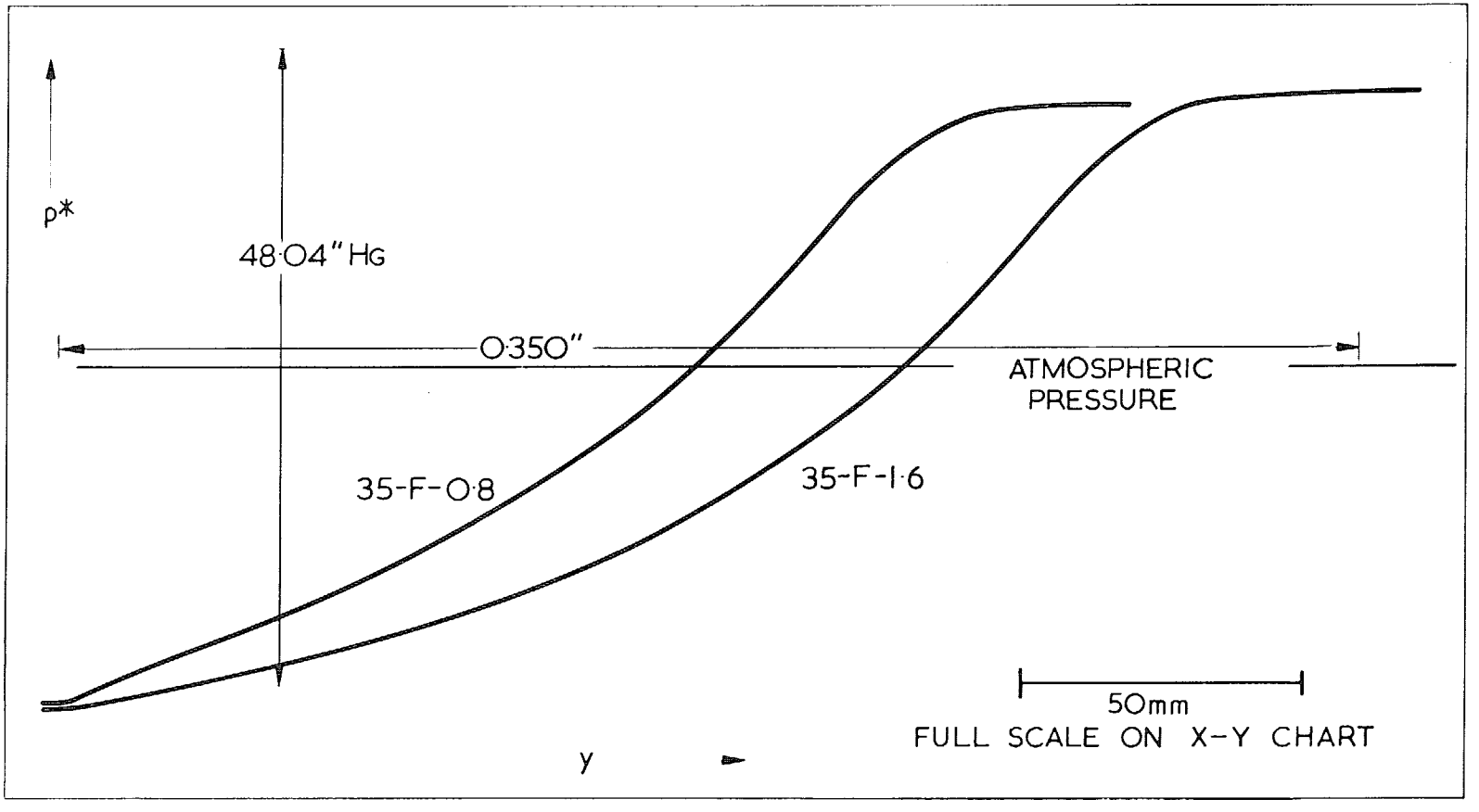

FIG. 6. Typical Pitot Profiles.

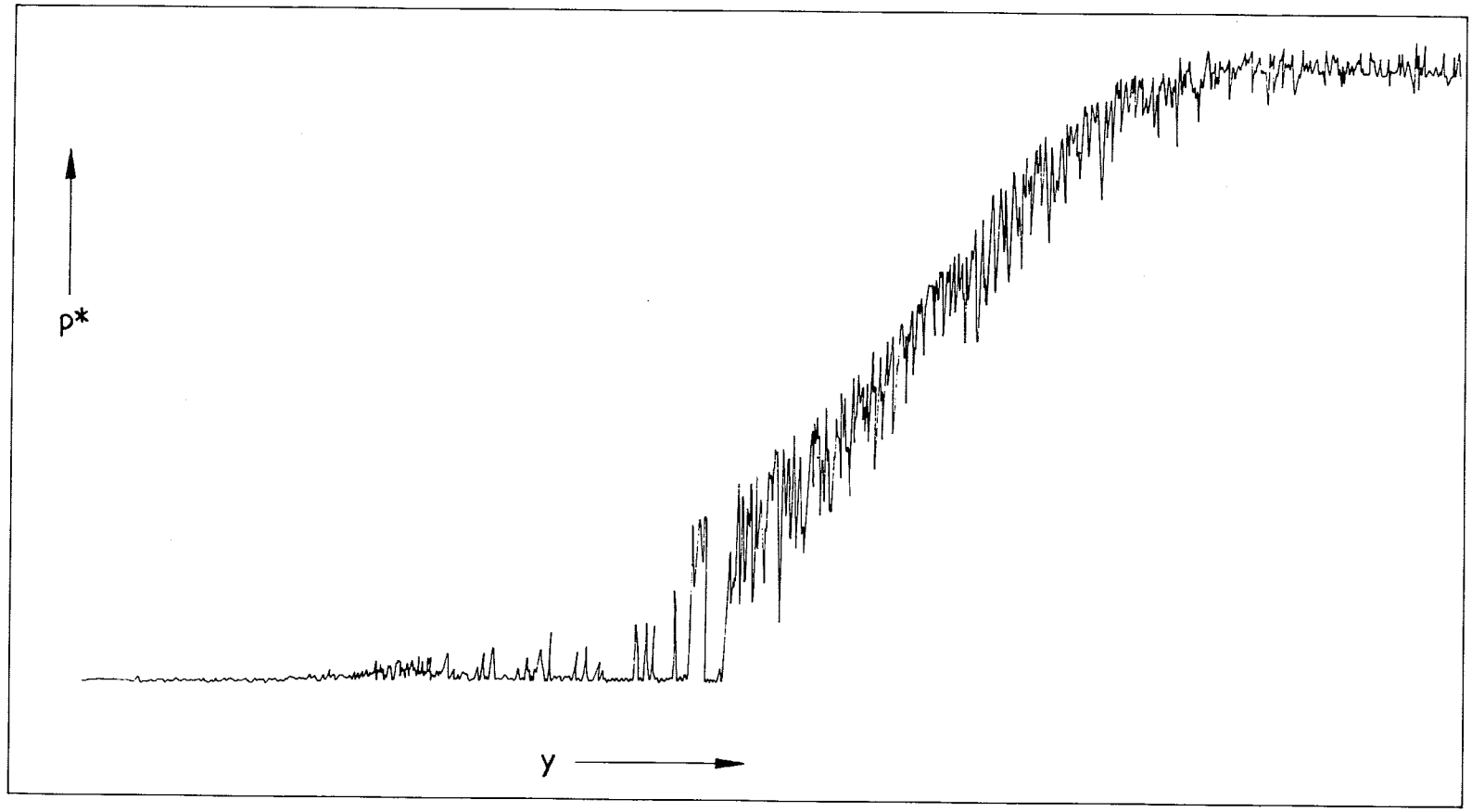

FIG. 7. Pitot Profile Near 'Blow-off'.

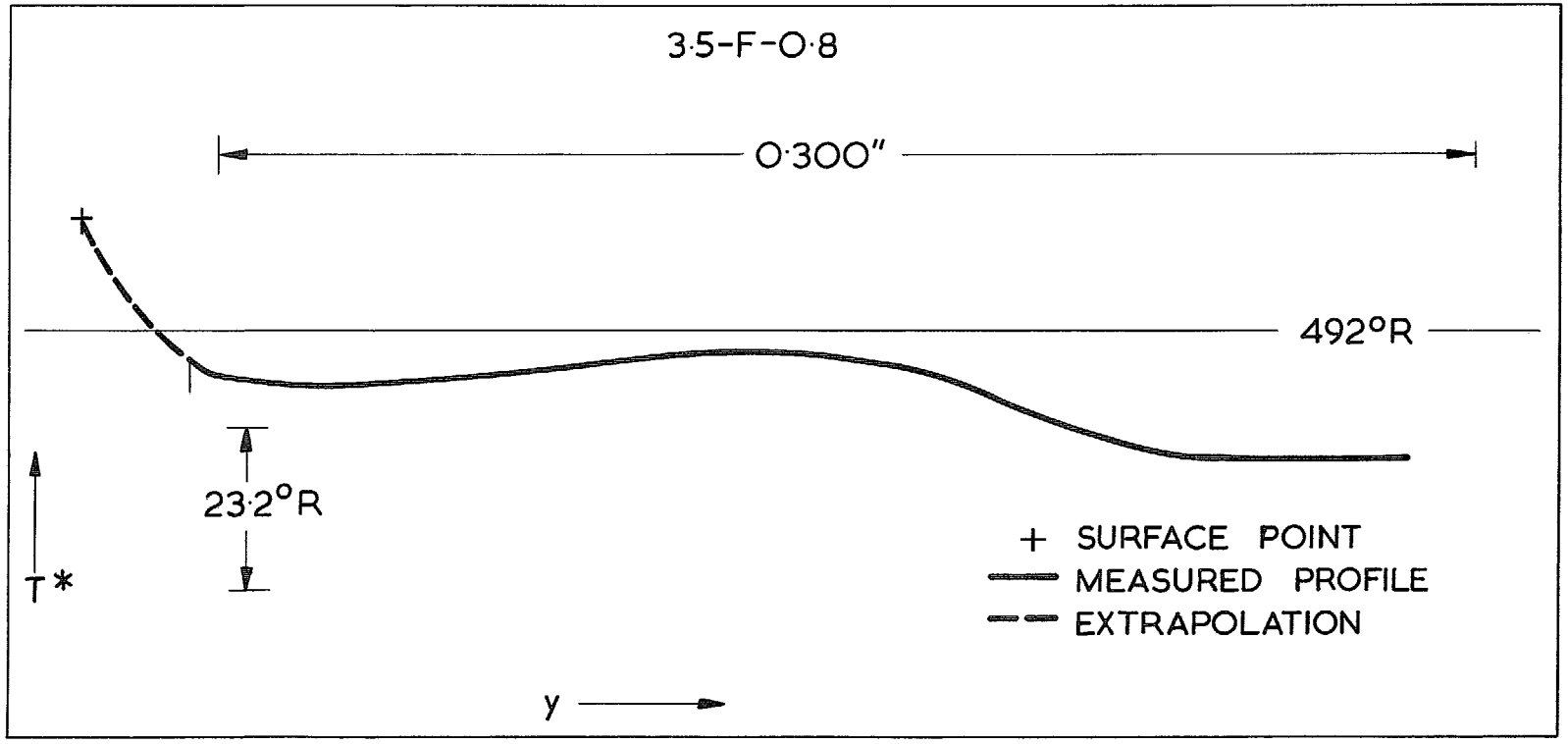

FIG. 8. Typical Probe Temperature Trace.

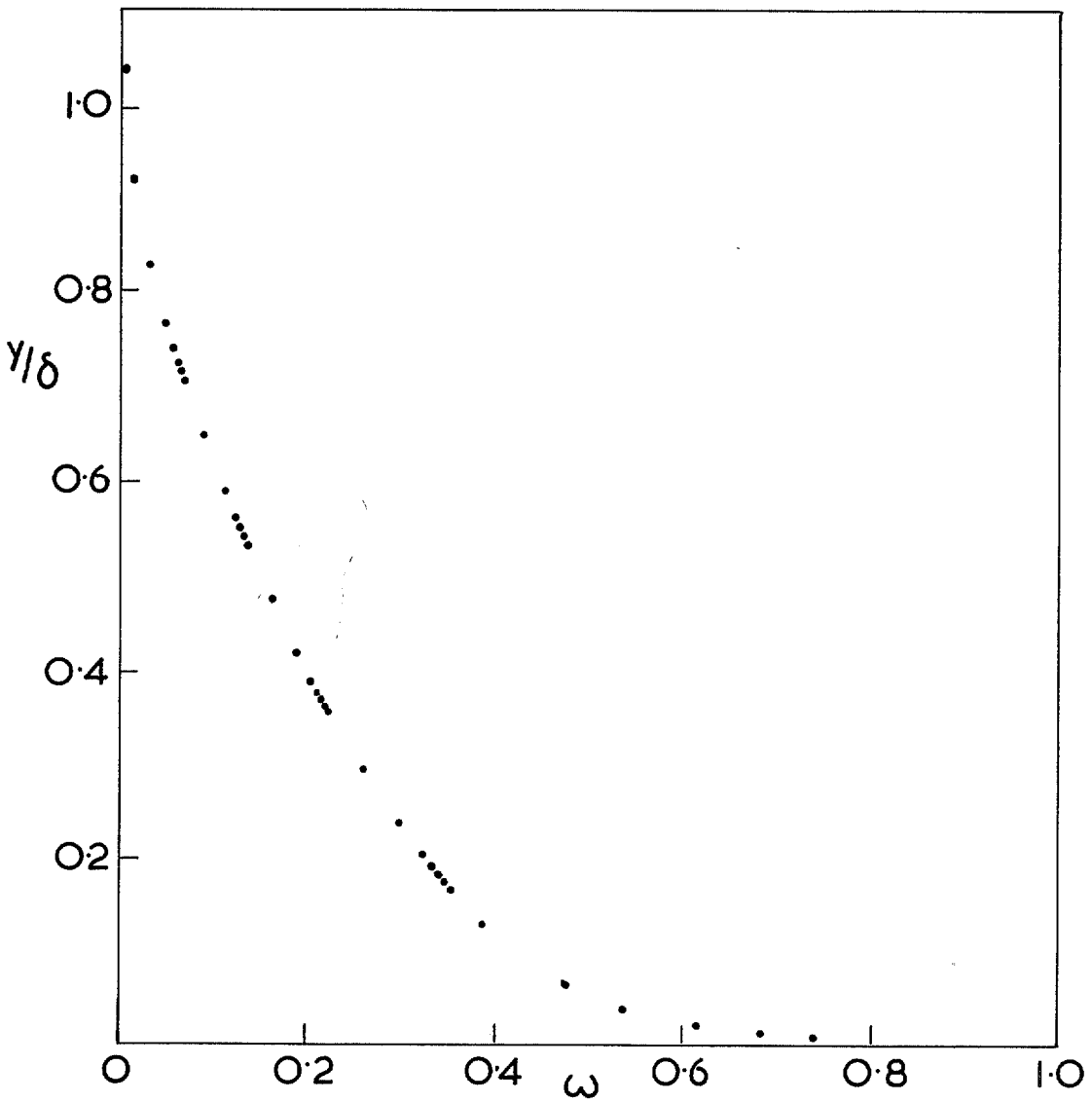

FIG. 9. Typical Concentration Traverse.

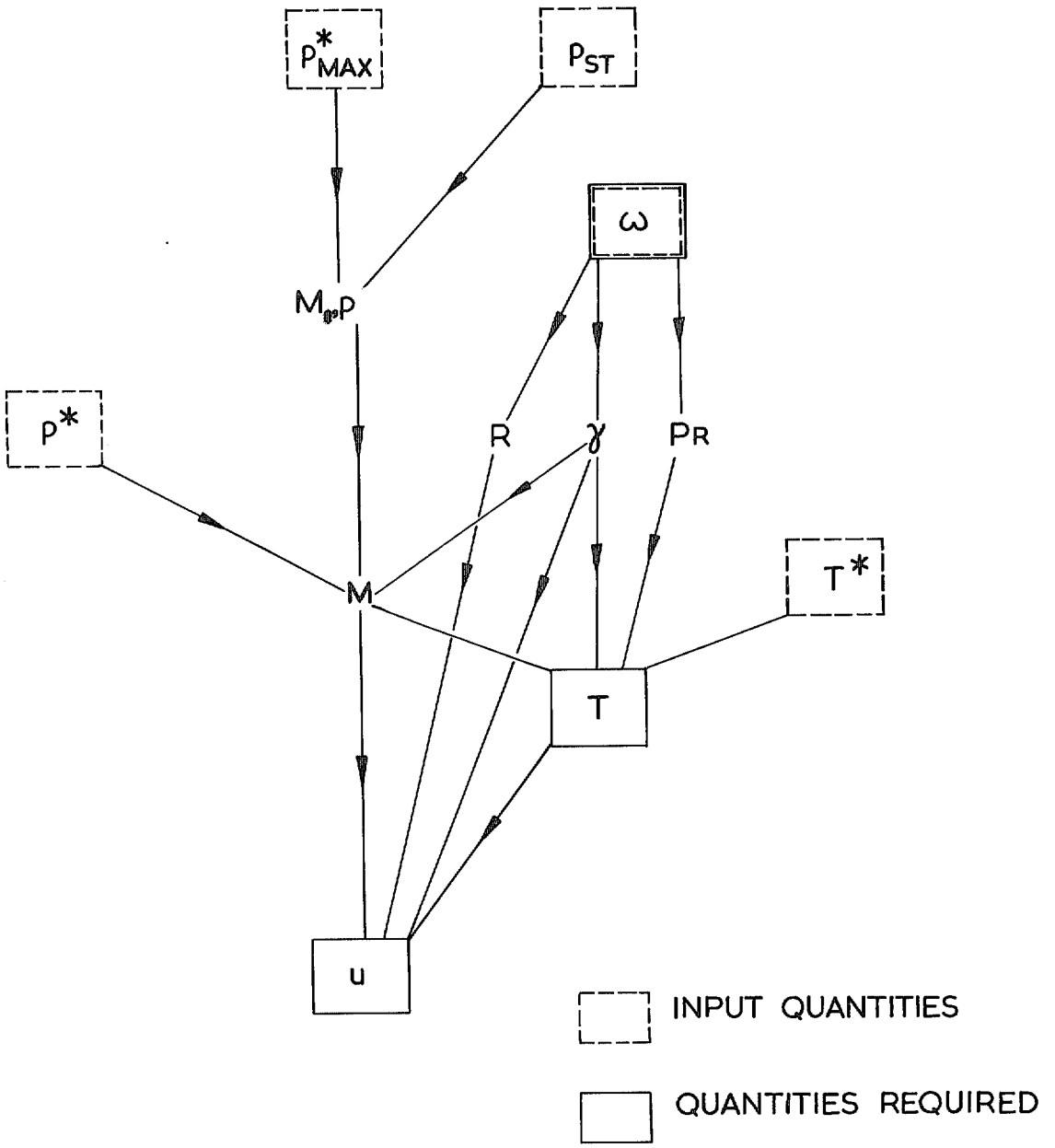

FIG. 10. Diagram of the Calculation Procedure.

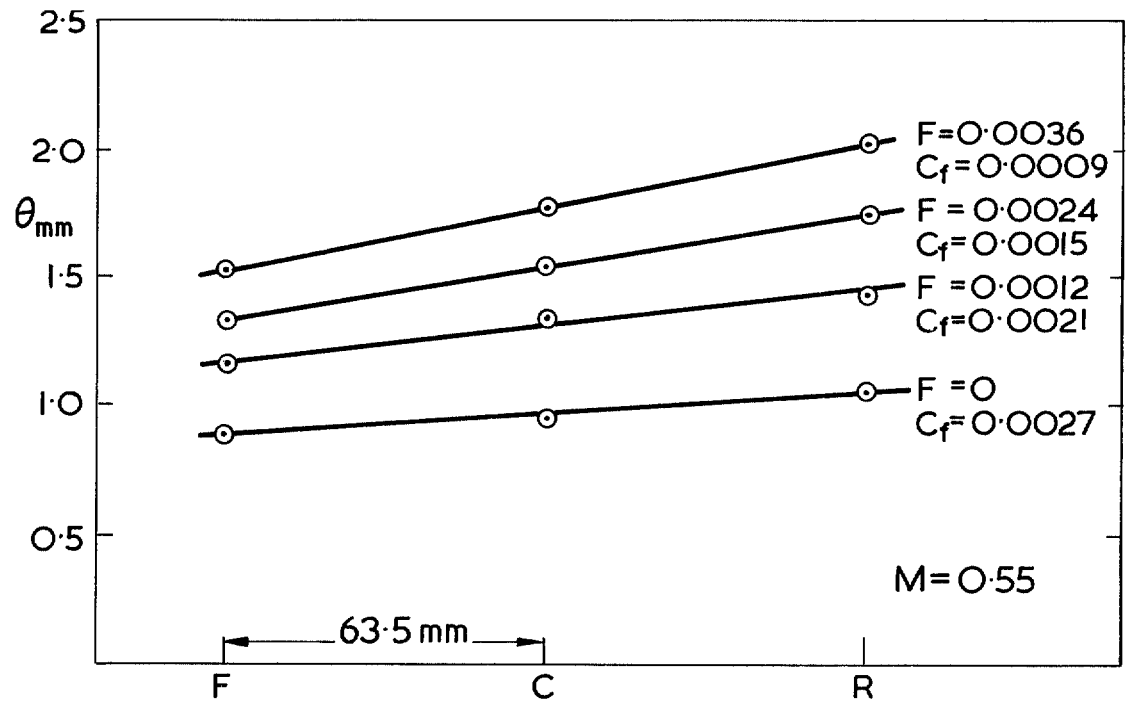

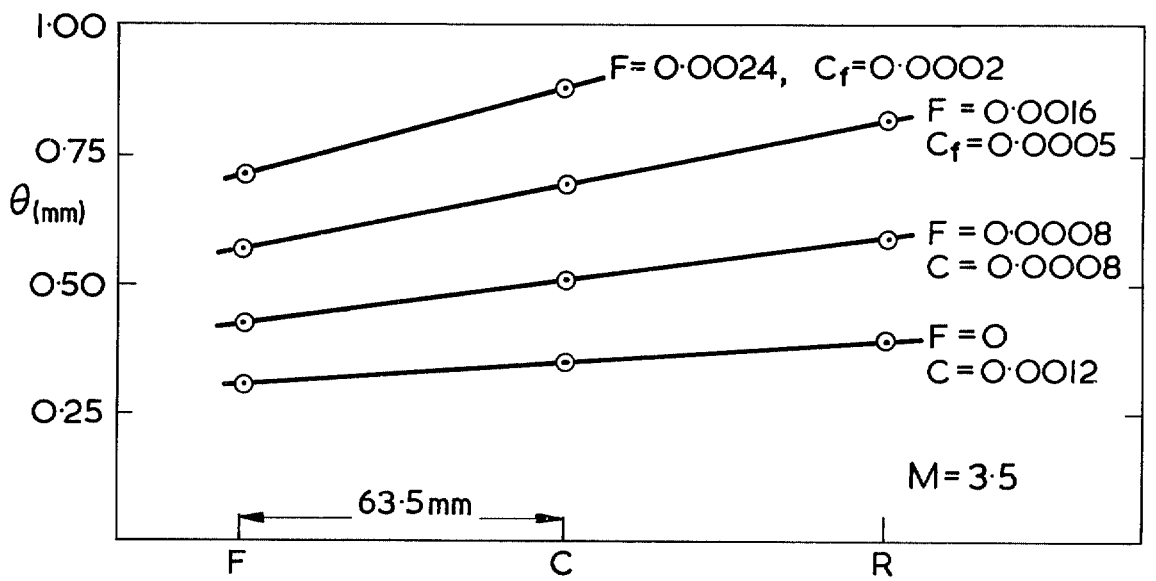

FIG. 11. Typical Momentum Developments.

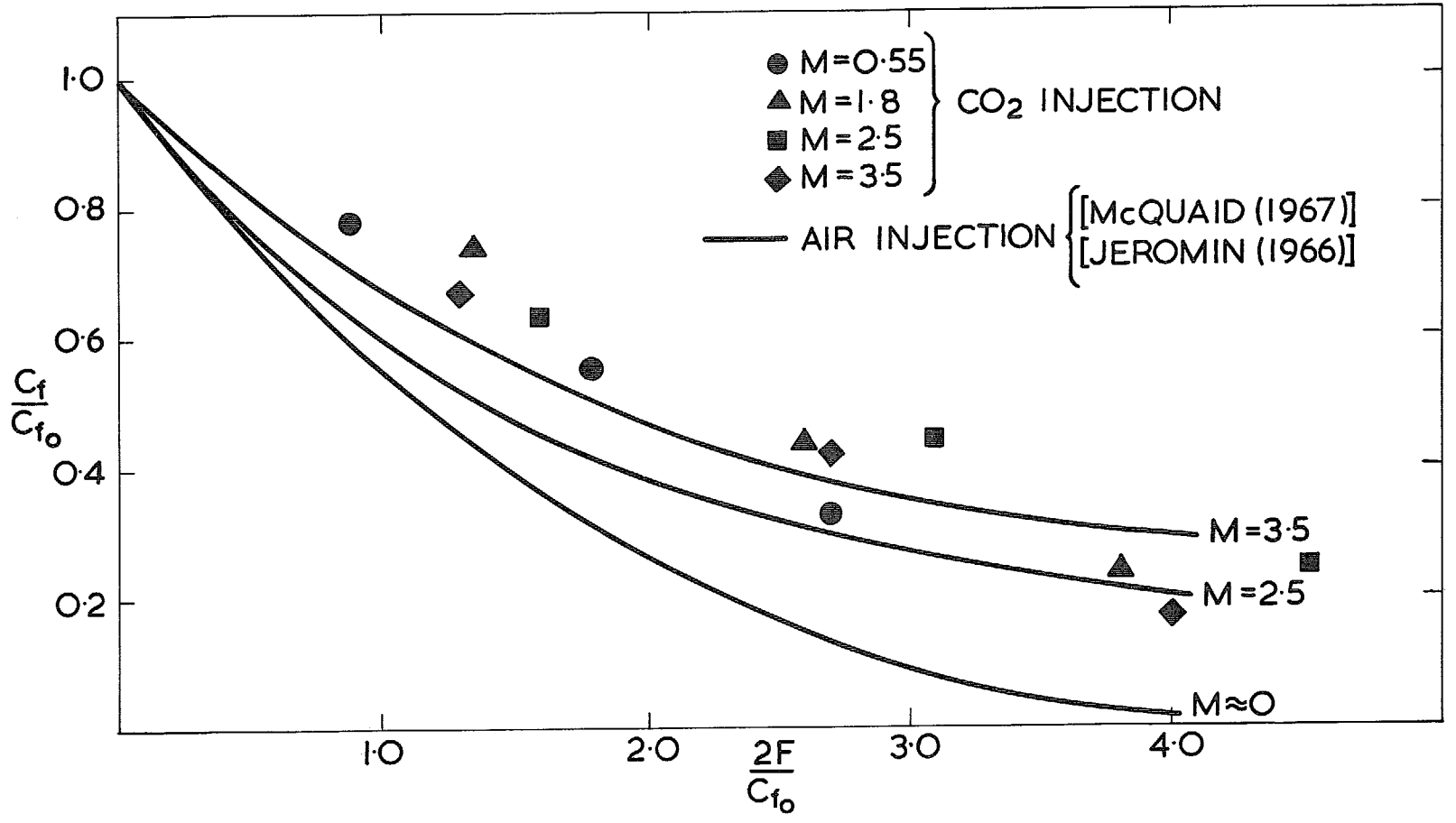

FIG. 12. Variation of Skin-friction Coefficient with Injection.

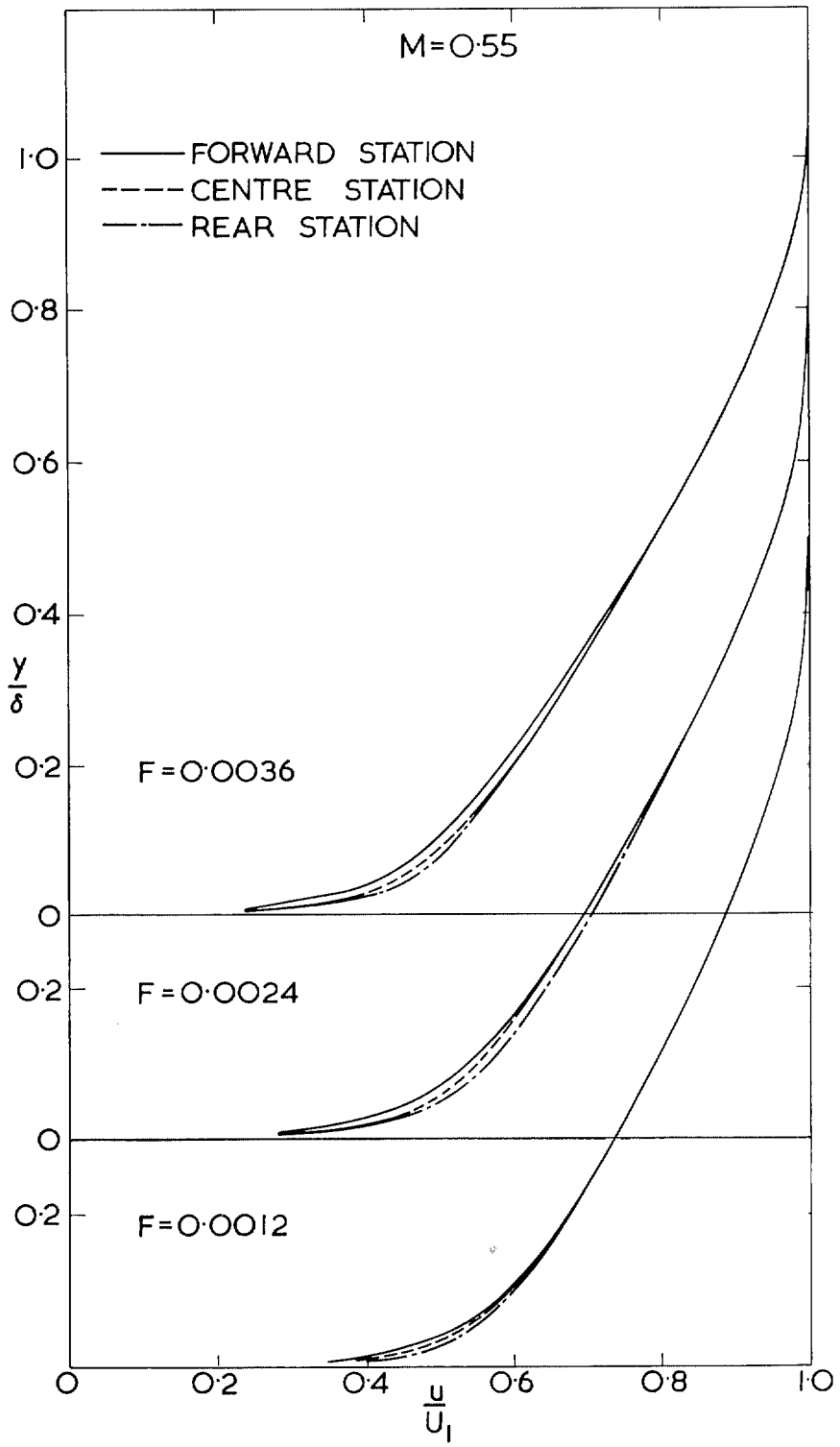

FIG. 13. Velocity Profiles at M = 0·55.

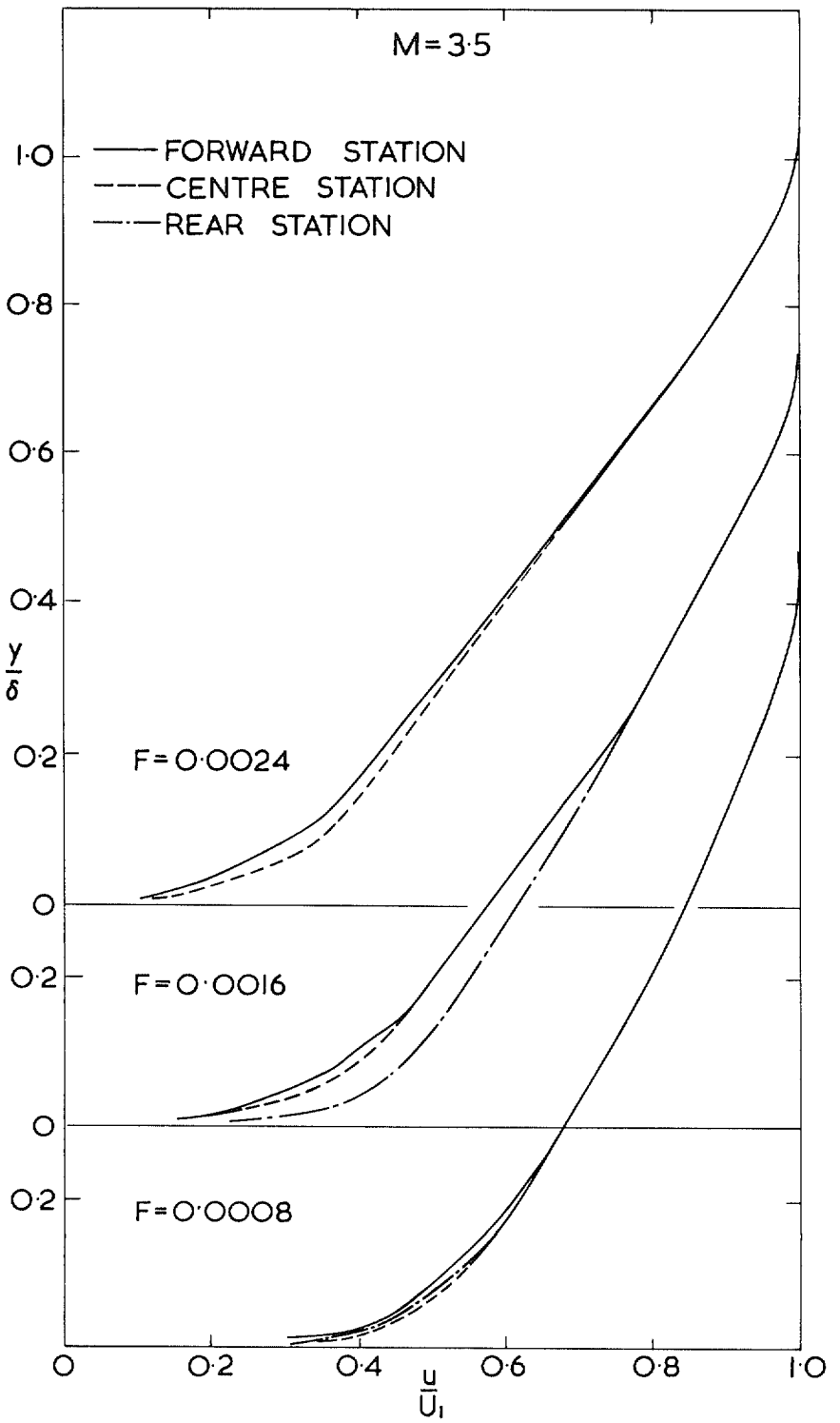

FIG. 14. Velocity Profiles at M = 3·5.

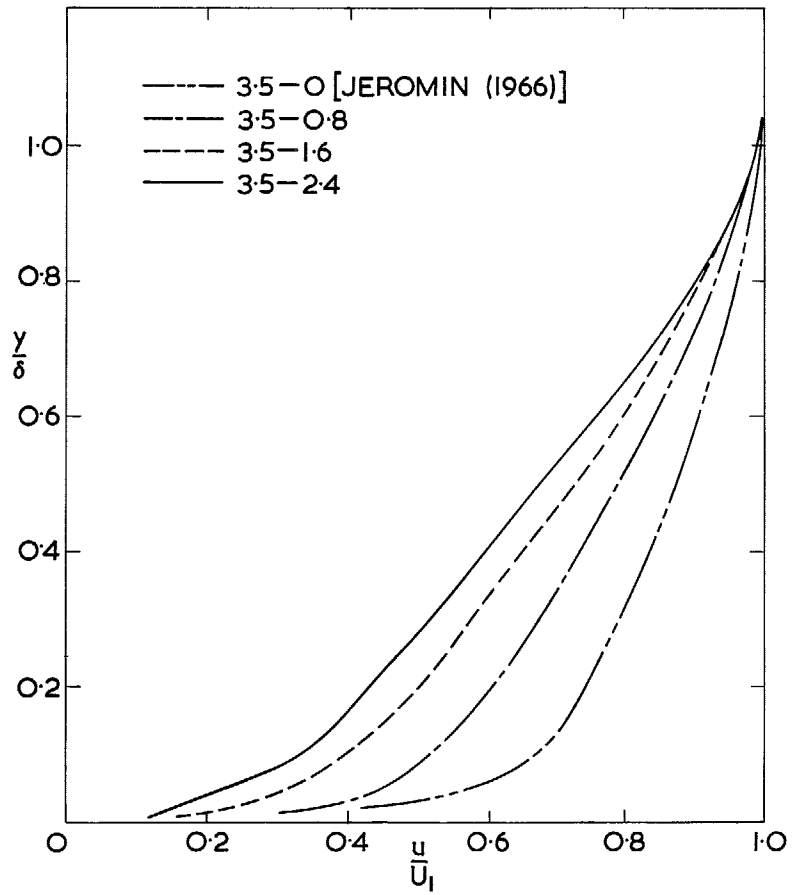

FIG. 15. Velocity Profiles with Injection—M = 3·5.

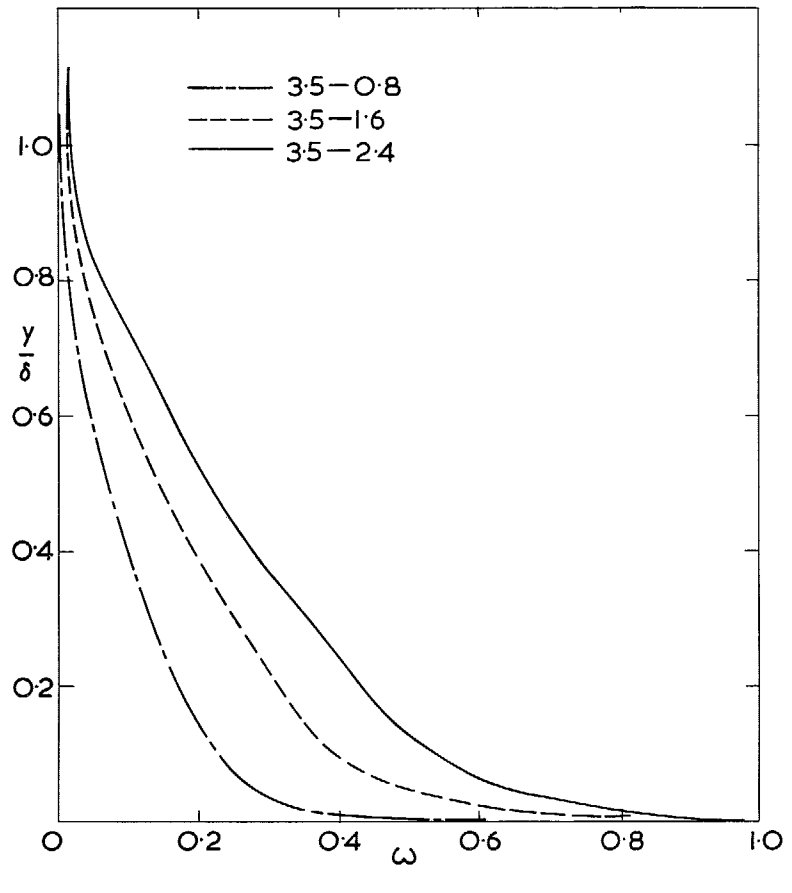

FIG. 16. Concentration Profiles with Injection—M = 3·5.

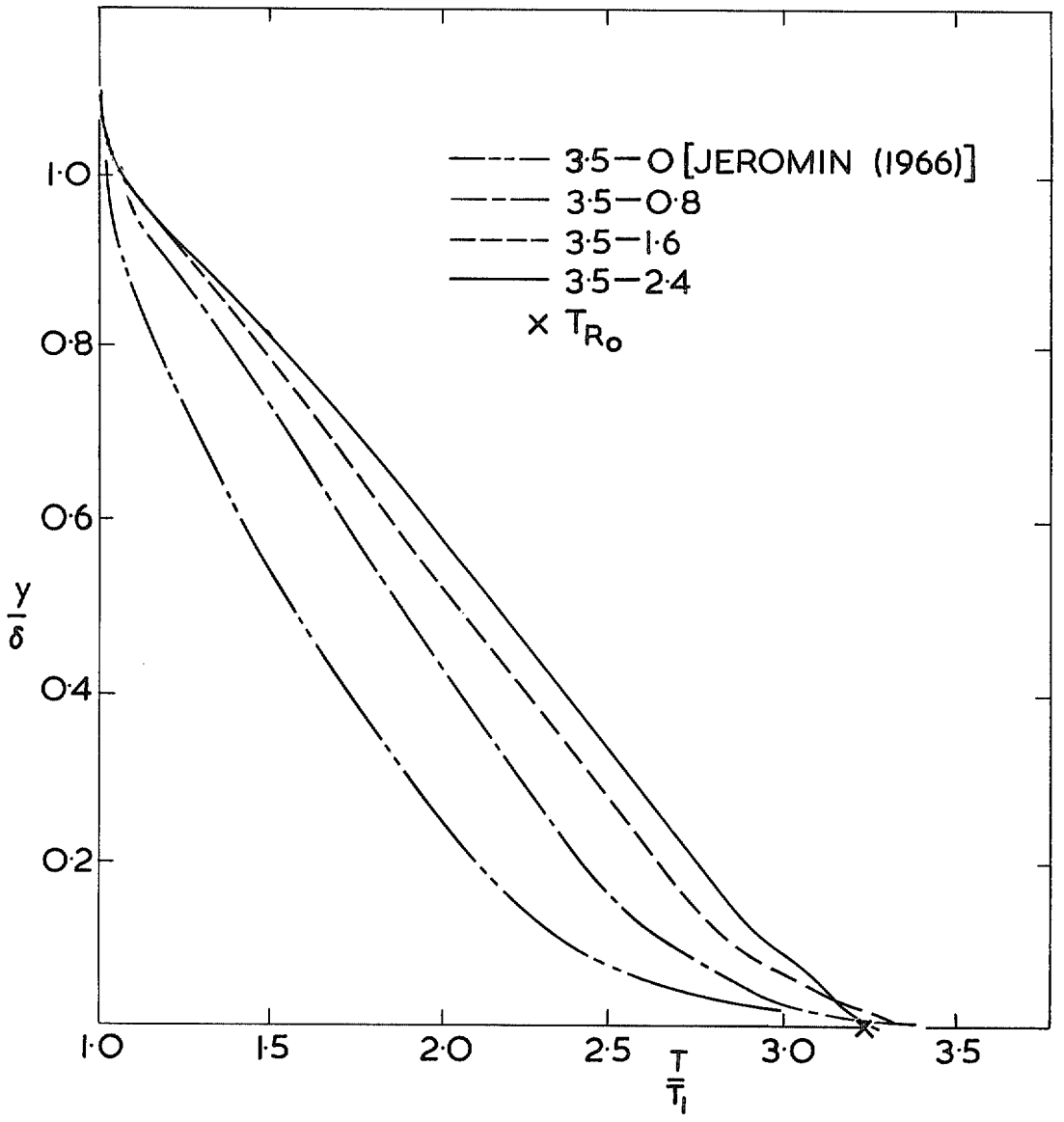

FIG. 17. Temperature Profiles with Injection—M = 3·5.

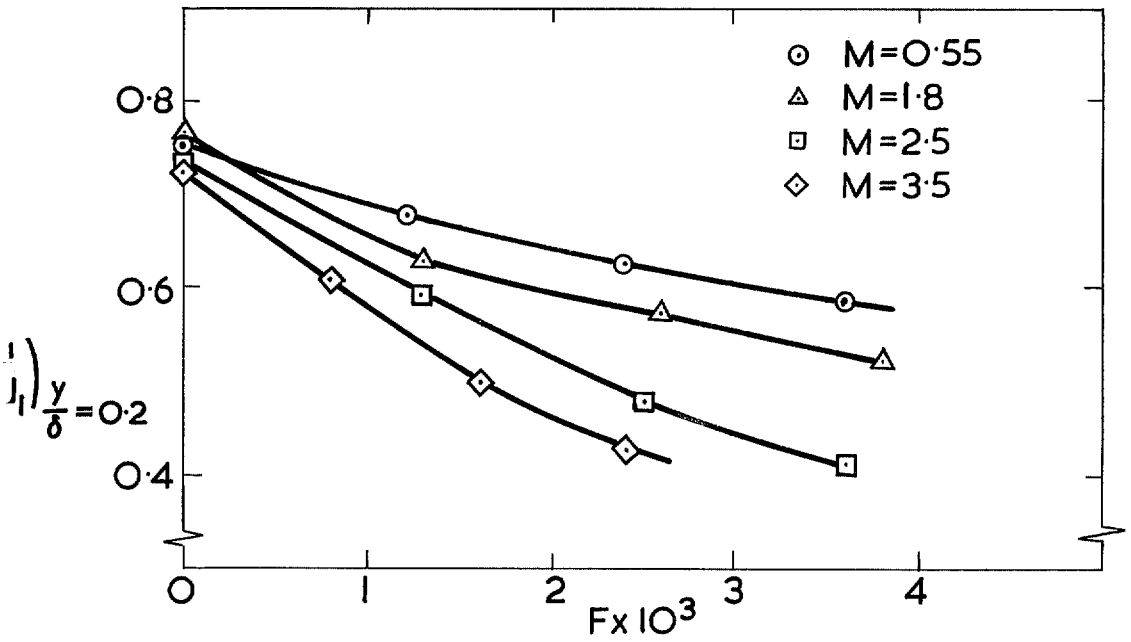

FIG. 18. Variation of the Velocity at $y/\delta = 0{\cdot}2$ with Injection.

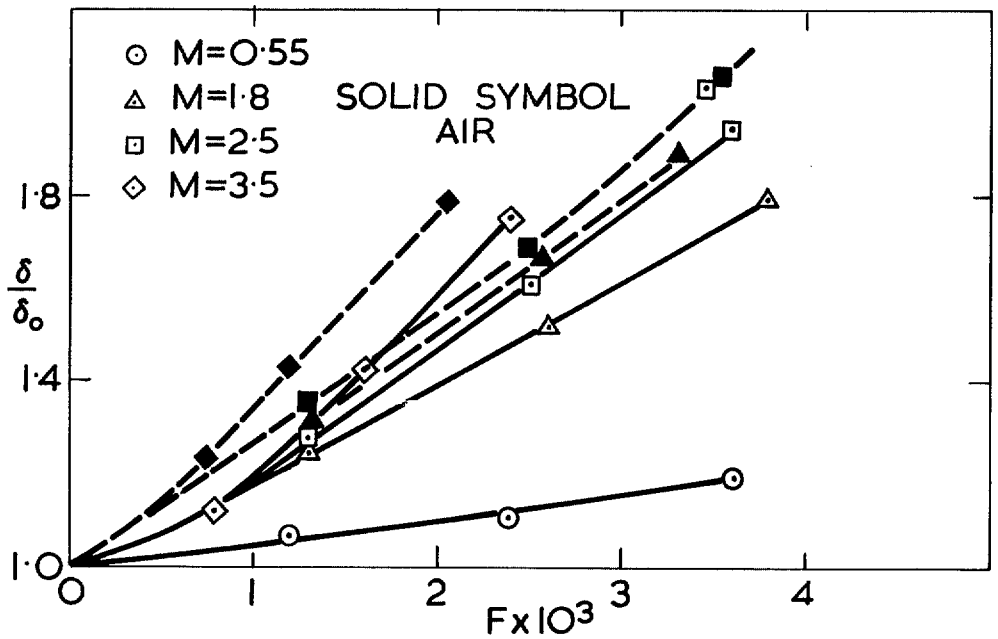

FIG. 19. Variation of the Boundary Layer Thickness with Injection.

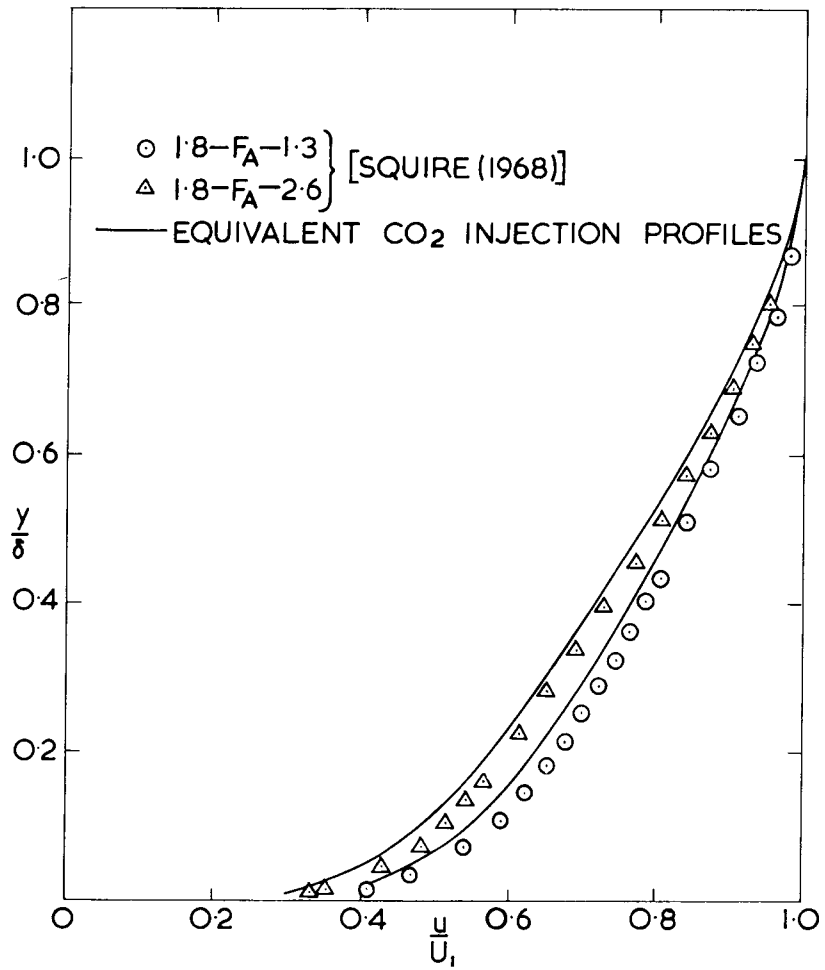

FIG. 20. Velocity Profiles with Air and Carbon Dioxide Injection at M = 1·8.

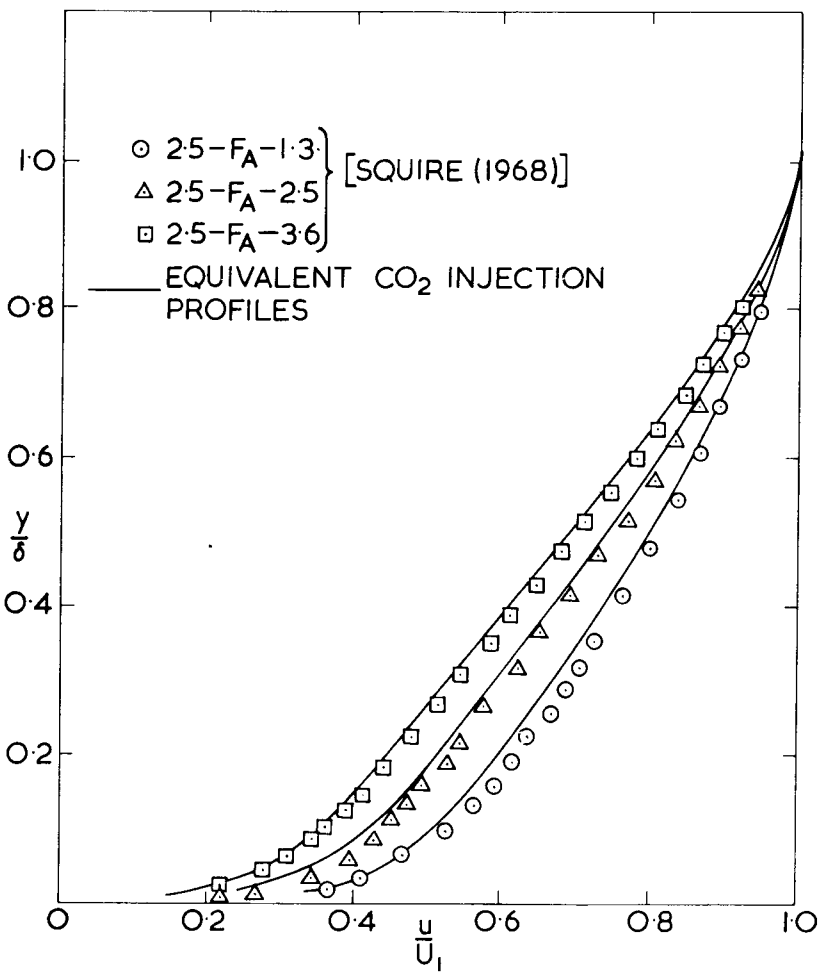

FIG. 21. Velocity Profiles with Air and Carbon Dioxide Injection at M = 2·5.

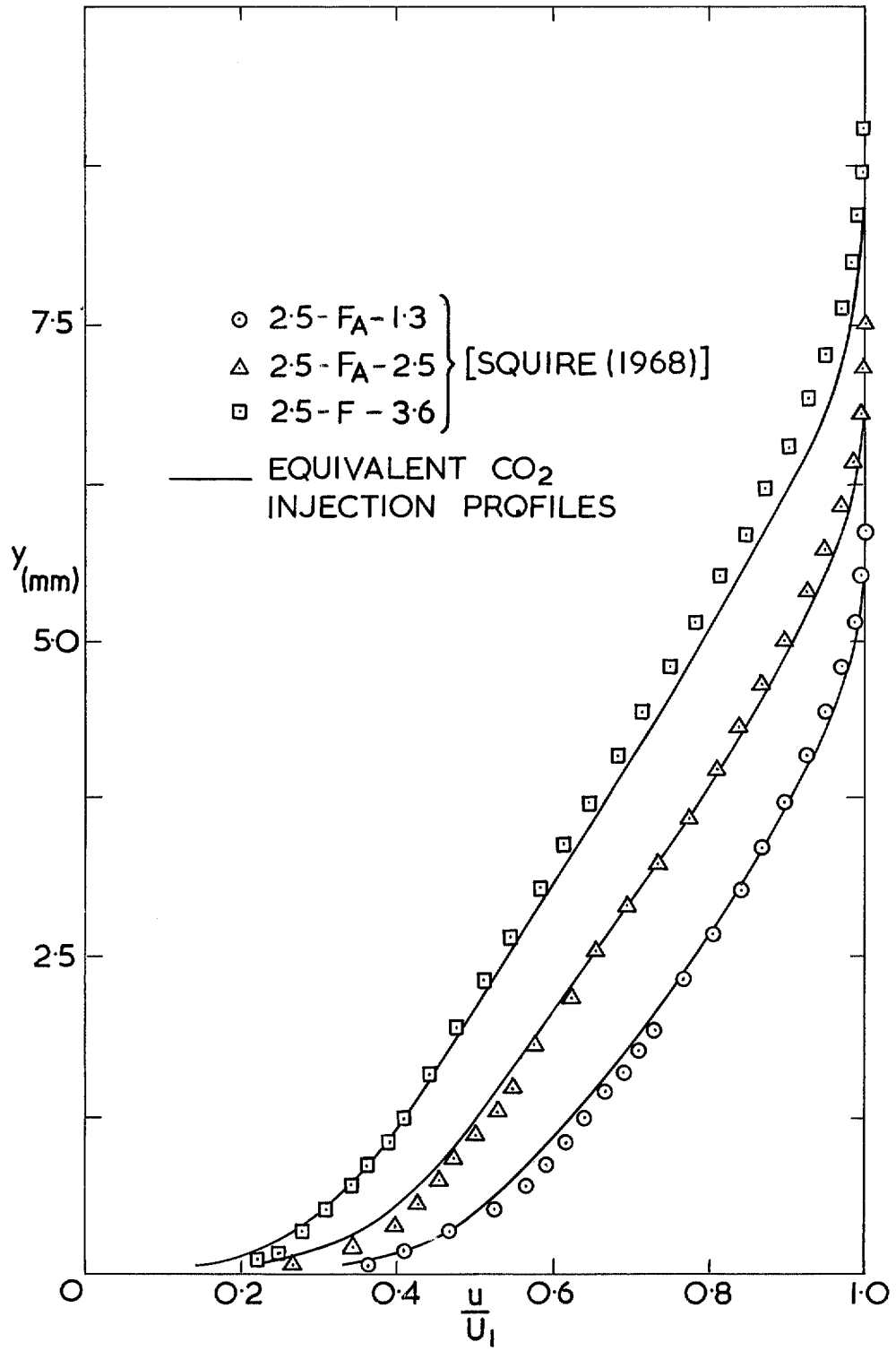

FIG. 22. Velocity Profiles with Air and Carbon Dioxide Injection at M = 2·5.

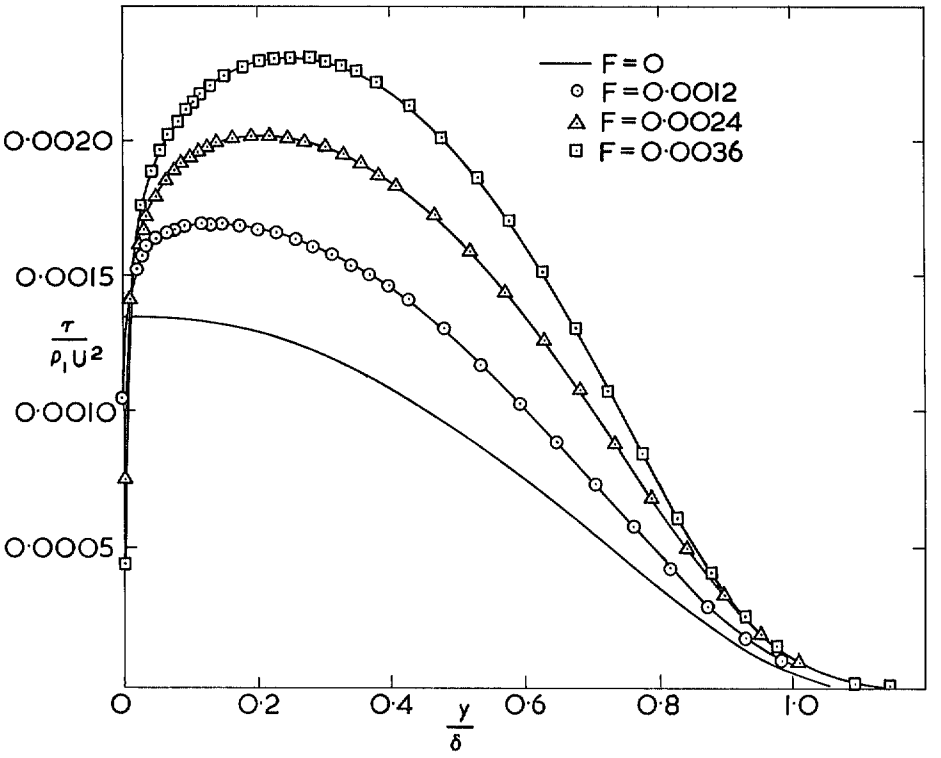

FIG. 23. Shear Stress Profiles at M = 0·55.

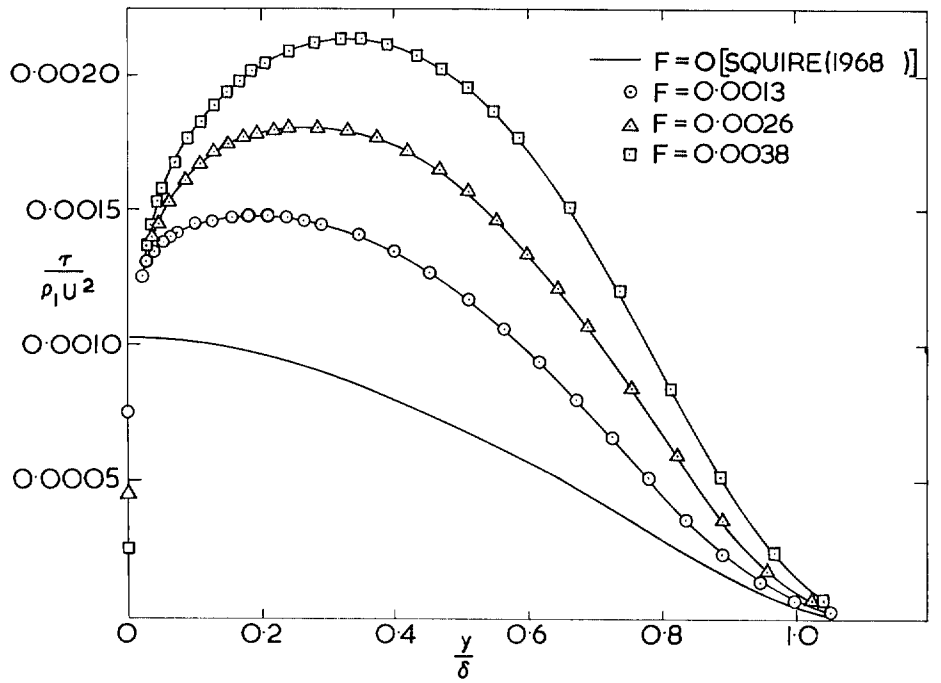

FIG. 24. Shear Stress Distributions: M = 1·8.

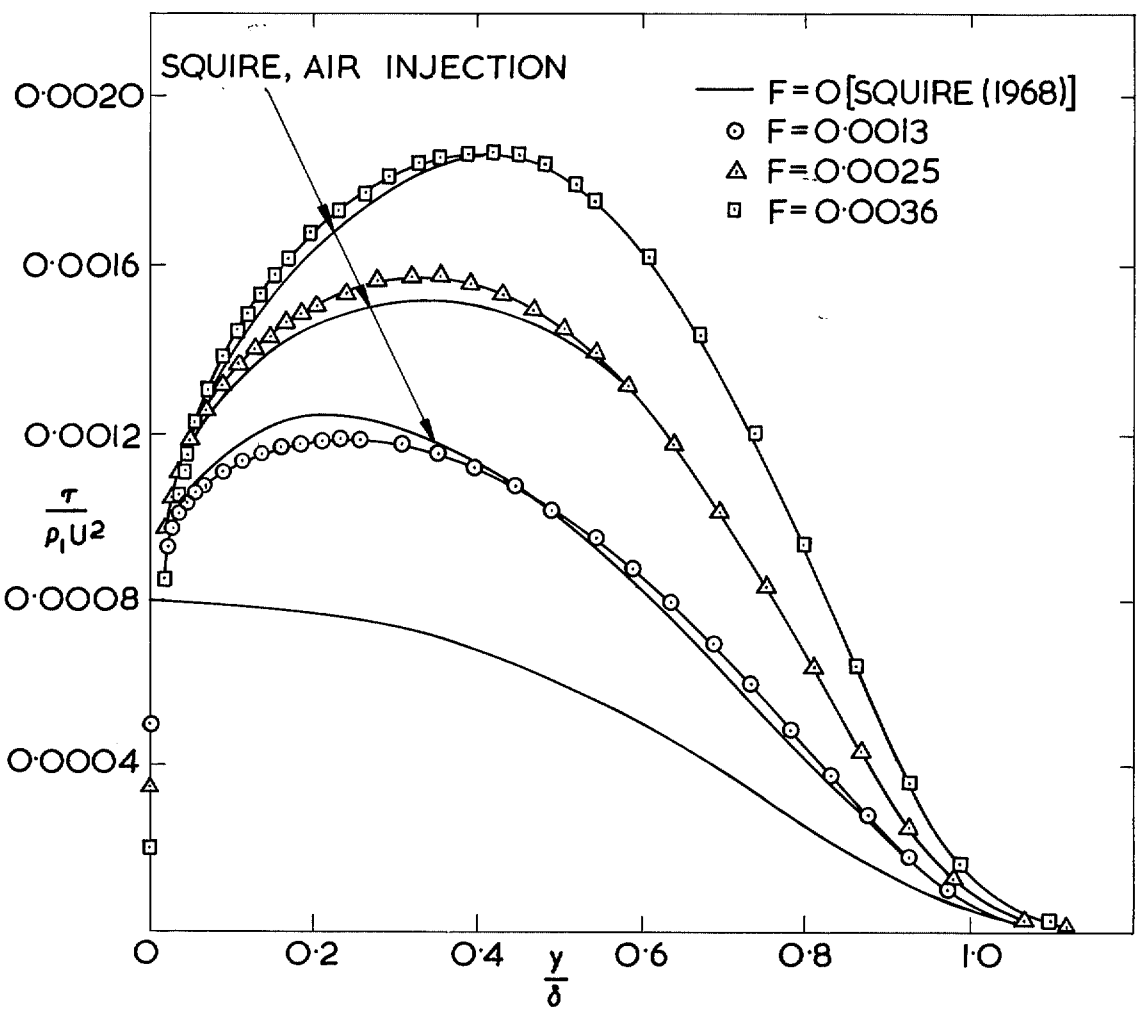

FIG. 25. Shear Stress Profiles at M = 2·5.

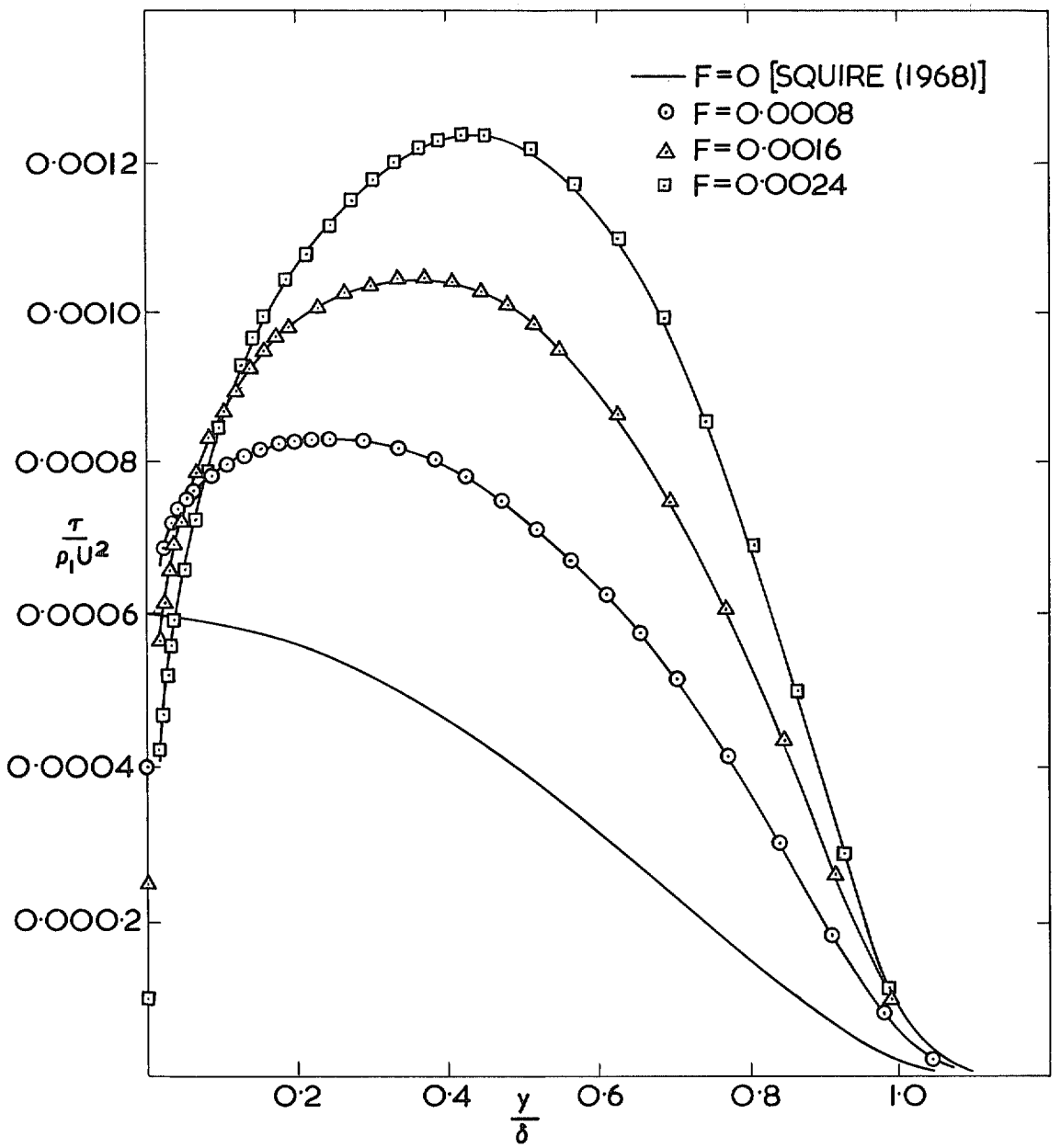

FIG. 26. Shear Stress Profiles at M = 3·5.

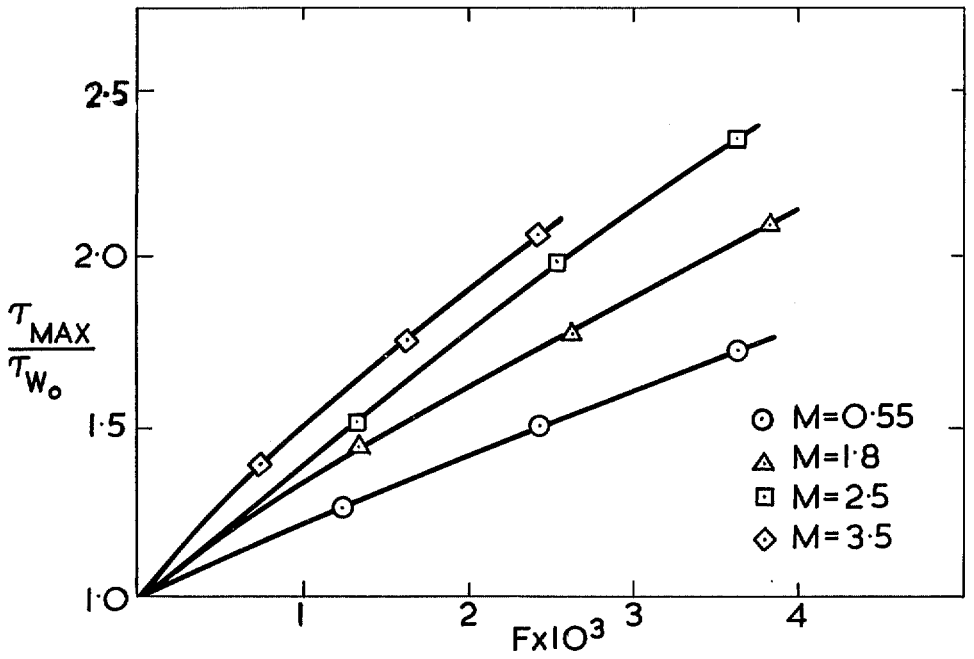

FIG. 27. Variation of Maximum Shear Stress with F.

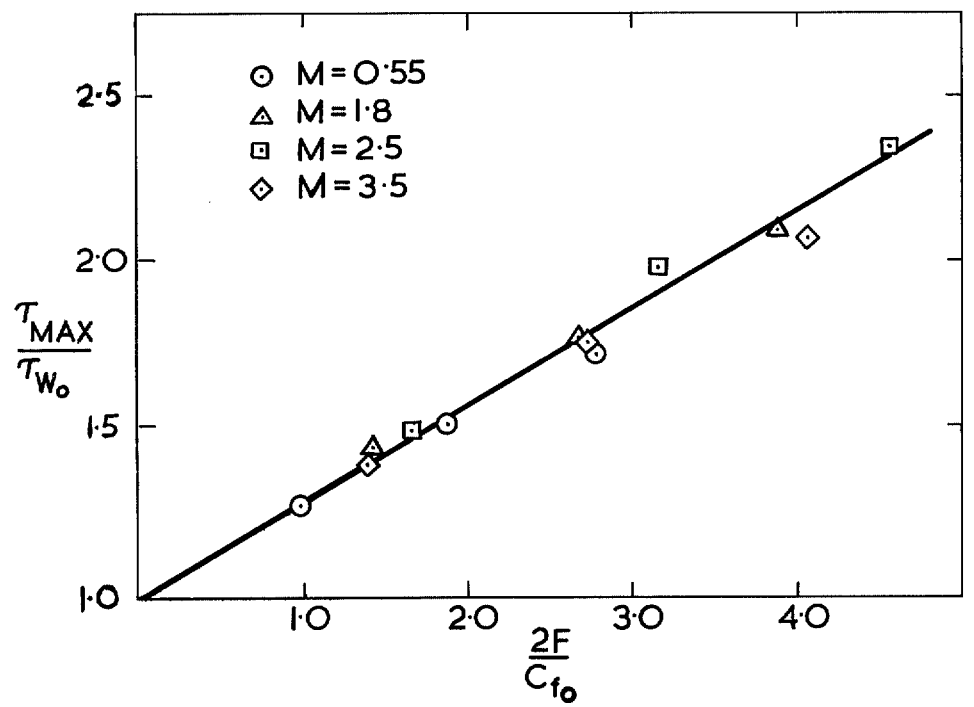

FIG. 28. Variation of Maximum Shear Stress with $2F/c_{f_o}$.

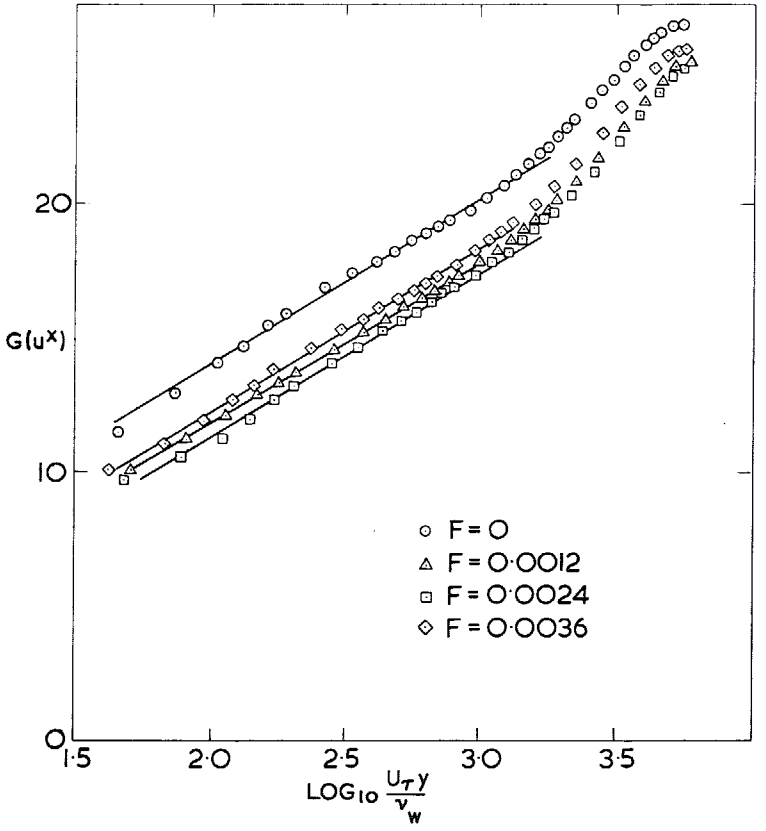

FIG. 29. Law of the Wall Curves: M = 0·55.

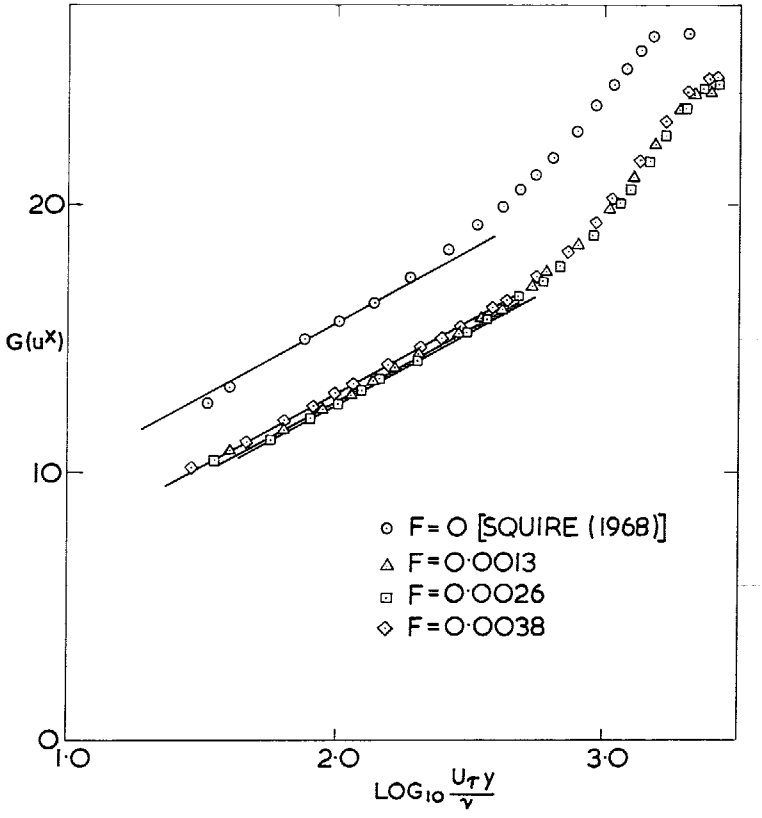

FIG. 30. Law of the Wall Curves: M = 1·8.

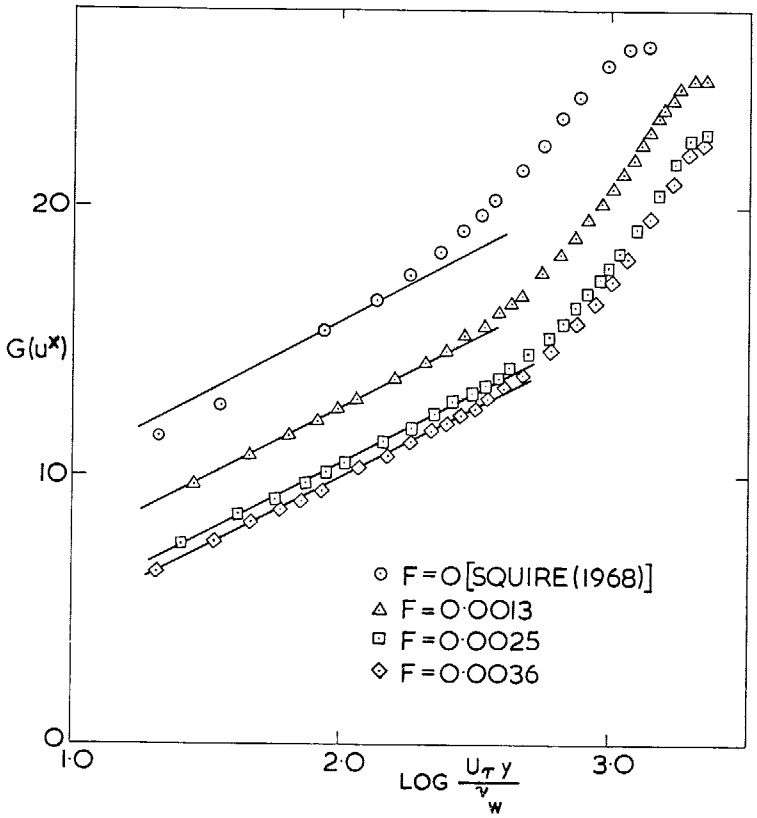

FIG. 31. Law of the Wall Curves: M = 2·5.

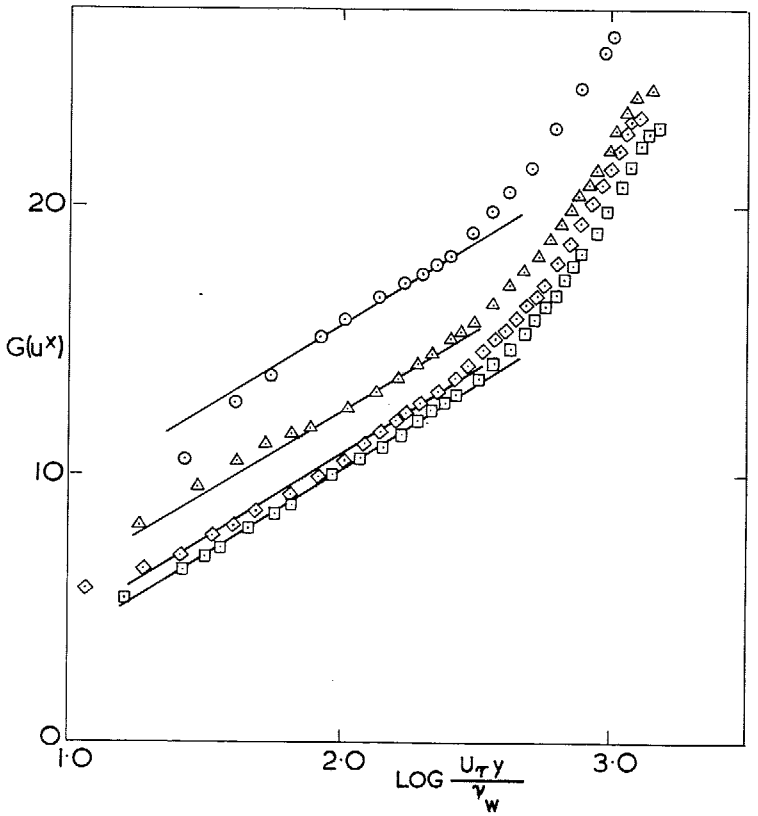

FIG. 32. Law of the Wall Curves: M = 3·5.

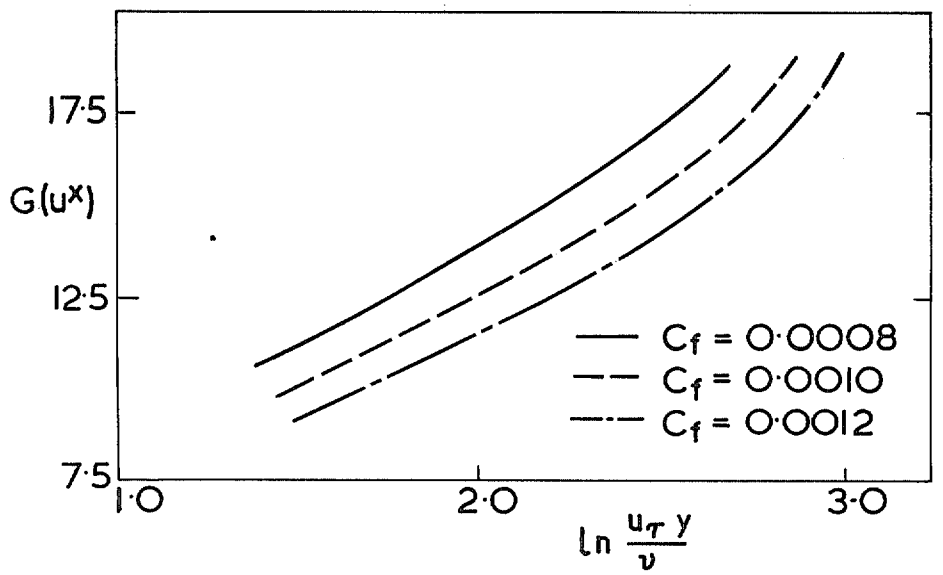

FIG. 33. Effect of Errors in c_f on the Wall Law.

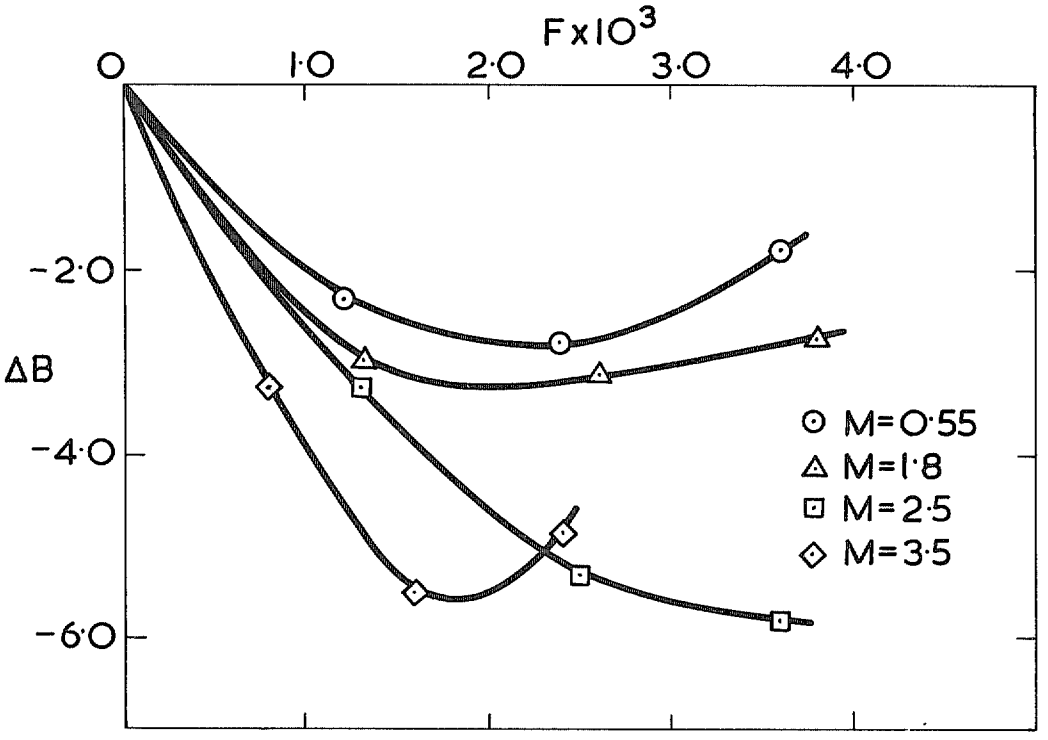

FIG. 34. Variation of ΔB with Injection Rate.

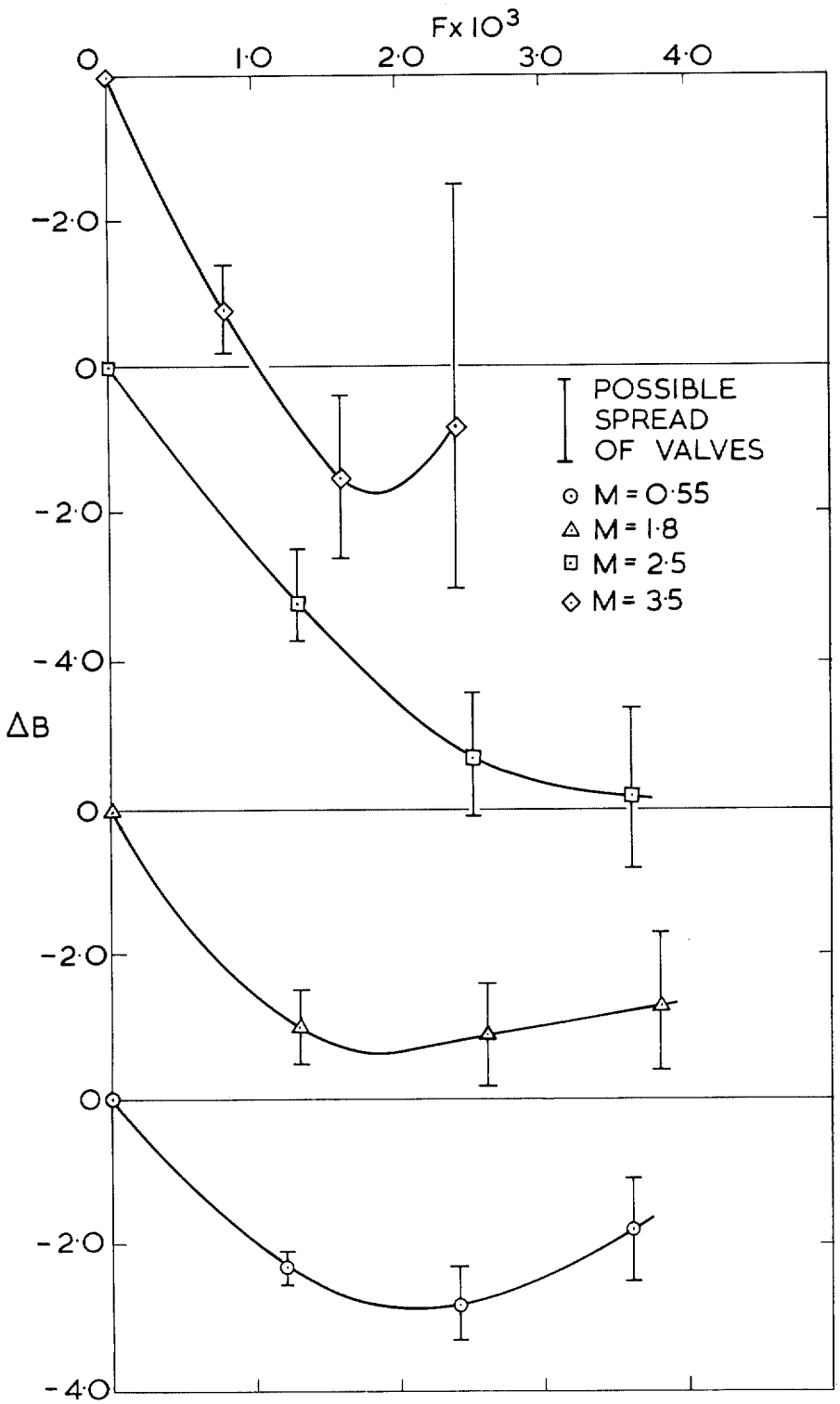

FIG. 35. Effect of Possible Errors on the Variation of B with Injection.

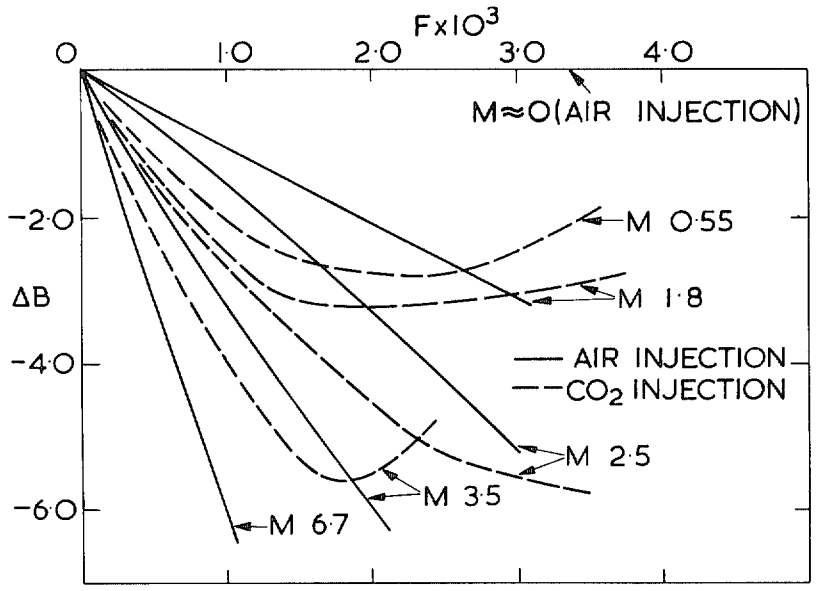

FIG. 36. Variation of ΔB with air and carbon dioxide injection.

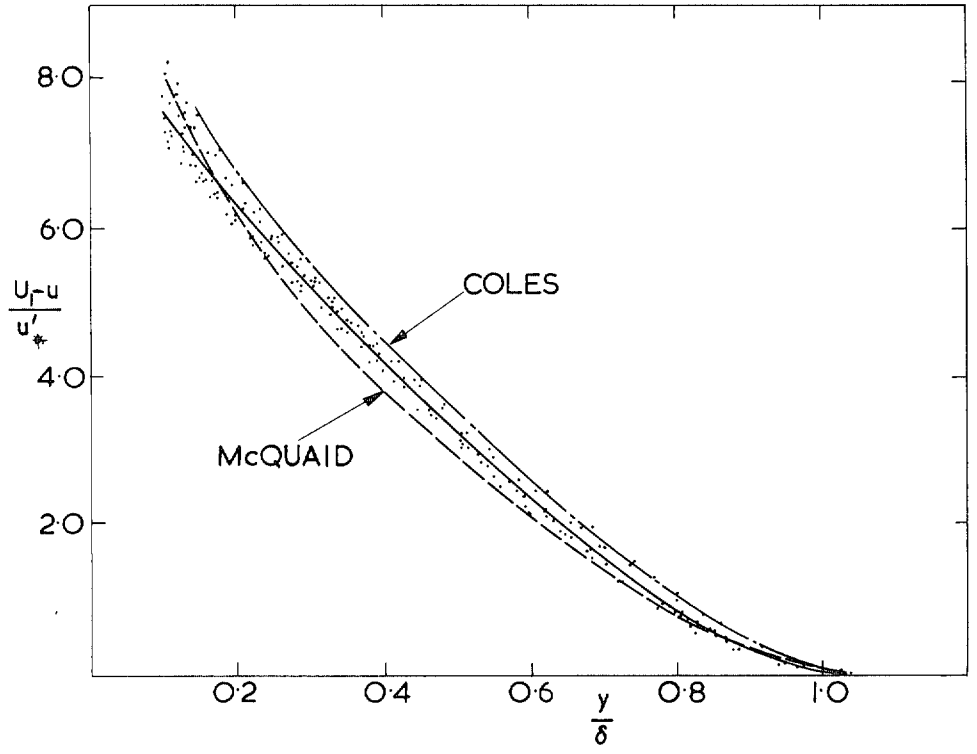

FIG. 37. Velocity Defect Law.

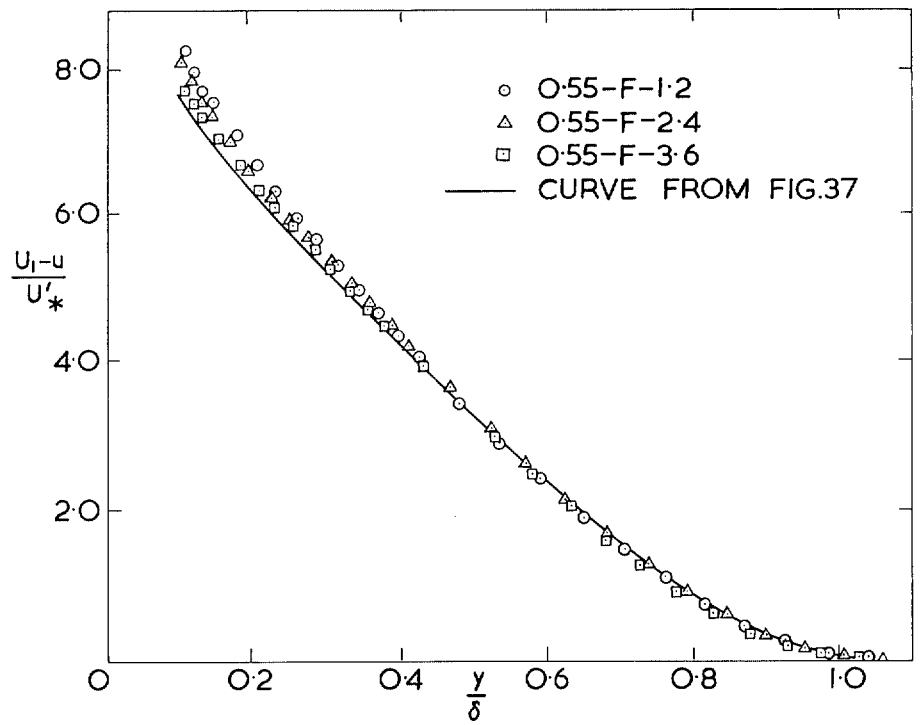

FIG. 38. Velocity Defect Law—M = 0·55.

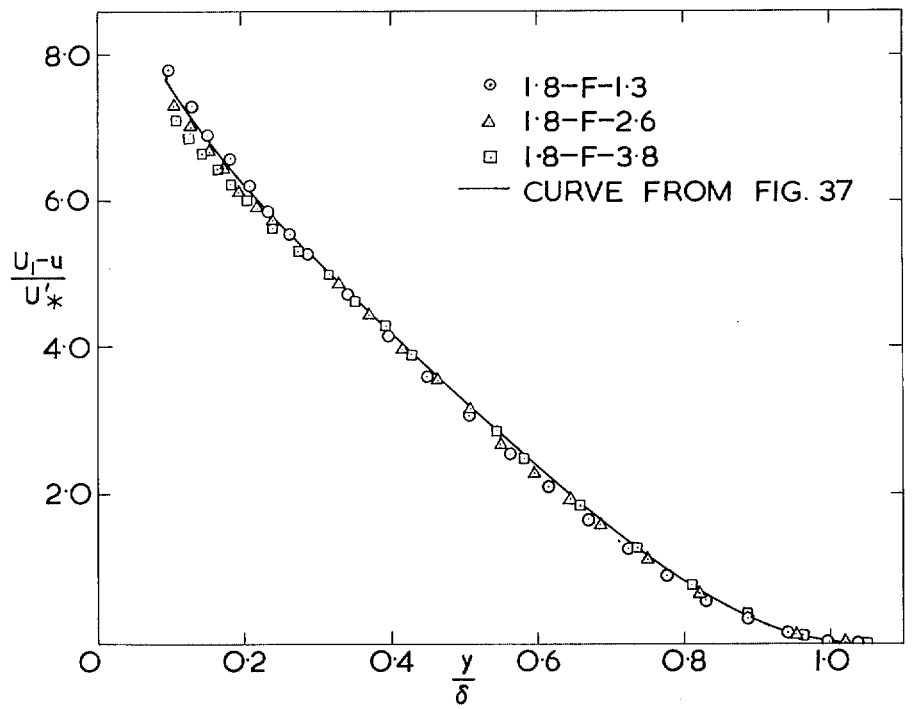

FIG. 39. Velocity Defect Law—M = 1·8.

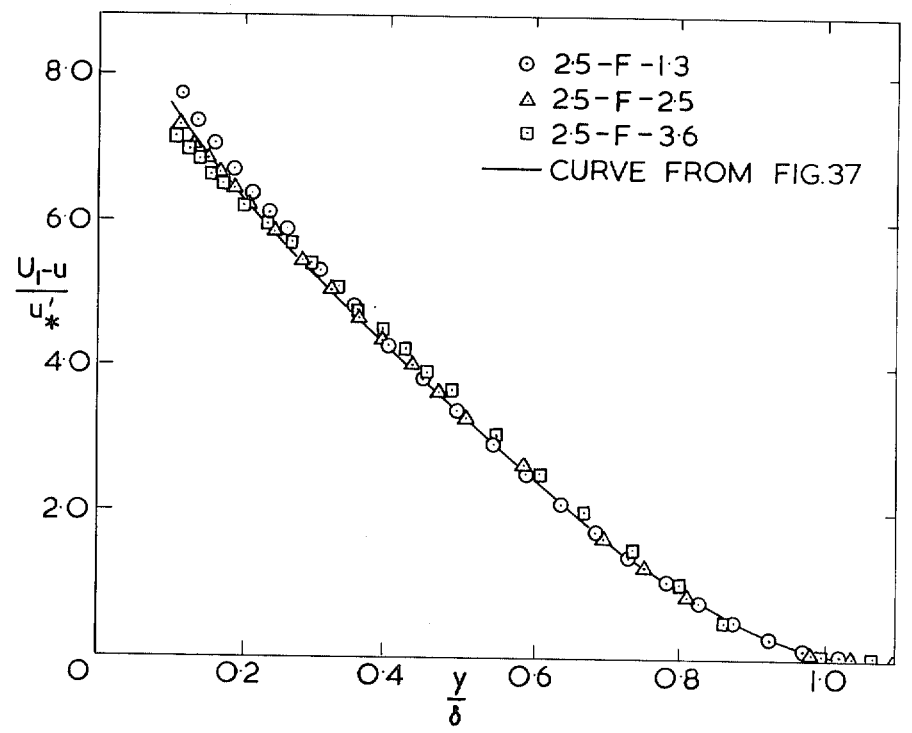

FIG. 40. Velocity Defect Law—M = 2·5.

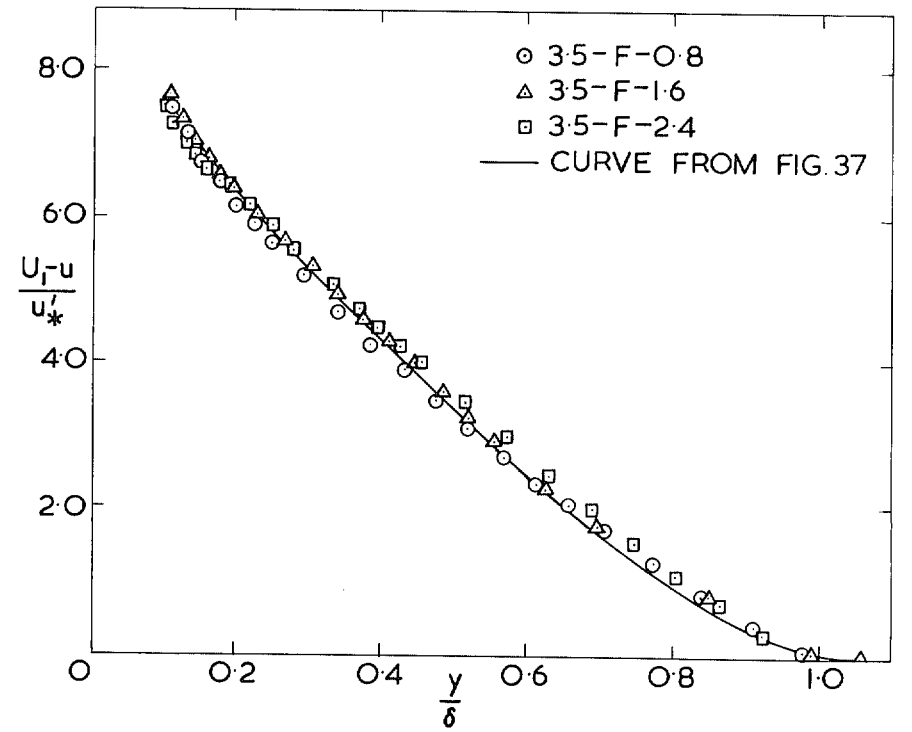

FIG. 41. Velocity Defect Law—M = 3·5.

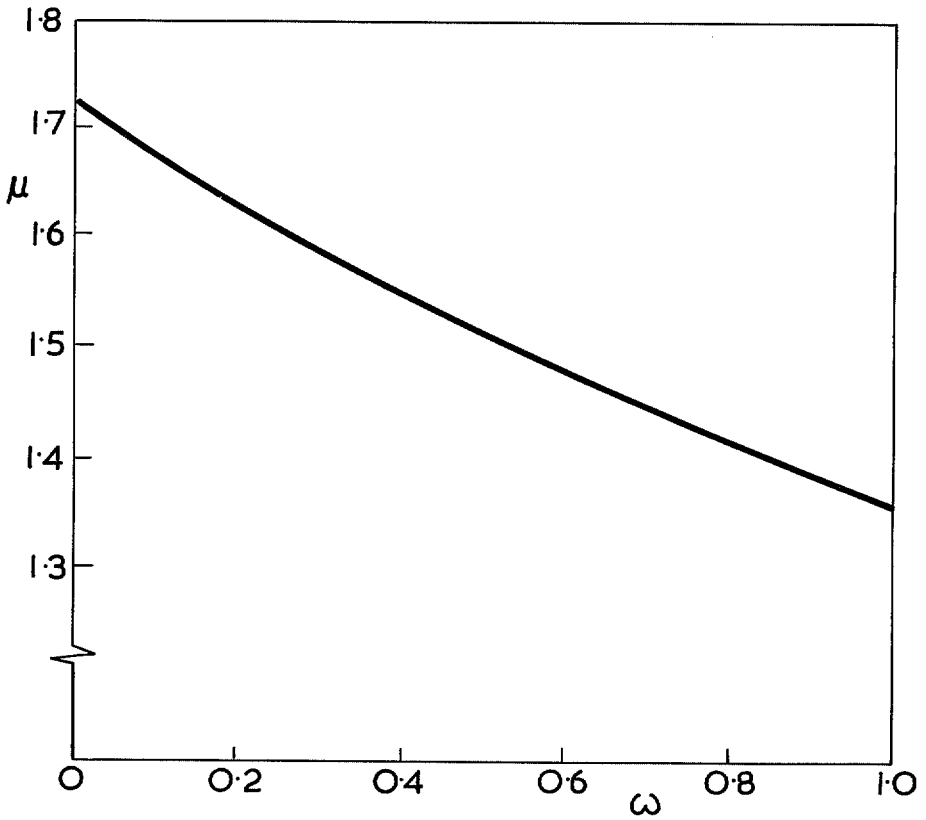

FIG. 42. Variation of Viscosity with Concentration of Carbon Dioxide.

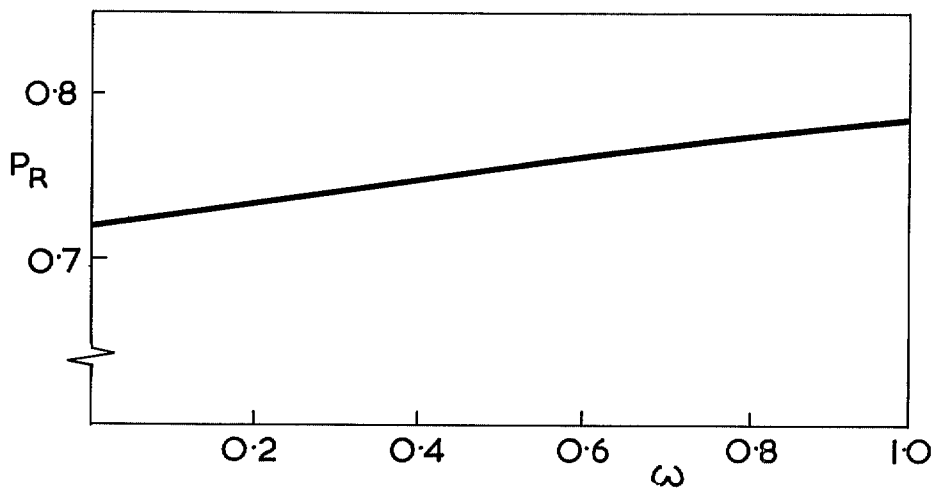

FIG. 43. Variation of Prandtl Number with Concentration of Carbon Dioxide.

Printed in Wales for Her Majesty's Stationery Office by Allens Printers (Wales) Limited

Dd. 502110 K.5 5/72

HER MAJESTY'S STATIONERY OFFICE

Government Bookshops

49 High Holborn, London WC1V 6HB
13a Castle Street, Edinburgh EH2 3AR
109 St. Mary Street, Cardiff CF1 1JW
Brazennose Street, Manchester M60 8AS
50 Fairfax Street, Bristol BS1 3DE
258 Broad Street, Birmingham B1 2HE
80 Chichester Street, Belfast BT1 4JY

Government publications are also available through booksellers

R. & M. No. 3696
SBN 11 470496 1*